UDK 66:54(05) CODEN HMIDA 8 ISSN 0367–598X

2

Hemijska industrija

Vol. 75

Časopis Saveza hemijskih inženjera Srbije

Chemical Industry

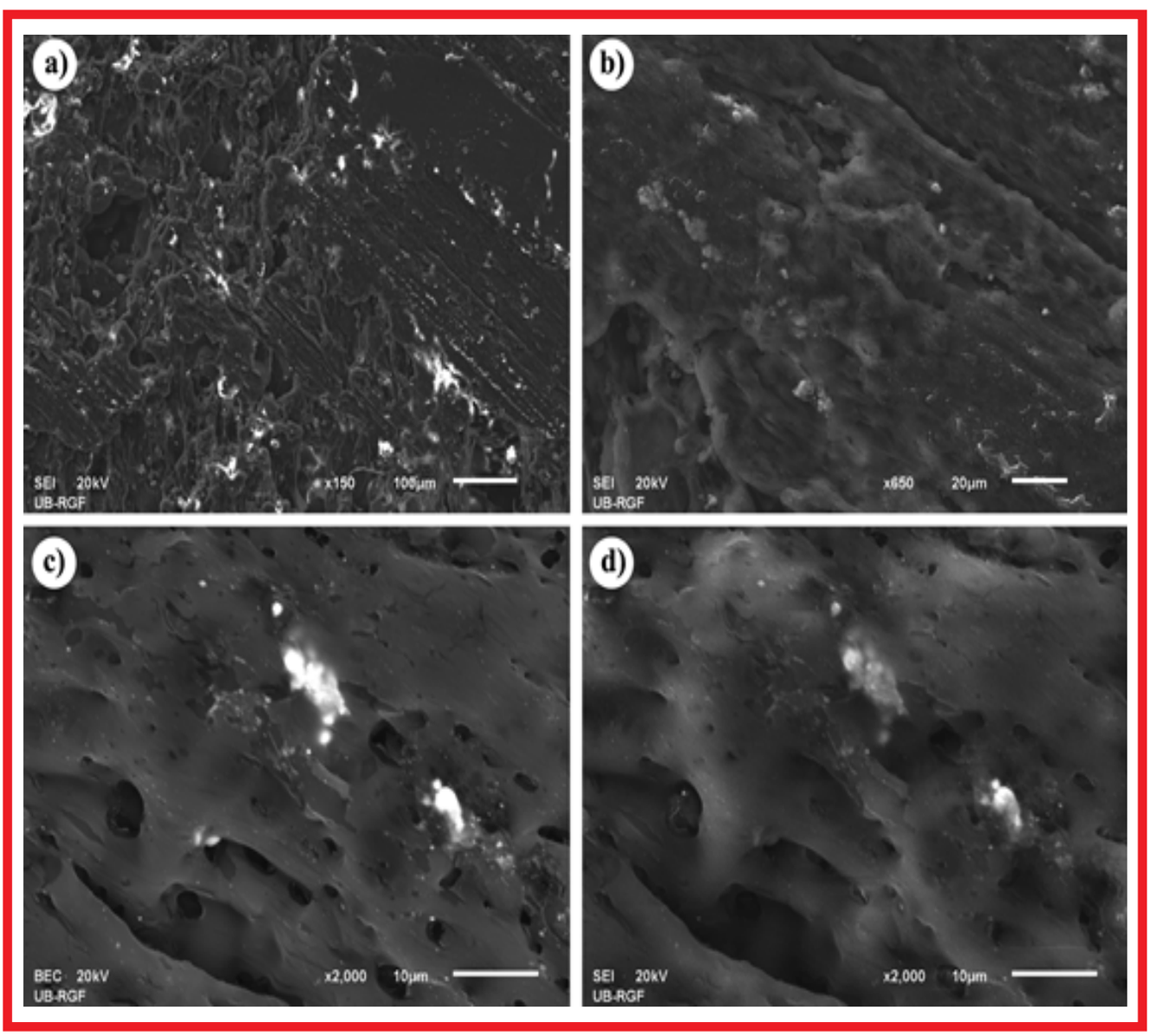

BEOGRAD, MART-APRIL 2021. HMIDA 8, 75 (2) 65-134 (2021)

Aktivnosti Saveza hemijskih inženjera Srbije pomažu:

**MINISTARSTVO PROSVETE,
NAUKE I TEHNOLOŠKOG RAZVOJA
REPUBLIKE SRBIJE**

Tehnološko-metalurški fakultet
Univerziteta u Beogradu, Beograd

Institut za tehnologiju nuklearnih i
drugih mineralnih sirovina, Beograd

Hemijski fakutet Univerziteta u
Beogradu, Beograd

Prirodno-matematički fakultet
Univerziteta u Novom Sadu, Novi Sad

Institut za opštu i fizičku hemiju,
Beograd

Tehnološki fakultet
Univerziteta u Novom Sadu, Novi Sad

NU Institut za hemiju, tehnologiju i metalurgiju
Univerziteta u Beogradu, Beograd

Institut IMS, Beograd

Tehnološki fakultet
Univerziteta u Nišu, Leskovac

Fakultet tehničkih nauka,
Kosovska Mitrovica

Chemical Industry
Химическая промышленность

Hemijska industrija

Časopis Saveza hemijskih inženjera Srbije
Journal of the Association of Chemical Engineers of Serbia
Журнал Союза химических инженеров Сербии

VOL. 75 **Beograd, mart-april 2021.** **Broj 2**

Izdavač
Savez hemijskih inženjera Srbije
Beograd, Kneza Miloša 9/I

Glavni urednik
Bojana Obradović

Zamenica glavnog i odgovornog urednika
Emila Živković

Pomoćnik glavnog i odgovornog urednika
Ivana Drvenica

Urednici
Enis Džunuzović, Ivana Banković-Ilić, Maja Obradović, Dušan Mijin, Marija Nikolić, Tatjana Volkov-Husović, Đorđe Veljović,

Članovi uredništva
Nikolaj Ostrovski, Milorad Cakić, Željko Čupić, Miodrag Lazić, Slobodan Petrović, Milovan Purenović, Aleksandar Spasić, Dragoslav Stoiljković, Radmila Šećerov-Sokolović, Slobodan Šerbanović, Nikola Nikačević, Svetomir Milojević

Članovi uredništva iz inostranstva
Dragomir Bukur (SAD), Jiri Hanika (Češka Republika), Valerij Meshalkin (Rusija), Ljubiša Radović (SAD), Constantinos Vayenas (Grčka)

Likovno-grafičko rešenje naslovne strane
Milan Jovanović

Redakcija
11000 Beograd, Kneza Miloša 9/I
Tel/fax: 011/3240-018
E-pošta: shi@ache.org.rs
www.ache.org.rs

Izlazi dvomesečno, rukopisi se ne vraćaju

Za izdavača: Ivana T. Drvenica

Sekretar redakcije: Slavica Desnica

Izdavanje časopisa pomaže
Republika Srbija, Ministarstvo prosvete, nauke i tehnološkog razvoja

Uplata pretplate i oglasnog prostora vrši se na tekući račun Saveza hemijskih inženjera Srbije, Beograd, broj 205-2172-71, Komercijalna banka a.d., Beograd

Menadžer časopisa i Kompjuterska priprema
Aleksandar Dekanski

Štampa
Razvojno-istraživački centar grafičkog inženjerstva, Tehnološko-metalurški fakultet, Univerzitet u Beogradu, Karnegijeva 4, 11000 Beograd

Indeksiranje
Radovi koji se publikuju u časopisu *Hemijska Industrija* ideksiraju se preko *Thompson Reuters Scietific®* servisa *Science Citation Index - Expanded™* i *Journal Citation Report (JCR*)

SADRŽAJ/CONTENTS

Optimizacija mlevenja aktivne komponente i hidrofobizacija dobijenog sredstva za gašenje požara

Slavica R. Mihajlović[1], Nataša G. Đorđević[1], Marina N. Jovanović[2], Milica M. Vlahović[3], Ljubinko D. Savić[4], Aleksandra S. Patarić[1] i Marina S. Blagojev[5]

[1]*Institut za tehnologiju nuklearnih i drugih mineralnih sirovina, Franše d'Eperea 86, Beograd, Srbija*
[2]*Univerzitet u Zenici, Metalurško-tehnološki fakultet, Travnička cesta 1, Zenica, Bosna i Hercegovina*
[3]*Univerzitet u Beogradu, Institut za hemiju, tehnologiju i metalurgiju, Njegoševa 12, Beograd, Srbija*
[4]*Univerzitet u Prištini sa sedištem u Kosovskoj Mitrovici, Fakultet tehničkih nauka, Kneza Miloša 7, Kosovska Mitrovica, Srbija*
[5]*Univerzitet u Beogradu, Rudarsko-geološki fakultet, Đušina 7, Beograd, Srbija*

Izvod

U radu je prikazan postupak mlevenja monoamonijum fosfata (MAP) kao aktivne komponente u praškastom sredstvu za gašenje požara (SGP). Cilj je bio da se utvrdi vreme mlevenja MAP koje je potrebno za dobijanje optimalne granulacije za potpuno gašenje požara i eliminisanje plamena. MAP je mleven u laboratorijskom keramičkom mlinu sa kuglama i vibro mlinu sa prstenastim radnim elementima. Proces je kontrolisan prosejavanjem na situ 100 μm. Utvrđeno je da se mlevenjem granula MAP veličine ≈3000 μm u laboratorijskom mlinu sa kuglama optimalna krupnoća od 64 % frakcije čestica veličine -100 μm dobija nakon 33 min mlevenja. Za postizanje iste finoće proizvoda u dvostepenom mlevenju vreme je skraćeno na 26 min (10 min u vibro mlinu i 16 min u mlinu sa kuglama). Stabilnost i hidrofobnost SGP je postignuta oblaganjem magnezijum stearatom (MgSt) pri udelu od 2 % u mlinu sa kuglama u trajanju od 15 min. Efikasnost gašenja je testirana na poligonu u realnim uslovima. Na tačno određenom mestu za testiranje, u kontrolisanim uslovima, izazvan je požar paljenjem čvrstih materijala i zapaljivih tečnosti. U oba slučaja je došlo do trenutne eliminacije plamena. Na taj način je potvrđena efikasnost formiranog SGP i mogućnost njegove upotrebe u praksi.

Ključne reči: monoamonijum fosfat; granulometrijski sastav; magnezijum stearat; oblaganje.

Available on-line at the Journal web address: http://www.ache.org.rs/HI/

STRUČNI RAD

UDK: 661.635.13:621.742.53:629.4.047.4

Hem. Ind. **75 (2)** 65-75 (2021)

1. UVOD

Sve veće opasnosti i rizici od izbijanja požara su uticali na razvoj i formiranje novih sredstava za gašenje požara (SGP) na bazi različitih hemijskih jedinjenja. SGP je materija koja dovođenjem u neposredni kontakt ili u prostor gde se odvija gorenje, svojim delovanjem trajno prekida započeti proces gorenja. Gorenje je fizičko-hemijski proces sjedinjavanja gorive materije sa kiseonikom uz oslobađanje znatne količine toplote i dima. Sredstva kao što su voda, pena i CO_2 gas nije moguće koristiti za sve vrste požara. Uvođenjem SGP u formi praha eliminisani su skoro svi nedostaci ranije korišćenih sredstava, a što je najvažnije postignuta je velika moć gašenja koja se ogleda u trenutnoj eliminaciji plamena [1-3]. Praktična primena praškastih materijala za gašenje požara počela je pojavom prvih ručnih aparata za gašenje požara prahom. Takođe, razvoj i usavršavanje vatrogasnih vozila i njihova tehnička opremljenost su doprineli sve većoj upotrebi sredstava za gašenje požara u formi praha. U poslednje vreme uvode se i stabilna postrojenja za gašenje požara velikih kapaciteta i to sa automatskim aktiviranjem. Veliku upotrebu praškastih materijala za gašenje požara omogućile su njihove dobre osobine kao što je postojanost i dugotrajnost, kao i to što nisu otrovni, ne provode električnu struju, ne izazivaju oštećenja na materijalima i objektima sa kojima dođu u dodir i dobro ističu iz tela aparata za gašenje i u uslovima kada dugo stoje u njemu, jer nisu podložni očvršćavanju i aglomeraciji pod uslovom da su tehnološki dobro obrađeni kako bi dobili trajna hidrofobna svojstva [4,5]. Sredstva za gašenje požara odlikuju se kombinovanim dejstvom na proces gorenja što znači da istovremeno mogu biti prisutna dva procesa koja dovode do eliminacije plamena kao što je slučaj kod gašenja penom.

Corresponding author: Slavica R. Mihajlović, Institut za tehnologiju nuklearnih i drugih mineralnih sirovina, Franše d'Eperea 86, Beograd, Srbija
E-mail: s.mihajlovic@itnms.ac.rs
Paper received: 14. januar 2021
Paper accepted: 29 March 2021
https://doi.org/10.2298/HEMIND210114012M

Dejstvo gašenja penom je delimično zagušujuće, pri čemu se pokriva i izoluje zapaljiva površina, a delimično i rashladno. Međutim, za svako sredstvo za gašenje požara karakteristično je jedno dominirajuće dejstvo. Tako na primer, osnovni efekat gašenja vodom je hlađenje žarišta i plamena, penom je izolacija, a prahom i halonima - inhibiranje [6-8].

Trenutna eliminacija plamena praškastim SGP vezana je za fenomen antikatalitičkog efekta, kao posledice sposobnosti materije za gašenje požara da prekida proces gorenja tako što sprečava oksidaciju. U postupku gašenja, na površini čestica praha gase se reakcioni lanci plamena što ima za posledicu trenutno dejstvo i trenutnu eliminaciju plamena [4]. Kod antikatalitičkog efekta treba razlikovati efekat inhibicije od efekta intoksikacije. Inhibicija može biti homogena (sve komponente sistema su u istom agregatnom stanju) i heterogena (komponente sistema se nalaze u više agregatnih stanja). Homogeni efekat inhibicije nastaje kada vatrogasno sredstvo odnosno produkti termičkog raspadanja kod homogenih reakcija isparavanja deluju kao negativni katalizator na proces gorenja. Heterogena inhibicija pri ugušenju plamena nastaje delovanjem čestica sredstva za gašenje i efekat heterogene inhibicije povećava delovanje sredstva za gašenje posebno pri gašenju vodenom maglom, prahom i CO_2 u obliku aerosola. Efekat intoksikacije sastoji se u "zaražavanju" kontakata. Ukoliko se taj kontakt ostvari sa česticom sredstva za gašenje, gorenje će se na tom "lancu" prekinuti. Imajući u vidu postojanje velikog broja čestica sredstva za gašenje na kojima će se desiti isti proces, logično je da kao rezultat kidanja velikog broja „lanaca" dođe do prekida gorenja. Gašenje požara efektom homogene i heterogene inhibicije povezan je sa hemijskom kinetikom odnosno sa faktorima koji utiču na brzinu odvijanja hemijske reakcije sagorevanja i uspostavljanja hemijske ravnoteže [9].

Efikasnost gašenja požara prahom zavisi od granulometrijskog sastava SGP i ostvarenog turbulentnog kretanja čestica praha. Čestice koje ulaze u sastav SGP ne smeju da budu previše krupne, jer bi prilikom izbacivanja smese iz aparata za gašenje zbog svoje težine pale na tlo jako brzo, pre dolaska do žarišta i ne bi ugasile požar. Suviše sitne čestice bi zbog male mase lebdele u vazduhu praveći oblak, pa takođe ne bi ugasile požar. Utvrđivanjem optimalnog granulometrijskog sastava za korišćeno SGP moguće je povećati njegovu efikasnost pri gašenju požara. Tako na primer, kada se prečnik čestice SGP smanji sa 400 μm na 40 μm sposobnost gašenja požara se poveća četiri puta. Dalje smanjenje veličine čestica ne dovodi do povećanja sposobnosti gašenja [4]. Rezultati istraživanja vezanih za utvrđivanje najoptimalnijeg granulometrijskog sastava praškastih SGP su pokazali da su to krupnoće između 10 i 75 μm, s tim da je većinski udeo čestica do 40 μm [10]. Pri tzv. bacanju smese na požar, najveći uticaj ima turbulentno kretanje praha koje zavisi od granulometrijskog sastava. "Uzburkani" prah i stvoreni slojevi na jednom požarnom objektu prouzrokuju brzo izjednačavanje temperature i brzo odvođenje velike količine toplote na hladniju okolinu periferije požara [4].

Da bi se SGP uz pomoć pogonskog gasa uspešno izbacio iz aparata za gašenje požara neophodna je njegova „tečljivost", odnosno forma neaglomerisanog praha. Pojava očvršćavanja SGP nastaje kao posledica upijanja vlage iz atmosfere zbog hidrofilnih osobina pre svega monoamonijum fosfata i kalcijum karbonata koji ulaze u sastav mešavine [11,12]. Smanjenje hidrofilnih svojstava čestica i njihovo potpuno prevođenje u stanje hidrofobnosti postiže se dodavanjem različitih aditiva. Naime, sa ciljem da se dobije hidrofobna površina SGP dodaju se različite površinski aktivne materije koje modifikuju površinu čestica praha. Najčešće se kao površinski aktivne materije koriste monokarboksilne kiseline sa alifatičnim ugljovodoničnim lancem, tzv. masne kiseline, kao i njihove soli [13,14]. Postignuta hidrofobna svojstva SGP su trajna, bez obzira da li je SGP u aparatu ili se nalazi u skladištenom prostoru pre punjenja aparata. Modifikovanje površine čestica SGP utiče i na smanjenje njihovih abrazivnih svojstava (posebno kod čestica kalcijum karbonata i kvarcnog peska) [15,16]. Takođe, poboljšavaju se reološka svojstva mešavine što je posebno važno kod faze izbacivanja SGP iz aparata za gašenje požara. Na efikasnost postupka modifikovanja veliki uticaj ima i postupak mlevenja. Naime, mlevenjem se ne vrši samo usitnjavanje komponenti već i povećanje slobodne površine sistema. Dodavanjem površinski aktivne supstance stvara se mogućnost njenog vezivanja za slobodne centre nastale mlevenjem sistema čime se postiže njegova stabilnost i hidrofobnost [17-19]. Treba naglasiti da sve sirovine pružaju određeni otpor mlevenju, odnosno imaju svoju meljivost. Otpor sirovine prema mlevenju zavisi od čvrstoće, tvrdoće, teksturnih i strukturnih karakteristika sirovine, tipa kristalne rešetke mineralne komponente i drugih fizičko-mehaničkih osobina [20]. Čvrstoća sirovine po pravilu ima glavni uticaj na meljivost, ali direktna proporcionalnost ova dva parametra nije ustanovljena [20].

U ovom radu autori su koristili magnezijum stearat (MgSt) za stabilizaciju i oblaganje komponenti koje ulaze u sastav SGP čime je hidrofilna površina čestica pretvorena u hidrofobnu. Na taj način je rešen problem upijanja vlage. Aktivna

komponenta koja ulazi u sastav ispitivanog SGP je monoamonijum fosfat (MAP), dok su ostale komponente punioci. Pored MAP mešavinu čini amonijum sulfat (AS), kalcijum karbonat (KK) i kvarcni pesak (KP). Procentualni udeo svake komponente zavisi od konkretne primene. Višenamenski prah (za požare A, B, i C klase) mora da sadrži min 40 % MAP. Rezultati prikazani u ovom radu odnose se na SGP koji ima maseni odnos komponenti MAP : AS : KK : KP : MgSt = = 55 :20 : 18 : 5 : 2. Cilj ovog rada je bio da se odredi optimalno vreme mlevenja MAP, kao aktivne komponente u SGP, i da se hidrofobizuje kompletna mešavina. Hidrofobizacijom SGP postiže se njegova stabilnost i eliminiše svaka mogućnost upijanja vlage i pojave aglomeracije kako u samom aparatu tako i stajanjem SGP van aparata u skladištenom prostoru.

2. EKSPERIMENTALNI DEO

2. 1. Materijali

Komponente korišćene za dobijanje SGP su: monoamonijum fosfat (MAP), $NH_4H_2PO_4$, kao aktivna komponenta, amonijum sulfat (AS), $(NH_4)_2SO_4$ i kalcijum karbonat (KK), $CaCO_3$, su iz fabrike „Elixir Zorka–Mineralna đubriva“ d.o.o. Šabac, Srbija. Kvarcni pesak (KP) je iz kompanije „Jugo Kaolin“, ogranak „Kopovi“-Ub, Srbija. Magnezijum stearat (MgSt), $Mg(C_{18}H_{35}O_2)_2$, je proizveden u fabrici „Centrohem“ d.o.o.-Stara Pazova, Srbija. Osnovne karakteristike magnezijum stearata dobijene od proizvođača su date u tabeli 1 [22].

Tabela 1. Osnovne hemijske i fizičke karakteristike MgSt
Table 1. The basic chemical and physical properties of MgSt

Naziv proizvoda	Magnezijum stearate
Hemijska formula	$Mg(C_{18}H_{35}O_2)_2$
Relativna molekulska masa, g	591,25
Kvalitet	Extra pure
Sadržaj Mg, %	4,46
Sadržaj hlorida, %	< 0,1
Sadržaj Pb, %	< 0,0001
Sadržaj Cd, %	< 0,0001
Gubitak žarenja, %	2,2
Osobine	Beo prah, slabog mirisa na stearin, nerastvoran u H_2O, koncentrovanom etanolu i etru

Polazni uzorci MAP i AS su krupnoće ≈ 3000 μm, a kvarcnog peska i kalcijum karbonata oko 1000 μm.

U istraživanjima prikazanim u radu korišćen je i komercijalni prah za gašenje požara uvezen iz Italije (SGPI) koji upotrebljava firma “Vatrosprem”, Srbija.

2. 2 Metode

Hemijska analiza je urađena na atomskom adsorpcionom spektrofotometru (AAS) Analyst 300 (proizvođač “Perkin Elmer”- SAD) i spektrofotometru Spekol 1300 (proizvođač “JENA”, Nemačka).

Postupak mlevenja. MAP je mleven u trajanju od 5, 12, 19, 26, 33, 40, 47, 60, 75, 90 i 100 min u laboratorijskom keramičkom mlinu sa kuglama. Masa uzorka je bila 3 kg. Kontrolno prosejavanje je bilo na situ otvora 100 μm. Takođe, za mlevenje MAP korišćen je i vibro mlin sa prstenastim radnim elementima, model „MN 954/3“, proizvođača „KHD Humboldt Wedag“-Nemačka. Mlevenje mase praha 200 g u vibro mlinu je bilo u trajanju od 10 min, a posle toga prah je mleven u laboratorijskom keramičkom mlinu sa kuglama u trajanju od 5, 12, 19, 26, 33, 40, 50 i 60 min. Kontrolno prosejavanje je rađeno na situ od 100 μm. MAP i AS su prosejavani na situ veličine otvora 200 μm, a kvarcni pesak i krečnjak na situ 100 μm što znači da se u sastavu SGP nalaze frakcije čestica veličine -200 i -100 μm. MgSt je korišćen u obliku kako je isporučen iz fabrike. Sito veličine 100 μm korišćeno je za kontrolno prosejavanje MAP u opitima mlevenja.

Određivanje vlage MAP

Sadržaj vlage (W) je određen prema formuli:

$$W = \frac{m_w - m_s}{m_w} 100 \quad (1)$$

gde je m_W– masa vlažnog uzorka, a m_s - masa suvog uzorka.

Postupak oblaganja SGP

Kao sredstvo za oblaganje SGP korišćen je magnezijum stearat koji je u mešavini zastupljen sa masenim udelom od 2 %. Oblaganje je vršeno u laboratorijskom keramičkom mlinu sa kuglama u trajanju od 15 min. Pre početka oblaganja, tačno odmerene mase pojedinačnih komponenti, su odvojeno sušene 30 min na 105 °C.

Provera obloženosti SGP

Provera je vršena je prema standardnoj metodi [21]. Petrijeva šolja prečnika 70 mm se napuni prahom SGP i izravna tako što se višak praha ukloni lenjirom. Zatim se na tri mesta iskapa oko 0,3 cm^3 destilovane vode. Petrijeva šolja se stavi u eksikator iznad zasićenog rastvora NaCl na 20 °C (75 % relativna vlažnost). Posle 60 min Petrijeva šolja se izvadi iz eksikatora, pa se postepeno naginje. Ako se kapi vode otkotrljaju znači da je SGP hidrofoban i da ne upija vlagu.

Određivanje granulometrijskog sastava SGP

Odmereno je približno 20 g SGP i prosejavano na uređaju za trešenje u trajanju od 10 min. Sita su bila otvora 200, 100, 63 i 36 µm. Merena je količina praha koja ostaje na svakom pojedinačnom situ (odsev) i računskim putem je dobijen kumulativni (zbirni) procenat mase odseva i proseva.

3. REZULTATI I DISKUSIJA

3. 1. Hemijska analiza

Hemijska analiza svih komponenti koje ulaze u sastav SGP: monoamonijum fosfata (MAP), amonijum fosfata (AS), kvarcnog peska (KP) i kalcijum karbonata (KK) prikazana je u tabeli 2.

Tabela 2. Hemijska analiza polaznih komponenti
Table 1. Chemical analysis of starting components

Komponenta	Sadržaj, %			
	MAP	**AS**	**KP**	**KK**
Al_2O_3	-	-	1,22	0,048
Fe_2O_3	-	-	0,48	0,05
MgO	-		0,013	1,3
K_2O	-	-	0,91	0,042
Na_2O	-	-	0,039	0,02
TiO_2	-	-	0,034	<0,02
Gubitak žarenja	-	-	0,25	43,14
CaO	-	-	0,293	53,86
SiO_2	-	-	95,38	
S	-	24,08	-	
K	0,15	-	-	
Na	0,054	-	-	
SO_4^{2-}	9,86	-	-	
Cl^-	0,17	-	-	
P rastvoren u vodi	21,56	-	-	
P ukupan	27,94	-	-	
P rastvoren u NAC*	23,1	-	-	

*NAC-neutralni amonijum-citrat

3. 2. Ukupna vlaga MAP

Na uzorku MAP, kao aktivne komponente u SGP, određen je ukupan sadržaj vlage od 2,7 %. Ukupnu vlagu čini zbir vlage od 1,5 % određene na granulama MAP od ≈3000 µm i vlage od 1,2 % uzorka MAP krupnoće 300 µm dobijenog usitnjavanjem granula u vibro mlinu u trajanju od 15 min.

3. 3. Mlevenje MAP i određivanje granulometrijskog sastava u funkciji od vremena mlevenja

Polazni uzorak MAP koji je u obliku granula veličine ≈3000 µm je mleven u laboratorijskom keramičkom mlinu sa kuglama u trajanju od 5 do 100 min. Kontrolno prosejavanje je bilo na situ otvora 100 µm sa ciljem praćenja udela frakcije čestica veličine -100 µm u zavisnosti od vremena trajanja mlevenja. Praćena je ova frakcija, jer su iskustva u

praksi pokazala da je za efikasno gašenje požara neophodno da udeo aktivne komponente frakcije čestica veličine -100 µm bude veći od 60 %. Dobijeni rezultati su prikazani na slici 1.

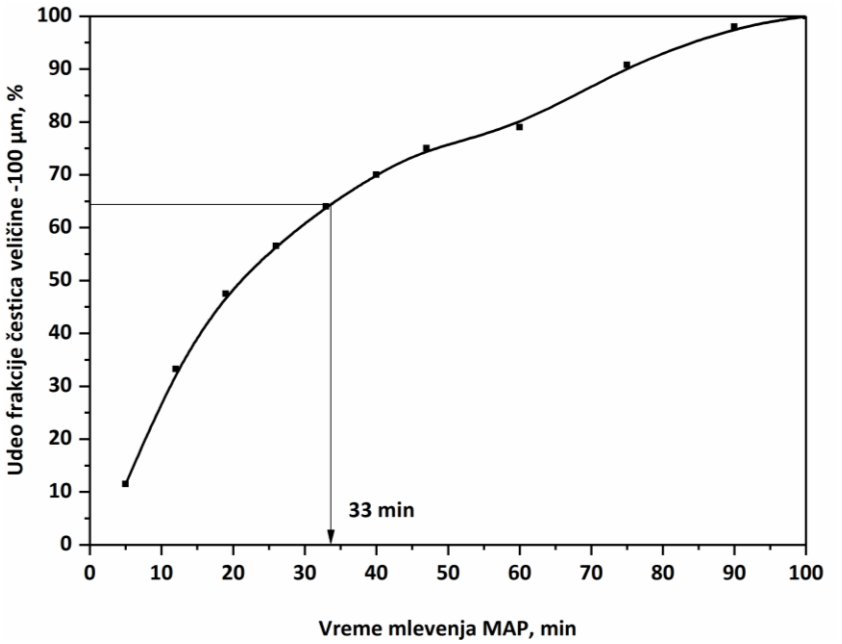

Slika 1. Udeo frakcije čestica veličine -100 µm MAP u funkciji od vremena mlevenja (polazna veličina granula ≈3000 µm)
Figure 1. Content of fraction of particle size -100 µm of MAP as a function grinding time (starting granule size ≈3000 µm)

Sa grafika (slika 1) je očitano da je za dobijanje 64 % frakcije čestica veličine -100 µm potrebno vreme mlevenja MAP u trajanju od 33 min. To je minimalno vreme mlevenja koje je potrebno da se 64 % polazne mase granula usitne do frakcije čestica veličine -100 µm u keramičkom mlinu. U daljem eksperimentu je ispitivana mogućnost dobijanja navedene frakcije za kraće vreme i to tako što je mlevenje prvo vršeno u vibro mlinu, a zatim u mlinu sa kuglama. Granule MAP od ≈3000 µm su usutnjene u vibro mlinu u trajanju od 10 min i određen je granulometrijski sastav prosejavanjem na sitima veličine otvora 100; 200 i 300 µm. Rezultati granulometrijskog sastava su prikazani u tabeli 3 i grafički na slici 2. Direktna kriva granulometrijskog sastava je dobijena na osnovu podataka druge kolone (*g* / %) u tabeli 3, a to je maseni procentualni udeo određene frakcije sa tačno definisanim graničnim veličinama čestica. Koordinate tačaka su frakcija i njen maseni procentualni udeo. Gornja granična krupnoća (*ggk*) se očitava sa grafika i predstavlja najkrupnija zrna u uzorku, dok je d_{sr} vrednost koja ukazuje koliki prečnik ima 50 % od ukupne mase uzorka.

Tabela 3. Granulometrijski sastav MAP posle usitnjavanja u vibro mlinu
Table 3. Particle size distribution of MAP after grinding in a vibro mill

Frakcija sa graničnim veličinama čestica, µm	*g* / %	*g*↓ / %*	*g*↑ / %**
+300	4,00	4,00	100,00
-300+200	9,00	13,00	96,00
-200+100	50,00	63,00	87,00
-100	37,00	100,00	37,00
Ukupno	100,00		

**g*↓- zbirni maseni procenat odseva; ***g*↑-zbirni maseni procenat proseva

Sa grafika (slika 2) se vidi da je usitnjavanjem u vibro mlinu dobijen uzorak MAP koji ima gornju graničnu krupnoću (*ggk*) od 300 µm i srednji prečnik zrna (d_{sr}) 120 µm. Prema podacima prikazanim u tabeli 3 *ggk* je nešto manji od 300 µm, ali je razlika minimalna, pa je usvojena vrednost od 300 µm. Nakon mlevenja u vibro mlinu, prah je mleven u laboratorijskom keramičkom mlinu sa kuglama u trajanju od 5 do 60 min dok je kontrolno prosejavanje izvedeno na situ od 100 µm. Dobijeni rezultati su prikazani na slici 3.

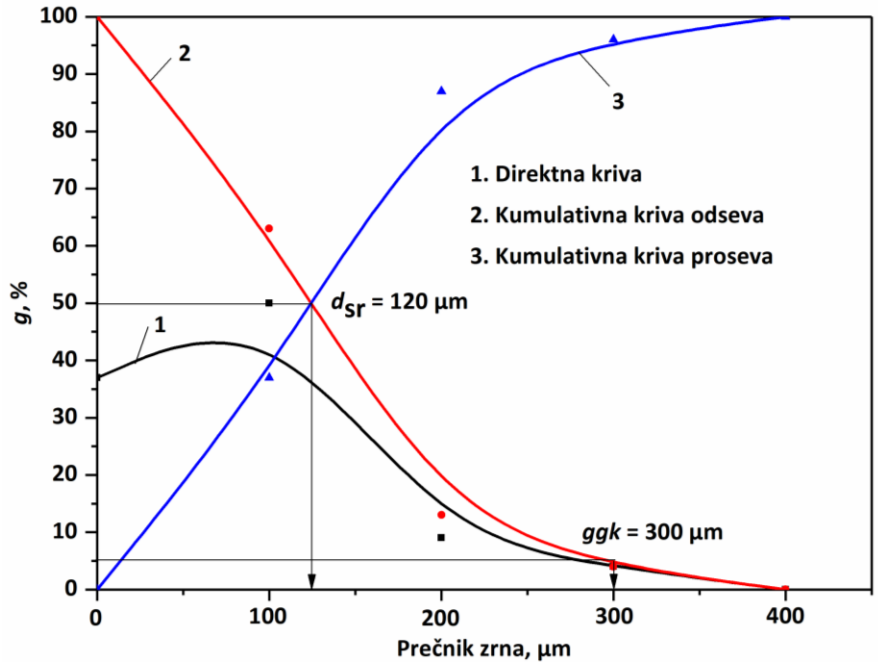

Slika 2. Granulometrijski sastav MAP posle usitnjavanja u vibro mlinu u trajanju od 10 min
Figure 2. Particle size distribution of MAP after grinding in a vibro mill for 10 min

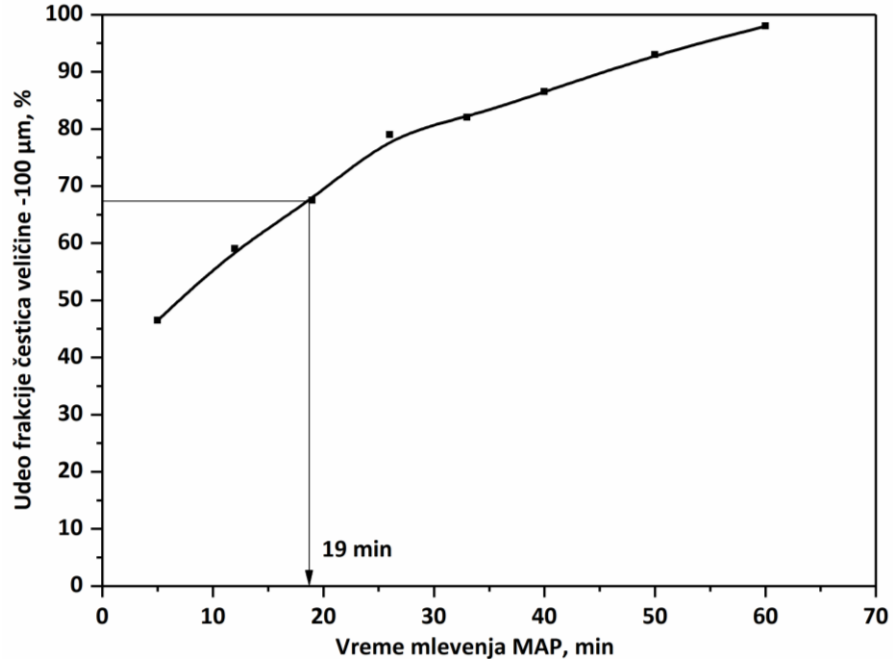

Slika 3. Udeo frakcije čestica veličine -100 µm MAP u zavisnosti od vremena mlevenja u laboratorijskom keramičkom mlinu sa kuglama posle mlevenja u vibro mlinu (ulaz ggk = 300 µm)
Figure 3. Content of the MAP fraction of particle size -100 µm as a function of the grinding time in the laboratory ceramic ball mill after milling in the vibro mill (input upper limit grain size 300 µm)

Sa grafika (slika 3) je očitano vreme mlevenja MAP od 19 min dovoljno da se dobije 67,5 % frakcije čestica veličine -100 µm koja ulazi u sastav SGP.

Cilj ovog eksperimenta sa vibro mlinom je bio da se utvrdi za koliko se dvostepenim mlevenjem u dva različita mlina skraćuje vreme mlevenja MAP za dobijanje neophodnog udela frakcije čestica veličine -100 µm (više od 60 %). Kada se MAP usitnjava samo u laboratorijskom keramičkom mlinu sa kuglama za 33 min mlevenja dobija se 64 % frakcije čestica veličine -100 µm. Međutim, kada se MAP prvo usitni u vibro mlinu u toku 10 min, a zatim u mlinu sa kuglama, vreme

mlevenja u keramičkom mlinu se skraćuje na 19 min pri čemu se dobija 67,5 % frakcije čestica veličine -100 μm (ukupno vreme mlevenja je 29 min). Analizirajući vreme mlevenja MAP koje je potrebno za dobijanje najmanjeg udela frakcije čestica veličine -100 μm koji obezbeđuje efikasnost SGP u čiji sastavu ulazi, zapaža se sledeće: kod jednostepenog mlevenja MAP, 64 % frakcije čestica veličine -100 μm se dobija za 33 min, a kod dvostepenog mlevenja za 26 min. U dvostepenom ciklusu, vreme mlevenja MAP se skraćuje za 7 min u odnosu na jednostepeni ciklus, pa se može govoriti i o određenoj uštedi energije neophodne za proces mlevenja.

Uvođenje drugog stepena mlevenja MAP i njegovu rentabilnost u proizvodnom pogonu treba analizirati u okviru ušteda koje bi se ostvarile eliminisanjem uvoza prahova stranih proizvođača što je predmet finansijske analize uvoznika sredstava za gašenje požara. Naravno, treba ukazati da se u Srbiji, od domaćih mineralnih sirovina, može napraviti efikasan prah za gašenje požara i pružiti neophodna pomoć u koncipiranju tehnološke šeme za njegovu proizvodnju.

3. 4. Oblaganje i stabilizacije SGP magnezijum stearatom

Da bi se postigla stabilnost SGP i eliminisala mogućnost upijanja vlage i aglomeracije prilikom stajanja u aparatu za gašenje požara ili skladištenom prostoru, sve komponente su obložene magnezijum stearatom (MgSt). Sadržaj MgSt u mešavini je bio 2 %. Ukupna masa SGP za postupak oblaganja je 3 kg, a pojedinačna zastupljenost komponenti u SGP koje su istovremeno oblagane 15 min u laboratorijskom keramičkom mlinu sa kuglama prikazana je u tabeli 4.

Tabela 4. Zastupljenost komponenti u SGP
Table 4. Component contents in powder fire extinguisher (PFE)

Komponenta	MAP	AS	KK	KP	MgSt	Ukupno
Sadržaj, %	55,00	20,00	18,00	5,00	2,00	100,00
Masa, kg	1,65	0,60	0,54	0,15	0,06	3,00

Nakon postupka oblaganja provera postignute hidrofobnosti je izvršena prema opisanoj metodi i rezultat je bila potpuna obloženost. Kapi destilovane vode koje su bile ukapane na površinu SGP u Petrijevoj šolji su se naginjanjem šolje otkotrljale.

3. 6. Karakterizacija dobijenog SGP

Uzorak SGP sa masenim odnosom komponenti datim u tabeli 4 koji je proizveden u ovom radu u laboratorijskim uslovima je analiziran u pogledu granulometrijskog i hemijskog sastava. Granulometrijska analiza je rađena sa ciljem da se vidi koliki je sadržaj najsitnije frakcije u SGP, a to je -36 μm. Testiranjem različitih SGP u realnim uslovima (na poligonu gde se izaziva požar u kontrolisanim uslovima u cilju testiranja određenog sredstva za gašenje) je zaključeno da veliki udeo ove frakcije, odnosno preusitnjeni uzorak SGP, ne gasi požar dovoljno efikasno. Naime, suviše male čestice ne mogu da padnu gravitacijski na žarište plamena, već se stvara oblak praha koji lebdi. Zbog toga je jako važno da SGP ima zadovoljavajuću krupnoću. Dobijeni rezultati granulometrijskog sastava SGP u ovom radu su upoređeni sa granulometrijskim sastavom komercijalnog SGP (SGPI). Uporedni rezultati granulometrijskog sastava prikazani su u tabelama 5 i 6 ($g\downarrow$ - zbirni maseni procenat odseva, $g\uparrow$ - zbirni maseni procenat proseva).

Tabela 5. Uporedni granulometrijski sastav SGP dobijenog u ovom radu i komercijalnog SGPI - „suvo" prosejavanje
Table 5. Comparative particle size distribution of the powder fire extinguisher produced in the present work (SGP) and a commercial product (SGPI) - „dry" sieving

Frakcija sa graničnim veličinama čestica, μm	SGP	SGPI	SGP	SGPI	SGP	SGPI	SGP	SGPI
	m / g	*m* / g	*g* / %	*g* / %	$g\downarrow$ / %	$g\downarrow$ / %	$g\uparrow$ / %	$g\uparrow$ / %
+200	0,35	0,49	1,91	2,54	1,91	2,54	100,00	100,00
-200+100	2,75	5,43	15,03	28,06	16,94	30,60	98,09	97,46
-100+63	5,20	4,83	28,41	24,96	45,35	55,56	83,06	69,40
-63+36	8,50	6,75	46,45	34,88	91,80	90,44	54,65	44,44
-36+0	1,50	1,85	8,20	9,56	100,00	100,00	8,20	9,56
Ukupna masa	18,30	19,35	100,00	100,00	-	-	-	-

$\boldsymbol{g}\downarrow$- zbirni maseni procenat odseva; $\boldsymbol{g}\uparrow$-zbirni maseni procenat proseva

Tabela 6. Uporedni granulometrijski sastav SGP dobijenog u ovom radu i komercijalnog SGPI - „mokro" prosejavanje
Table 6. Comparative particle size distribution of the powder fire extinguisher produced in the present work (SGP) and a commercial product (SGPI) - „wet" sieving

Frakcija sa graničnim veličinama čestica, µm	SGP	SGPI	SGP	SGPI	SGP	SGPI	SGP	SGPI
	m / g	*m* / g	*g* / %	*g* / %	*g*↓ / %	*g*↓ / %	*g*↑ / %	*g*↑ / %
+200	-	-	-	-	-	-	-	-
-200+100	0,50	0,27	2,50	1,35	2,50	1,35	100,00	100,00
-100+63	1,10	0,26	5,50	1,30	8,00	2,65	97,50	98,65
-63+36	1,40	0,19	7,00	0,95	15,00	3,60	92,00	97,35
-36+0	17,00	19,28	85,00	96,40	100,00	100,00	85,00	96,40
Ukupna masa	20,00	20,00	100,00	100,00	-	-	-	-

****g*↓- zbirni maseni procenat odseva; *****g*↑-zbirni maseni procenat proseva

Granulometrijski sastav SGP kod postupka „suvog" prosejavanja je pokazao da je udeo frakcije veličina čestica -36 µm od ≈8 % relativno nizak u odnosu na udeo frakcija čestica u graničnim veličinama -100+63 µm i -63+36 µm koji iznosi ≈28 % odnosno ≈46 %. Takođe, ≈92 % uzorka ima veličinu čestica iznad 36 µm što je približno vrednosti kod SGPI koja iznosi ≈90 %, a koji se pokazao kao dobar komercijalni proizvod sa maksimalnim učinkom pri gašenju požara. Poređenjem granulometrijskog sastava SGP i SGPI dobijenog postupkom „mokrog" prosejavanja uočava se određeno odstupanje (oko 10 %) u udelu frakcije čestica veličine -36 µm. Hemijska analiza SGP je prikazana u tabeli 7.

Tabela 7. Hemijska analiza SGP
Table 7. Chemical analysis of the powder fire extinguisher produced in the present work (SGP)

Komponenta	Sadržaj, %	Komponenta	Sadržaj, %	Komponenta	Sadržaj, %
P_2O_5	26,43	Ca	8,19	Cd	0,0008
S	6,41	Si	2,87	P	11,54
Mg	0,40	Cl^-	0,22	$NH_4H_2PO_4$	42,85
Na	0,113	Pb	<0,002	SiO_2	6,14
K	0,367				

Rezultati analize hemijskog sastava SGP su pokazali da je sadržaj aktivne komponente MAP 42,85 % što je više od minimalne vrednosti od 40 % koja je neophodna za efikasno gašenje požara. Imajući u vidu da je MAP najskuplja komponenta u sastavu SGP, može se konstatovati da je sa minimalnim sadržajem MAP postignuta maksimalna efikasnost formiranog SGP u gašenju požara izazvanog na poligonu predviđenom za testiranje. Upotrebom SGP koje je proizvedeno u ovom radu u laboratorijskim uslovima dobijeni su odlični rezultati prilikom gašenja požara izazvanim gorenjem čvrstih materijala i gorenjem zapaljivih tečnosti, jer je došlo do trenutne eliminacije plamena. Time je pokazano da je moguće napraviti sredstvo za gašenje požara u obliku praha od domaćih mineralnih sirovina koje zadovoljava sve kriterijume koji su neophodni za trenutno eliminisanje plamena.

Trenutna eliminacija plamena prilikom gašenja požara upotrebom formiranog SGP u kome je MAP aktivna komponenta se objašnjava sledećom hemijskom reakcijom:

$$NH_4H_2PO_4 + CaCO_3 = NH_4CaPO_4 + CO_2 + H_2O \quad (2)$$

Na visokim temperaturama, pri kojim se javljaju požari i pojava plamena prilikom gorenja, dolazi do hemijske reakcije MAP i kalcijum karbonata pri čemu se formira monoamonijum kalcijum fosfat, ugljen dioksid i vodena para. Nastali CO_2 gas, koji je u obliku mehurića, istopljenu mešavinu praha pretvara u penastu masu koja prekriva površine. Na taj način se prekida proces gorenja antikatalitičkim efektom, jer se sprečava oksidacija materije koja gori. Nastala penasta masa koja je zasićena CO_2 gasom ima četiri i više puta veću zapreminu u odnosu na zapreminu iste mase čistog MAP kao aktivne komponente u SGP [23, 24].

4. ZAKLJUČAK

Na osnovu rezultata prikazanih u radu može se izvesti sledeći zaključci:

1. Mlevenjem MAP kao aktivne komponente u SGP moguće je dobiti granulometrijski sastav koji je neophodan za efikasno gašenje požara i trenutnu eliminaciju plamena izazvanog gorenjem čvrstih i tečnih zapaljivih materija.

Efikasnost gašenja je utvrđena testiranjem na poligonu u realnim uslovima. Naime, na tačno određenom mestu za testiranje, u kontrolisanim uslovima, izazvan je požar paljenjem čvrstih materijala i zapaljivih tečnosti. U oba slučaja je došlo do trenutne eliminacije plamena. Na taj način je potvrđena efikasnost formiranog SGP i mogućnost njegove upotrebe u praksi.

2. Mlevenjem MAP krupnoće ≈3000 μm u laboratorijskom keramičkom mlinu sa kuglama u trajanju od 33 min dobijeno je 64 % frakcije čestica veličine -100 μm koja predstavlja optimalnu veličinu čestica praha.
3. Pokazano je da je vreme mlevenja MAP od 33 min moguće skratiti ako se uzorak prvo samelje u vibro mlinu, a zatim u mlinu sa kuglama. Mlevenjem u vibro mlinu, u trajanju od 10 min, granule MAP od ≈3000 μm su usitnjene u čestice praha veličine *ggk* = 300 μm i d_{sr} = 120 μm što je bio ulaz u mlin sa kuglama. Kontrolnim prosejavanjem na situ otvora 100 μm, utvrđeno je da se optimalna krupnoća MAP od 67,5 % frakcije čestica veličine -100 μm u mlinu sa kuglama dobija za kraće vreme, odnosno 19 min, pri čemu je ukupno vreme mlevenja u ovom procesu 29 min.
4. Vreme mlevenja MAP koje je potrebno za dobijanje najmanjeg udela frakcije čestica veličine -100 μm koji obezbeđuje efikasnost SGP u čijem se sastavu nalazi, zapaža se sledeće: kod jednostepenog mlevenja MAP 64 % frakcije čestica veličine -100 μm se dobija za 33 min, a kod dvostepenog mlevenja za 26 min.
5. Procentualni odnos komponenti u SGP dobijenom tokom istraživanja je: MAP : AS : KK : KP : MgSt = 55 : 20 : 18 : 5:2.
6. Oblaganjem SGP, sa dodatih 2 % magnezijum stearata, u trajanju od 15 min u laboratorijskom keramičkom mlinu sa kuglama, postignuta je potpuna hidrofobnost i stabilnost dobijenog sredstva.

Zahvalnica: Autori se zahvaljuju Ministarstvu prosvete, nauke i tehnološkog razvoja Republike Srbije na finansijskoj podršci istraživanju čiji su rezultati prikazani u radu (ugovor 451-03-9/2021-14/200023 i 451-03-9/2021-14/200026).

LITERATURA

[1] Zhao J, Yin Z, Shahid UM, Xing H, Cheng X, Fu Y, Lu S. Superhydrophobic and oleophobic ultra-fine dry chemical agent with higher chemical activity and longer fire-protection. *J Hazard Mater*. 2019; 380: 120625.

[2] Huang Ch, Chen X, Yuan B, Zhang H, Shang, Sh, Zhao Q, Dai H, He S, Zhang Y, Niu Y. Insight into suppression performance and mechanisms of ultrafine powders on wood dust deflagration under equivalent concentration. *J Hazard Mater*. 2020; 394: 122584.

[3] Xiaomin N, Chow WK. Fundamental suppression chemistry of clean fire suppressing agents: A Review. *J Appl Fire Sci*. 2011; 21(3): 223-251.

[4] Ewing CT, Faith FR, Huges JT, Carhart HW. Flame extinguishment properties of dry chemicals: Extinction concentrations for small diffusion pan fires. *Fire Technol*. 1989; 25: 134-149.

[5] Zhao G, Xu G, Jin Sh, Zhang Q, Liu Zh. Fire-Extinguishing efficiency of superfine powders under different Injection pressures. *Int J Chem Eng*. 2019; Article 2474370.

[6] Su Ch, Chen Ch, Liaw HJ, SC Wang. The assessment of fire suppression capability for the ammonium dihydrogen phosphate dry powder of commercial fire extinguishers. *Procedia Eng*. 2014; 84: 485-490.

[7] Huang X, Liu L, Zhou X. Experimental study on fires extinguishing performance of ammonia phosphate sub -nanometer powders. *Fire Saf Sci*. 2011; 4: 200 -205.

[8] Trees D, Seshadri K. Experimental studies of flame extinction by sodium bicarbonate ($NaHCO_3$) powders. *Combust Sci Technol*. 1997; 122(1/6): 215-230.

[9] Dondur V. *Hemijska kinetika*. Beograd, Fakultet za fizičku hemiju; 1992.

[10] Fudang S, Zhiming D, Xiaomin C, Linshuang Zh, Ye Y, Linming L. Experimental study on fires extinguishing properties of melamine phosphate powders. *Procedia Eng*. 2014; 84: 535-542.

[11] Mihajlović S, Sekulić Ž, Radulović D, Jovanović V. Investigation the calcite hydrophobisation of different grain sizes. *MME-Bor*. 2016; 2: 31-40.

[12] Mihajlović S, Sekulić Ž, Petrov M, Krstović P, Matejević B. Mikronizacija i oblaganje krečnjaka. *Izgradnja*. 2003; 319-321.

[13] Mihajlović SR, Vučinić DD, Sekulić ŽT, Milićević SZ, Kolonja BM. Mechanism of stearic acid adsorption to calcite. *Powder Technol*. 2013; 245: 208-216.

[14] Mihajlović S, Sekulić Ž, Radulović D, Stevanović D, Kašić V. Hidrofobizacija krečnjaka iz ležišta „Cancar" Aranđelovac upotrebom stearinske kiseline. *Tehnika*. 2015; 66(6): 943-946.

[15] Mihajlović S, Sekulić Ž, Daković A, Vučinić D, Jovanović V, Stojanović J. Surface properties of natural calcite filler treated with stearic acid. *Ceram-Silik*. 2009; 53(4): 268-275.

[16] Mihajlović SR, Daković AS, Sekulić ŽT, Ileš DA, Kragović MM. Površinska adsorpcija stearinske kiseline na prirodnom kalcitu. *Hem Ind*. 2009; 63(2): 101-106.

[17] Đorđević N, Jovanić P. Influence of mechanical activation on electrical properties of cordierite ceramics. *Sci Sinter*. 2008; 40: 47-53.

[18] Obradović N, Đorđević N, Filipović S, Nikolić N, Kosanović D, Mitrić M, Marković S, Pavlović V. Influence of mechanochemical activation on the sintering of cordierite ceramics in the presence of Bi_2O_3 as a functional additive. *Powder Technol*. 2012; 218: 157-161.

[19] Obradović N, Đorđević N, Filipović S, Marković S, Kosanović D, Mitrić M, Pavlović V. Reaction kinetics of mechanically activated cordierite-based ceramics studied via DTA. *J Therm Anal Calorim*. 2016; 124(2): 667–673.

[20] Magdalinović N. *Meljivost mineralnih sirovina*. Beograd, Nauka; 1997.

[21] SRPS ISO 7202:2019: Zaštita od požara-Sredstva za gašenje požara-Prah. 2019

[22] Izveštaj o analizi, Sistem menadžmenta kvalitetom preduzeća „Centrohem“ sertifikovan u skladu sa zahtevima ISO 9001:2008. Br. sertifikata: 75.100.9854-TUV Rheinland InterCert

[23] Lobos ZJ. Dry chemical fire extinguisher composition. US Patent 3,214,372A, 1965

[24] Xu Z, Guo X, Yan L, Kang W. Fire-extinguishing performance and mechanism of aqueous film-forming foam in diesel pool fire. *Case Stud Therm Eng*. 2020; 17: Article 100578.

ABSTRACT

Optimization of the active component grinding process and hydrophobization of the obtained powder fire extinguisher

Slavica R. Mihajlović[1], Nataša G. Đorđević[1], Marina N. Jovanović[2], Milica M. Vlahović[3], Ljubinko D. Savić[4], Aleksandra S. Patarić[1] and Marina S. Blagojev[5]

[1]*Institute for Technology of Nuclear and Other Mineral Raw Materials, Franchet d`Esperey 86, Belgrade, Serbia*
[2]*University of Zenica, Faculty of Metallurgy and Technology, Travnička cesta 1, Zenica, Bosnia and Herzegovina*
[3]*University of Belgrade, Institute of Chemistry, Technology and Metallurgy- National Institute of the Republic of Serbia, Njegoševa 12, Belgrade, Serbia*
[4]*University of Pristina situated in Kosovska Mitrovica, Faculty of Technical Sciences, Kneza Miloša 7, Kosovska Mitrovica, Serbia*
[5]*University of Belgrade, Faculty of Mining and Geology, Đušina 7, Serbia*

(Technical paper)

This work presents a grinding process of monoammonium phosphate (MAP) as an active component in a powder fire extinguisher (PFE). The aim was to determine the grinding time for reaching the optimal particle size of MAP necessary for permanent fire extinguishing. MAP grinding was performed by using a laboratory ceramic ball mill and a vibrating cup mill. The grinding process was controlled by sieving using a 100 μm sieve at precisely defined time intervals. The efficiency of a PFE depends on the share of the -100 μm fraction of the active component, which has to exceed 60 %. The optimal grain size with 64 % of fraction of particle size -100 μm was obtained after 33 min of grinding of ≈3000 μm mm grain size MAP by using a ball mill (single-stage grinding). In two-stage process, by grinding the same initial MAP sample (≈3000 μm) in the vibro mill for 10 min, powder with the upper limit grain size of 300 μm and the mean grain diameter of 120 μm was obtained. This sample with a reduced size was further ground in the ceramic ball mill yielding 67.5 % of the fraction of particle size -100 μm after 19 min. The total time of the two-stage grinding process was 29 min. By analyzing the grinding time of MAP required to get the lowest required share of the fraction of particle size -100 μm that provides the effectiveness of formed PFE it can be concluded that 64 % of this fraction was obtained after 33 min of single-stage grinding, while only after 26 min in the two-stage process. Thus, the grinding time was reduced by 7 min indicating certain energy savings. Stability and hydrophobicity of the obtained PFE were achieved by coating with magnesium stearate (MgSt) at the content of 2 % in a ball mill for 15 min. The coating was confirmed by the standardized procedure for verification of PFE hydrophobic properties in contact with water drops. To obtained PFE had component mass ratios of MAP:AS:CC:QS:MgSt=55:20:18:5:2 (AS-ammonium sulfate; CC-calcium carbonate, QS-quartz sand) and was further characterized by chemical and granulometric analyses. The fire extinguishing efficiency of the PFE was tested in controlled conditions, whereby fires were initiated by burning solid materials and flammable liquids. In both cases, immediate elimination of flames was achieved, thus proving the efficiency of the PFE obtained in this work for practical applications..

Keywords: monoammonium phosphate; granulometric composition; magnesium stearate; coating

Influence of the Ringer's solution on wear of vacuum mixed poly(methyl methacrylate) bone cement in reciprocating sliding contact with AISI 316L stainless steel

Fatima Zivic[1], Nenad Grujovic[1], Slobodan Mitrovic[1], Jovan Tanaskovic[2] and Petar Todorovic[1]

[1]*University of Kragujevac, Faculty of Engineering, Kragujevac, Serbia*
[2]*University of Belgrade, Faculty of Mechanical Engineering, Belgrade, Serbia*

Abstract

This paper presents microstructural properties and damage behaviour of a vacuum mixed poly(methyl metacrylate) (PMMA) bone cement, during the sliding contact with AISI 316L stainless steel, under micro-loads. Influence of the Ringer's solution on the wear was analysed in comparison to dry contact. The variation of load did not produce any significant change of the wear factor while the increase in the sliding speed induced significant increases in the wear factor, more pronounced in the case of dry sliding. The obtained wear factors were in average higher for the sliding in Ringer's solution than those obtained under dry conditions. Significant fragmentation of the worn tracks, of irregular shapes with broken edges, was observed, slightly more pronounced for the dry contact. Many cavities and voids were formed on the wear track surface, but they did not extend into the bulk material. Higher loads produced more uniform and less fragmented wear tracks. Abrasive, adhesive wear and plastic deformation grooves were observed, as well as fatigue and erosive wear. Fatigue cracks developed in the direction normal to sliding. Network of fine craze cracks was exhibited on the surface of wear tracks, especially pronounced in the case of dry sliding. These results are important since they contribute to understanding the sites of crack initiation, and development mechanisms on the surface of PMMA bone cements, also including synergistic effects of physiological environments pertaining to the non-steady crack and craze behaviour and crack pattern development in PMMA.

Keywords: craze cracks; erosive grooves; fracture; densification; friction heating; fatigue crack.

Available on-line at the Journal web address: http://www.ache.org.rs/HI/

ORIGINAL SCIENTIFIC PAPER

UDC: 678.744.32+ 691.714.018.8: 620.178.16

Hem. Ind. **75 (2)** 77-92 (2021)

1. INTRODUCTION

Polymers for biomedical applications are designed to be either biostable or bioabsorbable. Biologically stable polymers provide a permanent support during the life-time of the patient. Poly(methyl methacrylate) (PMMA) $[(C_5O_2H_8)_n]$ based bone cements belong to a group of synthetic nondegradable, biocompatible polymeric hard biomaterials. Acrylic bone cements have versatile applications such as: cemented hip implants [1], spinal treatments [2], custom made bone implants [3], dental applications like orthodontic brackets [4] and occlusal splints [5]. PMMA is an isotropic, elasto-visco-plastic solid and amorphous/glassy polymer material. Bone cement is basically a mixture of PMMA powder obtained by in situ polymerization of the monomer methyl methacrylate (MMA). Diameter of PMMA beads usually lies in the range of 1 - 125 μm. These beads are soluble in the MMA monomer. The resulting polymer is amorphous, optically transparent, has a high refraction index, is hard and brittle and suitable for a number of biomedical applications. The bone cement commercially used is a complex mixture of the monomer, PMMA powder, an initiator, a promoter of polymerization (or curing), a protector to prevent premature polymerization during mixing and a filler [2]. They are mixed prior to use under well controlled conditions mainly to prevent the formation of large pores and voids,

Corresponding author: Fatima Zivic, University of Kragujevac, Faculty of Engineering, Sestre Janjić 6, 34000 Kragujevac, Serbia
E-mail: zivic@kg.ac.rs
Paper received: 05 January 2021
Paper accepted: 24 March 2021
https://doi.org/10.2298/HEMIND210105011Z

since these would significantly affect mechanical properties of the final product. An effective technique to decrease the bone cement porosity is vacuum mixing during the material preparation [6] and different benefits of such a procedure have been reported [1,2].

According to many literature resources, appearance of cement defects is highly related to the implant loosening and osteolysis [7,8]. Osteolysis is a process of bone matrix destruction, or removal of the bone mineralized matrix and destruction of the organic bone phase (composed of ~90 % collagen). Predicting the long-term mechanical behaviour of an implant is difficult because reported studies indicate large variations in mechanical properties of the interface between the bone matrix and the implant [7]. In the case of cemented joint prosthesis, essential properties which determine *in vivo* stability are related to the bone cement fatigue and fracture behaviour and many investigations are focused on the cause of failure and micromechanics [9]. Porosity and various material defects (*e.g*. agglomerates of radiopaque phases) have a prominent role in the process of crack development. It has been shown experimentally that cements with lower porosities exhibit better compressive and flexural properties [9,10]. However, relations of the porosity reduction to void size, morphology, number or spatial distribution are rarely specified, usually considering only one of these variables. Addition of radiopaque agents and different additives to PMMA bone cements further increases the complexity of material responses [2].

The role of the bone cement is to transfer complex load forms between the prosthesis and the bone. The loosening process is still under consideration, even though specific aspects have been determined, such as fracture and fatigue behaviour of PMMA cements [10]. Nguyen et al. [10] considered a cyclic fatigue crack growth as the major governing factor of the bone cement failure, considering approximately five million steps per year for one person, meaning that the joint prosthesis should endure around 10^8 cyclic motions during its lifetime. Also, in dentistry, steel brackets are in close contact with PMMA [4]. On the other hand, articulating surfaces of loose joint replacements generate wear debris during the contact. The particulate wear debris produced during the micro-contact between the loose cement surfaces and bone can have different unwanted effects. Part of that particulate wear debris consists of the bone cement particles, originating from the low amplitude reciprocating motion under low loads of the loose implant. The extent and rate to which cement particles are generated determine the life of the prosthesis.

In other cases of custom implants made of PMMA bone cements, such as thoracic bones, the implants are connected to the remaining bones usually by using metal wires (*e.g*. sternal wires made of AISI 316L stainless steel) [3]. The connection is made by drilling holes through the cement implant on one side and the living bone on the other, where the sternal wires are tightly setup, but certain wire micro-motions over the cement must exist during normal daily activities. Therefore, in such cases, the tribological behaviour of the contact pair PMMA bone cement - AISI 316L stainless steel determines the life of sternal wires which hold the implant at place. The potential fracture mechanism of such sternal wires was reported to be based on the presence of crevice corrosion and severe transversal cracks detected in broken wires [11].

Friction and wear mechanisms are largely unexplored in the case of PMMA bone cements, even though there are several studies related to specific aspects, such as corrosion influence on the friction behaviour or the effects of oscillatory motion at small amplitude, during the contact between AISI 316L steel and PMMA [12]. There are several studies on the friction coefficient dependence on hardness, surface roughness and chemical reaction of AISI 316L steel for bone screws [13] as well as on wear of occlusal splints and PMMA in dentistry [5,14]. Still, formation of a third body between articulating surfaces as well as different superposing influences such as that of a corrosive environment have to be included in considerations. The presence of a third body usually enhances further particle production as reported in studies of the accompanying phenomena and ways to reduce wear [8]. Phenomena such as wear and fracture mechanisms of PMMA bone cements need to be fully understood to quantify the occurring wear debris.

Questions related to sites of crack initiation, development mechanisms and the final failure point in the case of PMMA bone cements still remain, even though there are many studies focused on some specific aspects, like the surface finish in dental applications [4], or mechanisms that govern crack branching [15]. Some reports indicate that the start of separation of the cement from the metal stem is initiated by large fractures within the cement layer [10]. In the case of the cemented metal prosthesis, there are several opinions on the initiation site of the cement crack: (1) on the surface

of the loose cement; (2) in voids associated with porosity in the cement layer or at the metal-cement interface; or (3) in the vicinity of a pore in the cement [9, 10]. Yet another issue is related to the presence of stress concentrations within the bone cement that is related to porosity, different additives, and radiopaque agents. Nonsteady crack and craze behaviour in PMMA, crack growth rate and crack pattern development, additionally including synergistic effects of physiological environments have not been well understood yet [16] and better understanding of these phenomena are needed. From the materials engineering point of view, it is of great interest to relate the material performance to the microstructure, helping to understand all parameters that influence the long-term sustaining of loads and to prolong the implant durability.

This paper presents the influence of Ringer's solution on contact phenomena between a vacuum treated PMMA bone cement and AISI 316L stainless steel during reciprocating sliding. A micro-scale load range was applied, under dry and wet contact. Wear mechanisms were investigated in response to different normal force and linear speed values applied.

2. EXPERIMENTAL

2. 1. Materials

Commercially available PMMA bone cement for orthopaedic surgery (Palacos R, Schering Corporation, USA) was used as a test material. The PMMA bone cement is composed of: polymer powder components (methylacrylate - copolymer (PMMA beads); benzoyl peroxyde; zirconium dioxyde and chlorophyll) and liquid components (methyl methacrylate monomer; N,N-dymethyl-p-toludine and chlorophyll). The mixing procedure was performed according to the instructions of the manufacturer and by applying vacuum. Details of the material preparation procedure are reported previously [6]. The vacuum treated cement used in this study had the final porosity of 5.1 % and surface roughness of Ra = 10.5 μm. Flat block samples (30 mm x 20 mm x 15 mm) were prepared for testing in accordance with ASTM F732-00, ASTM F86-01 and ASTM F2025-00 standards. Each PMMA sample was washed with neutral soap and water. They were stored in a desiccator, prior to testing.

2. 2. Reciprocating sliding contact

Sliding tests of the flat cement samples were realised by using the ball-on-flat configuration at CSM Nanotribometer (CSM, Switzerland). Details of the device configuration are presented previously [17]. Tribological tests realised linear reciprocating sliding of the ball (AISI 316L stainless steel ball; diameter of 1.5 mm) on the flat PMMA sample, with dry contact and in Ringer's solution (simulation of body fluid environment; purchased, Hemofarm AD Vrsac, Serbia), at room temperature (approximately 25 °C). We tested five values of the normal load, Fn (100, 250, 500, 750, and 1000 mN) and three values of the maximal linear speed, v (4, 8 and 12 mm/s). Calculated values of the maximum elastic contact stress (according to the applied normal loads) were: 71.9, 97.6, 123.0, 140.8, and 154.9 MPa, respectively. Duration of each test was 10000 cycles (total distance of 16 m), where the one cycle is represented by two full amplitudes of the sliding distance (*i.e.* half amplitude, 0.4 mm; full amplitude, 0.8 mm; 1 cycle, 1.6 mm). Sliding speeds were selected as the most probable motion range within a body. Laboratory investigations using Ringer's solution instead of fat-based solutions represent the worst-case scenario [18]. The composition of the Ringer's solution used is as follows: 8.6 g dm^{-3} NaCl, 0.30 g dm^{-3} KCl and 0.33 g dm^{-3} $CaCl_2$. Articulating surfaces were completely immersed in the solution during sliding. A ball-on-flat contact configuration at a nanotribometer is commonly used to represent the circular contact point between a rigid sphere (alumina ball) and a flat sample (PMMA) and is modeled by the Hertzian contact theory in contact mechanics. Therefore, the contact zone was immersed in the solution, by applying 5 cm^3 of Ringer's solution on the flat sample at the beginning of each test, since it was shown by our previous tests that this quantity of the solution can provide full immersion of the contact pair during the whole test. Tests were repeated three times.

Optical images of the wear track on a PMMA sample were recorded after each test by using optical microscope (Meiji Techno MT-8530). It is important to note that care is required during the scanning electron microscopy (SEM) examination of the surface, since an intense electron beam will cause PMMA sample to decompose. The samples for

the SEM analysis were prepared, by coating them with an ultra-thin layer of gold, by a sputter coater LEICA EM SCD005 (Leica Microsystems, Austria), immediately prior to the SEM imaging at Scanning Electron Microscope JSM-6610LV, with EDS, JEOL Ltd, Japan. EDS analysis was also performed. Nanotribometer continuously measures the penetration depth (PD) parameter, representing the depth to which the ball penetrates the flat sample surface during sliding, and determines the depth of the wear track on the flat sample. The wear behaviour was monitored in accordance to the previously used procedure [17], by measuring the wear scar width and length, after the test and considering the geometry of the contact pair, as well as by using the PD parameter for each test. The wear factor, k, was calculated for each conducted test, according to the following equation:

$$k = V / Fs \quad (1)$$

where F is the normal load, s is the sliding distance, and V is the wear volume. The wear volume of each flat sample was calculated by using the average surface area of the wear track from the image obtained by optical microscopy and the maximum penetration depth (PD) parameter, recorded by the nanotribometer for each test. It was assumed that the cross-sectional area is a flat segment of a sphere, with PD representing the height of that flat segment while further details are shown previously [17]. Since the wear of the stainless-steel ball can be described as "no measurable wear", only the wear of the flat sample was calculated, as per the ASTM G133 standard.

3. RESULTS AND DISCUSSION

SEM images of the wear tracks on PMMA samples, after dry sliding against AISI 316L stainless steel, are shown in Fig. 1. Different magnifications are shown with specific details. *Backscattered* Electron (BSE) image is also shown in Fig. 1 (denoted as BEC).

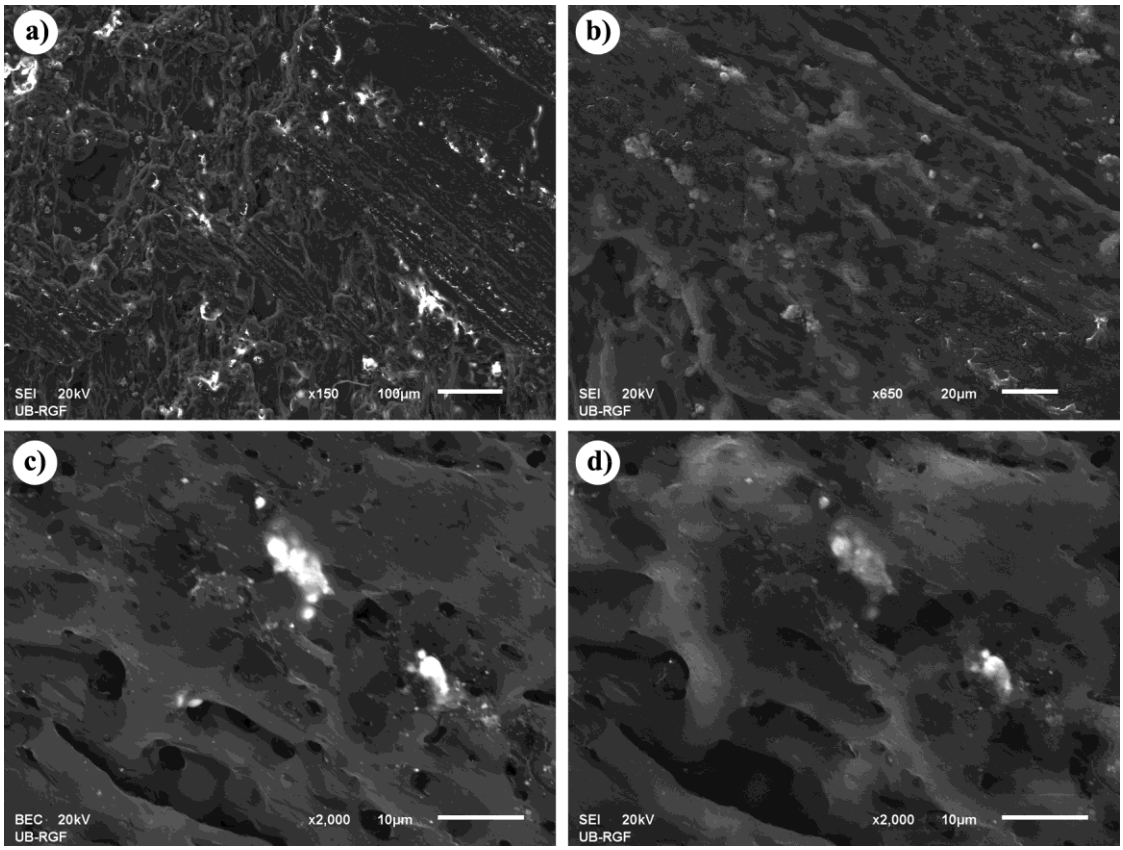

Figure 1. SEM images of the sample surface (dry sliding; 12 mm/s sliding speed; 750 mN normal load): a), b), d) SEM images showing details in the worn track at different magnifications (scale bars: 100, 20 and 10 µm, respectively); c) Backscattered Electron (BSE) image showing difference in chemical compositions in the worn track

The BSE image mode provides elemental contrast, *i.e*. chemical contrast, allowing distinction of the layers with different chemical compositions based on differences in color contrasts. Small white spots in Figure 1c designate ZrO_2 while the grey area represents the PMMA matrix. Secondary electron images obtained by SEM (denoted by *SEI* in Fig. 1) are high-resolution images of shapes of sample surfaces. ZrO_2 particles originate from additives in the PMMA powder component, whereas ZrO_2 is considered as one of the most common radiopaque agents in PMMA [27]. Since these particles are uniformly distributed throughout the PMMA matrix, the PMMA behaviour can be considered as that of a particle reinforced composite. Uniform distribution of these brittle, hard ZrO_2 particles throughout the PMMA matrix has a significant influence on the contact behaviour of the PMMA composite. It can be noticed (Fig. 1) that the wear track is of irregular shape. The evidence of abrasive wear can be clearly observed with many abrasive grooves in the wear track along the direction of sliding. The wear track is discontinued in those areas where pores or cavities occurred on the PMMA surface. ZrO_2 is distributed evenly throughout the whole PMMA surface except in the wear track.

The wear track at the highest investigated sliding speed (Fig. 1a-c) exhibited smooth surface, with shallow scratches and grooves, thus indicating governing adhesive wear. Plastic deformation of the PMMA material during sliding can be also observed in the form of plastic grooving. Areas of plastic deformation are more pronounced within the areas close to the edge of the wear track, along the sliding direction. The central part of the wear track is mainly subjected to abrasive and adhesive wear mechanisms. If the wear track is compared to the rest of the PMMA surface, it can be noticed that ZrO_2 particles are not evenly distributed throughout the wear track as on the rest of the PMMA surface (Fig. 1a). These particles appear smeared on the wear track and less present. A higher magnification (Fig. 1c, d) showed that clusters of ZrO_2 particles (approximately 5 μm in length) were distributed along the direction of sliding. The porous nature of PMMA can be clearly observed in Fig. 1c and d. It appears that PMMA wear tracks undergo plastic deformations – similar to 'work hardening' observed in the strengthening of metals. Increased densification (shrinkage) of PMMA can be observed in the area of the sliding contact (wear tracks) under all contact conditions, while more pronounced under higher sliding speeds and in Ringer's solution, as shown in Figs. 1a, 3a, 5 and 6, and in Supplementary material (Figs. S-1 to S-6).

EDS analyses of the wear tracks on PMMA samples were realised by using the spectrum analysis of selected positions on the sample surface, shown in Figure 2. It was proved that small white spots on the PMMA samples were ZrO_2 (Fig. 2b). Evidence of the abrasive wear, adhesive wear and plastic deformation grooves can be clearly observed in Figure 2a. Larger clusters of ZrO_2 particles were mainly positioned in cavities and pores. Only very small ZrO_2 particles can be observed in areas of pronounced abrasive and adhesive wear. The EDS analysis also proved that there was a transfer of stainless steel to the PMMA surface during sliding, but only in very small amounts, as shown in Figure 2c, approximately up to 0.04 atomic % in the total composition. The EDS analysis was performed at numerous positions and traces of steel transfer were found only at few positions, indicating that the transfer of steel onto PMMA existed at dry sliding, but only to a very small extent. Traces of gold (Au) shown in Figures 2b and c originate from gold deposition on the PMMA surface prior to SEM analysis due to the preparation procedure of PMMA for SEM analysis. Distribution of all elements in spectrums denoted in Fig. 2a is given in in Supplementary material (Table. S-1).

SEM images of cleaned wear tracks on a PMMA sample after sliding in the presence of Ringer's solution is shown in Figure 3 at different magnifications while BSE images indicate zones with different chemical compositions. As in the previous case of dry sliding, ZrO_2 particles can be observed on the PMMA surface. In the case of low sliding speeds, many small ZrO_2 particles were evenly distributed on the PMMA surface, as shown in Supplementary material (Fig. S7). However, in the case of the high sliding speeds (Fig. 3) these particles were present in the smaller extent. Unlike for dry sliding, smearing of ZrO_2 particles clusters along the sliding direction was not noticed (Fig. 3a, b). Clusters of ZrO_2 particles stayed approximately round in shape and larger clusters can hardly be seen in the wear track, while only very small ZrO_2 particles can be observed (Fig. 3c, d). Abrasive grooves can be seen but scratches were not as deep as in the case of dry sliding and adhesive wear was more prominent. Wear tracks are discontinuous, consisting of many small round-shaped areas. This was also observed in the case of dry sliding, but in the case of wet sliding, wear tracks were much more distributed as a number of small round tracks, each exhibiting similar wear mechanisms. In that case, increased densification of PMMA can be observed within the area of the sliding contact (wear tracks) under all contact conditions, also more pronounced under

higher sliding speeds as it was the case of dry sliding. Pores, cavities and PMMA beads clusters can be observed next to edges of the wear tracks (Fig. 3b). Higher magnification (Fig. 3c, d) revealed a similar PMMA structure as in the case of dry sliding, except for the obvious difference in the lack of large clusters of ZrO_2 particles.

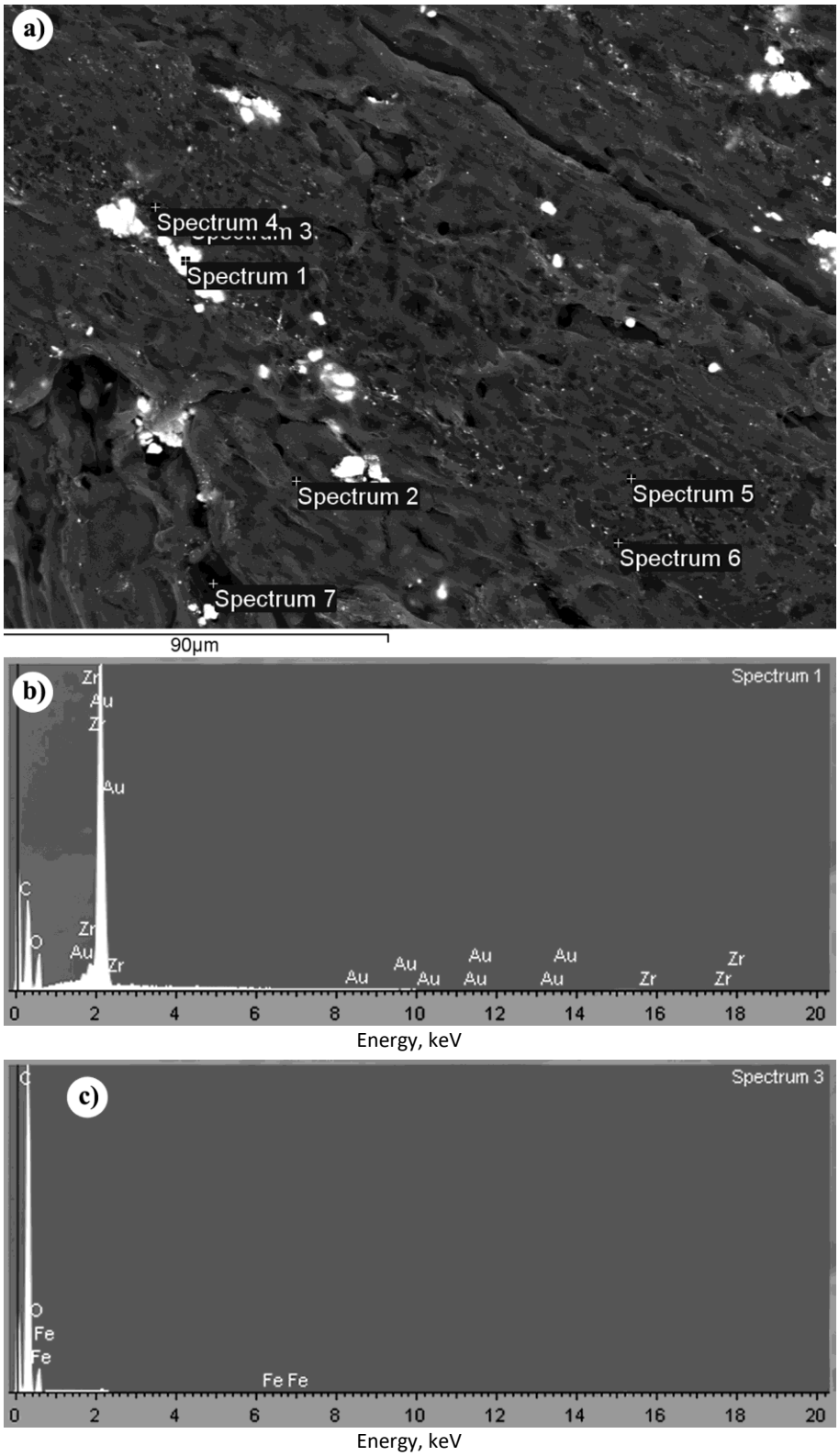

Figure 2. EDS microanalysis of the wear track (dry sliding; 12 mm/s; 500 mN): a) SEM image of the wear track with denoted positions of EDS spectrum analyses; b) EDS analysis (chemical composition) for the position 1; c) EDS analysis for the position 3.

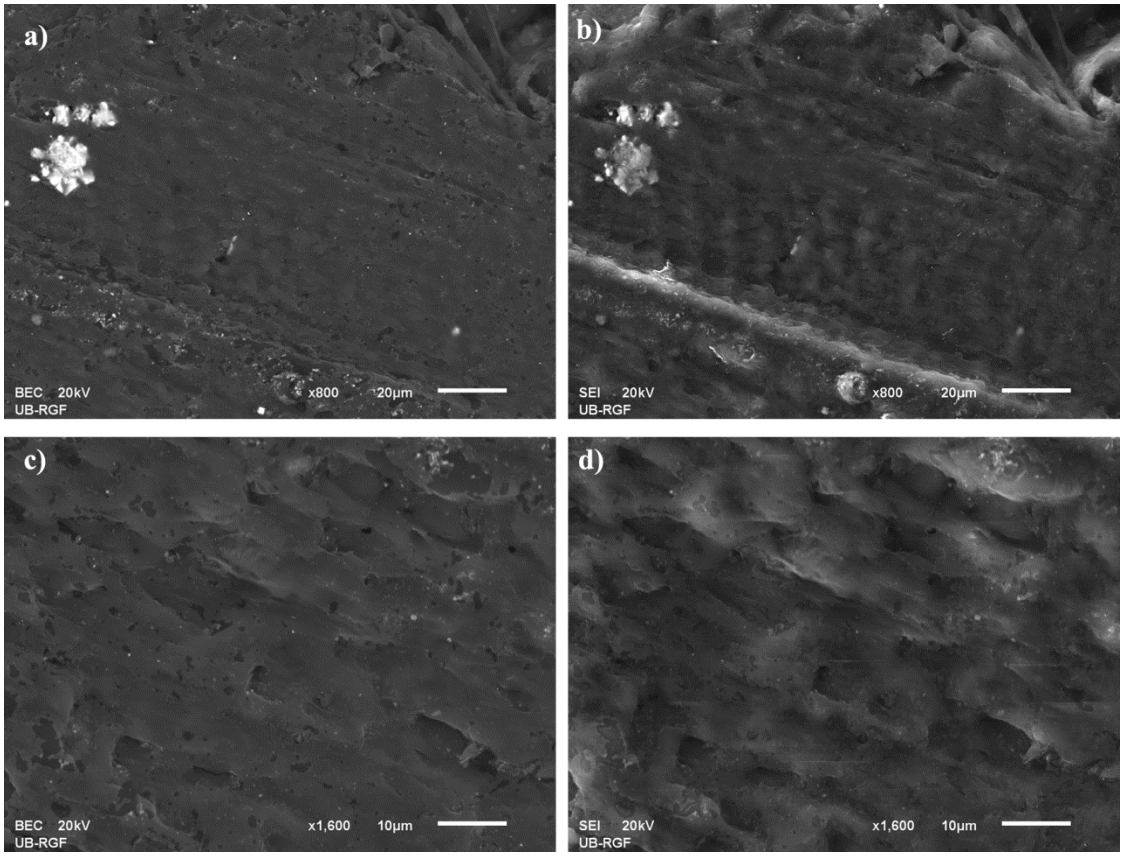

Figure 3. SEM images of the of the wear track (sliding in Ringer's solution; 12 mm/s; 750 mN): a), c) BSE images showing differences in the chemical composition in the wear track; b), d) SEI images of the wear track at different magnifications

EDS analyses of the wear tracks on PMMA samples in the case of wet sliding is shown in Fig. 4. Spectrum positions in Fig. 4 were selected to analyse residuals observed at the surface after sliding. Only elements originating from the PMMA composition and Ringer's solution were detected. The EDS analysis showed traces of Zr (originating from ZrO_2) and Cl (originating from the Ringer's solution) mainly within cavities observed on the surface, just outside of the wear track zones (small round-shaped areas of wear tracks). Small sized ZrO_2 particles can be observed. The EDS analysis in the case of wet sliding showed that the transfer of the steel to the polymer was not occurring unlike for dry sliding. Only residual contents of Na, Cl and K originating from the Ringer's solution were detected. Distribution of all elements in spectrums denoted in Fig. 4a is given in in Supplementary material (Table. S-2).

Several observed phenomena during sliding of PMMA against AISI 316L stainless steel are shown in the following images. A detail in the wear track in the case of dry sliding is shown in Fig. 5. Evidence of fatigue wear, fatigue crack initiation and a crack development pattern are clearly seen. A network of fine random cracks or fissures on the surface of the PMMA wear track (Fig. 5) can be observed, termed craze cracks. These small craze cracks are probably associated with the plastic shrinkage cracking, due to rapid hardening of the surface. They penetrated to a very shallow depth, and further represent the stress initiators.

Fatigue cracks developed normal to the sliding direction (perpendicular to abrasive scratches) growing into large cracks eventually leading to chipping, spalling and detachment of large pieces of densified PMMA surface leaving irregular empty spaces on the surface along the edges of the wear track as clearly observed in Figure 5. Large deep abrasive grooves (Fig. 5) were probably made by detached PMMA particles acting as a third-body abrasive during the contact. Figure 5 shows the evidence of particulate wear debris. In the case of dry sliding, wear tracks were often formed over large voids on the PMMA surface, where these voids originated from the PMMA original structure, which is highly influenced by the initial cement mixing method, surely affecting the sliding contact behaviour. However, development of microcracks within these wear track regions followed the same previously described pattern as well (shown in Fig. 5). Discontinuity of the PMMA matrix material at the position of the void did not change the wear mechanisms: abrasive, adhesive wear, and fatigue. It is

probable that some of the detached PMMA particles are being captured by larger voids and do not further interfere with the sliding process.

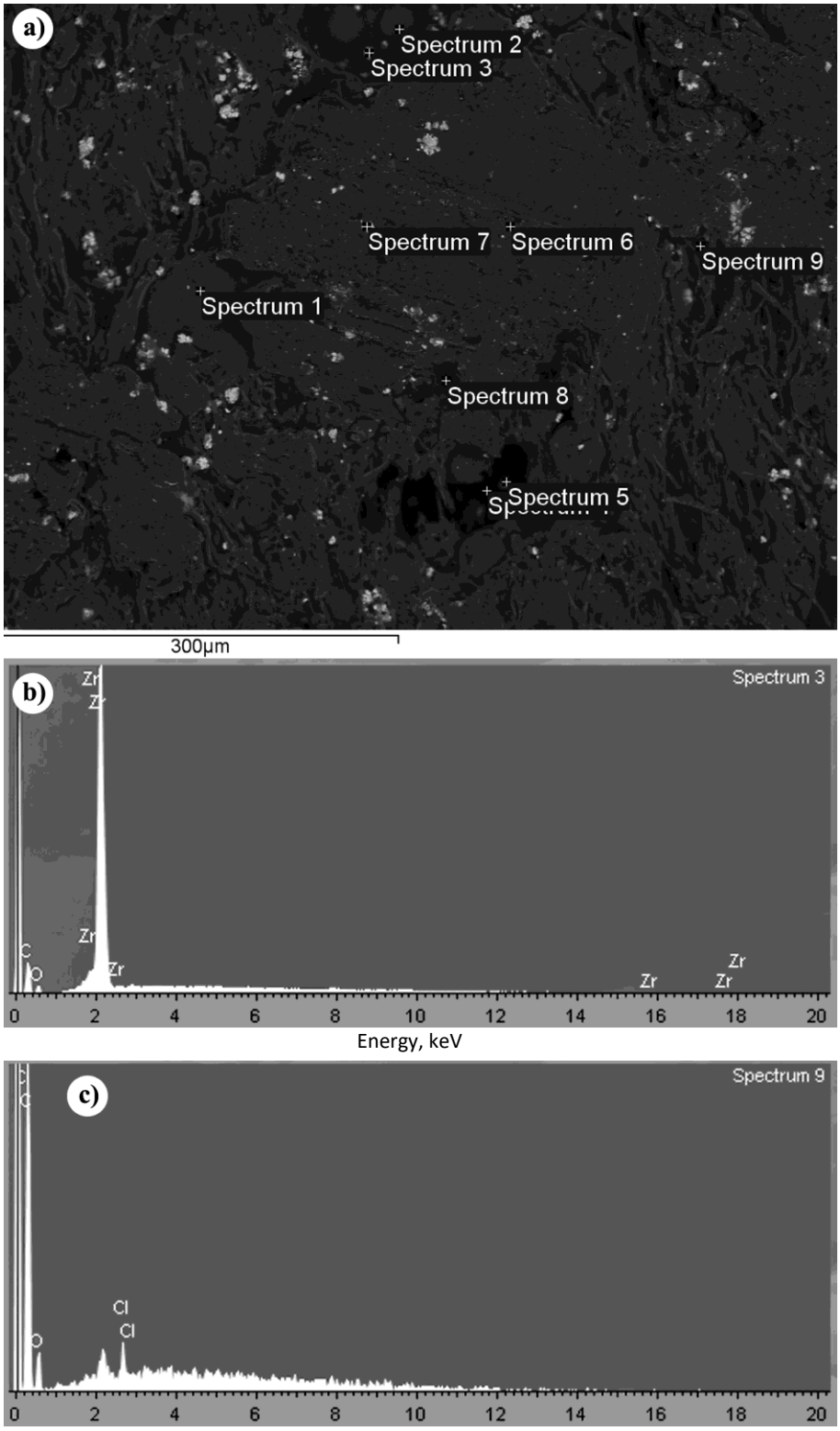

Figure 4. EDS microanalysis of the wear track (sliding in Ringer's solution; 12 mm/s; 750 mN): a) SEM image of the cleaned wear track with denoted positions of EDS spectrum analyses ; b) EDS analysis (chemical composition) for the position 3; c) EDS analysis for the position 9.

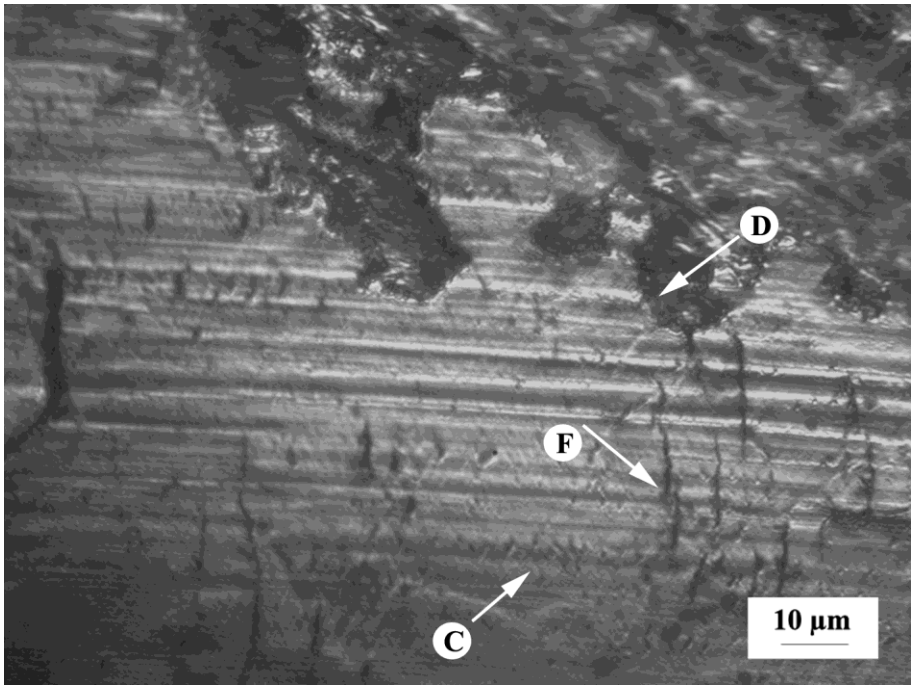

Figure 5. Irregular edges of the wear track, delamination (as denoted by the arrow, D) surface crazing (as denoted by the arrow, C) and fatigue cracks (as denoted by the arrow, F) along the wear track: normal to the sliding direction (dry sliding; 4 mm/s; 500 mN)

It is probable that some of the detached PMMA particles are being captured by larger voids and do not further interfere with the sliding process. However, some part of small PMMA particles affected the wear mechanism producing the three-body wear, clearly evident in Fig. 5 (deep abrasive groove). Detached areas of the PMMA wear track surface shown in Figure 5 in a form of broken edges of irregular shapes have occurred under all test conditions during the dry sliding.

In the case of wet sliding this phenomenon was also observed but with one difference. Detached areas are surrounded with smooth edges as opposed to ragged edges in the previous case and these further developed into regular ellipsoid-shaped cavities as shown in Figure 6b. This was obviously the result of the influence of the Ringer's solution flowing through empty spaces (discontinued material) within the contact zone. These cavities in both cases, dry and wet sliding occurred only on the surface of wear tracks not extending into the bulk material beyond the densified area of the wear track. The cavities were formed by peeling off the surface layers of the wear track on PMMA samples, very similar to spalling of a coating.

In the case of wet sliding, these round cavities were larger in diameters under lower speeds and loads (Fig. 6b) while of significantly smaller sizes under higher speeds and loads. Also, in the case of wet sliding, several small pits can be observed in central regions of the wear tracks, which would probably grow into these large cavities. In the case of dry sliding, such small pits were not observed. These observations are consistent with the published results showing that the increase in the chlorides concentration produced the increase in the number of pits [12]. Fragmentation of wear tracks observed under both sliding conditions was significantly higher in the case of the wet sliding. Large grooves and gouges can be observed throughout the wear tracks under all test wet sliding conditions, as shown in Figure 6, originating from spalled surface layers of the wear track. Fragmentation of the wear track together with the abrasive effect of detached PMMA particles can be clearly observed in Figure 6a.

The wear track appearance shown in Figure 6 is typical for erosion and abrasive wear. Erosion initially is produced by the flow of Ringer's solution within the contact zone. Later when the wear debris starts to form, small PMMA particles mix with Ringer's solution making an erosive slurry, which intensifies the erosion wear by the action of the slurry sliding and flowing on the surface causing additional increases in PMMA particles/layers detachment. The erosive action of the slurry produced significantly wider gouges and grooves under higher speeds and loads, which is consistent with the higher flow of the slurry through these openings at higher sliding speeds. Large erosion grooves and a number of small pits and microcracks developing within the fracture can be observed in Figures 6b and c. A half-detached piece of the

surface layer of the wear track on the PMMA sample can be seen in Figure 6d. It is obvious that the flow of Ringer's solution promoted separation of this half-detached piece of the surface layer.

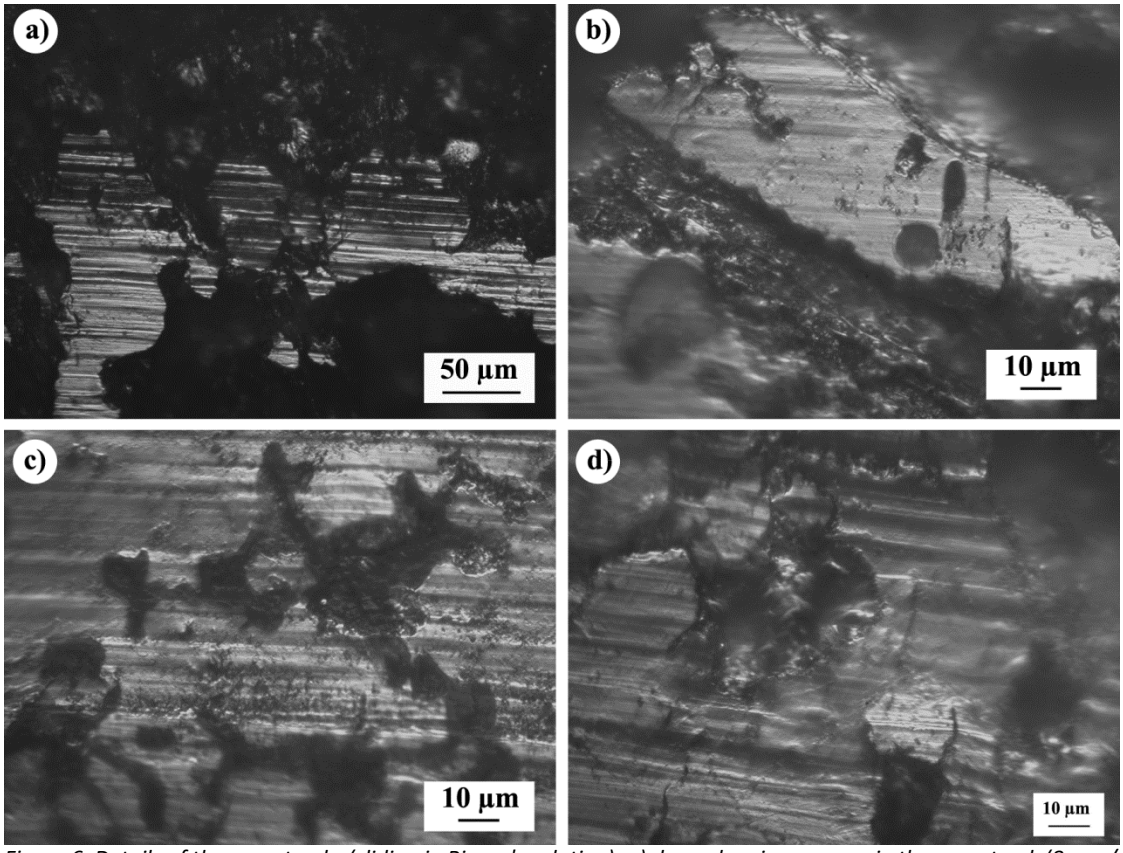

Figure 6. Details of the wear tracks (sliding in Ringer's solution): a) deep abrasive grooves in the wear track (8 mm/s; 250 mN; scale bar: 50 µm); b) details of the wear tracks at 4 mm/s; 100 mN (scale bar: 10 µm); c) deep erosive grooves in the wear track made by the Ringer's solution flow (12 mm/s; 500 mN; scale bar: 10 µm); d) fatigue debris particle in the process of being spalled off the PMMA surface as a result of crack growth at 12 mm/s; 750 mN

Effects of the load and sliding speed on the calculated wear factors in all experiments are shown in Figure 7. The load variations did not induce any significant changes of the wear factor under both test conditions (dry or wet). On the other hand, the increase in the sliding speed induced a significant increase in the wear factor (Fig. 7b, d), more pronounced in the case of dry sliding (Fig. 7b).

Polymers, in general, and PMMA as a visco-elasto-plastic material, are extremely sensitive to frictional heating. It is well known that friction is a typical dissipative process in which mechanical energy is converted into heat (up to 90 - 95 % according to experimental data) [19]. Considering the fact that the increase in the sliding speed is directly associated with the increase in the contact temperature, the wear increase is expected, as it is actually obtained in this study. It should be noted that the increase in the wear factor with the sliding speed increase is significantly higher under dry than under wet conditions (Figs 7 b and d, respectively). The Ringer's solution as a lubricating environment obviously induced lowering of the contact temperature to some extent. On the other hand, wear factors were in average higher for sliding in Ringer's solution than under dry conditions (Fig. 7).

Tiainen [20] studied tribological behaviour of PMMA in contact with different materials (4/10 MPa loads; pin-on-plate reciprocating tests) and reported wear factors of PMMA as: $33/25\times10^{-6}$ mm^3/Nm and $0.086/0.047\times10^{-6}$ mm^3/Nm for CoCrMo and DLC-coated pins, respectively. Recent studies of PMMA wear reported wide ranges of wear rates depending on the PMMA preparation procedure [5,14]. Wear factors of the order of 7×10^{-6} mm^3/Nm can be found in the literature for dry sliding of a steel pin on PMMA, but without details on the steel type or test conditions [5,14]. Wear factors obtained in our study were in the range of $25\text{-}90\times10^{-6}$ mm^3/Nm for dry tests and $90\text{-}130\times10^{-6}$ mm^3/Nm for wet

sliding. Comparison of all produced wear tracks within our study, for the same test regimes for dry and wet sliding, evidently indicated that in the former case the wear tracks were irregularly shaped with uneven edges. On the opposite, wet sliding produced more regularly shaped, often rounded wear tracks. Under reciprocating sliding, the investigated bone cement displayed a true mechanical fatigue failure in both environments. In the case of wet sliding, lower loads produced deep abrasive grooves along the sliding direction, while higher loads produced lower number of scratches not as deep as in the case of dry sliding and sliding under lower loads.

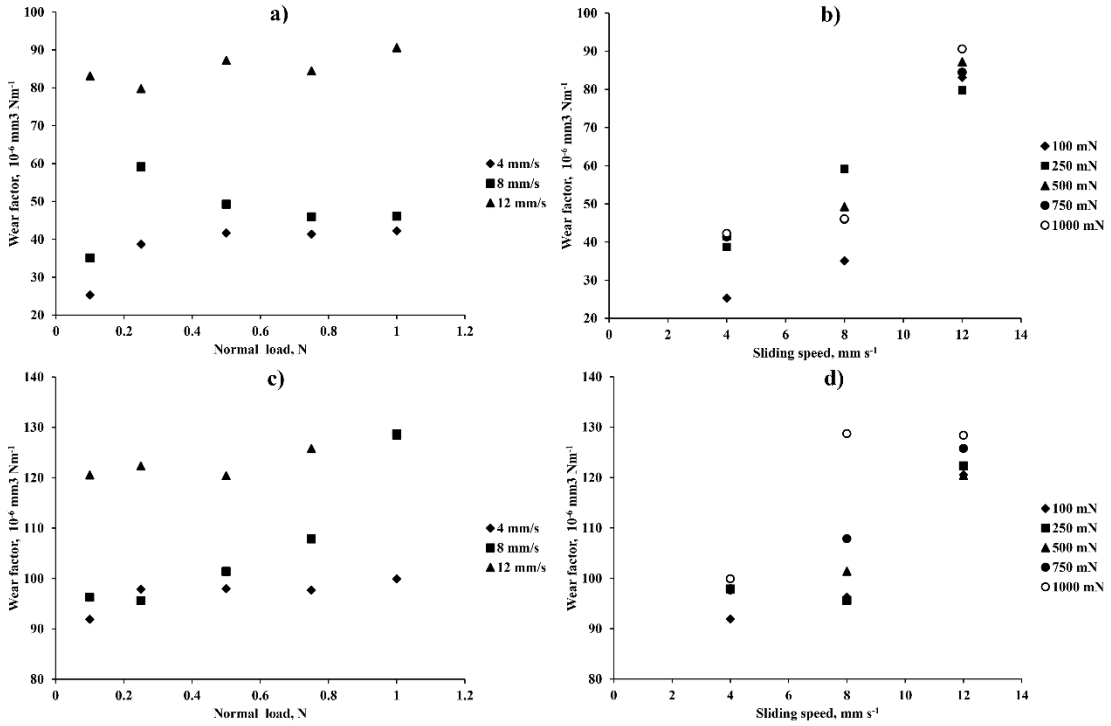

Figure 7. Wear factor of PMMA samples as a function of the normal load at different sliding speeds under: a) dry sliding, c) sliding in Ringer's solution; as a function of the sliding speed at different normal loads under: b) dry sliding, d) sliding in Ringer's solution

Several authors investigated the fracture properties (constant amplitude fatigue, fatigue crack propagation and plane-strain fracture toughness) of bone cements [2] or the fatigue failure process and the earliest stages of crack initiation in an acrylic bone cement [9,10]. It was reported that in the presence of a pore, crack initiation may occur away from the pore due to the combined influence of pore morphology and the presence of defects within regions of stress concentration. Small cracks associated with porosity have not been seen in the control specimens, whereas a fatigue crack initiation site occurred in the vicinity of a pore [9]. In a study of the impact and compression damage of PMMA spheres over a range of loads and velocities it was found that radial crazing always formed under compressive loads indicating large amounts of energy dissipation by inelastic deformations [21]. This is in consistence with observed cracks in Figure 5 where surface crazing and fatigue cracks are evident.

Several studies investigated the non-steady crack and craze behaviour of PMMA under cyclical loading [16,22]. The traditional engineering approach to fatigue description in metals and in the presence of a crack is to relate the stress intensity factor to the average crack propagation rate (per cycle). With respect to polymers there exist two features that set these materials apart. One is the fact that because of their intrinsic time or rate sensitive characteristics the growth of a crack does not depend greatly on the number of cycles but (also) on the frequency as a parameter representing the time history [22]. Furthermore, it seems that the crack does not propagate steadily but in 'spurts' and that these spurts depend on the load level and time history. Under the test conditions conducted in our study, increases in the load and sliding speed produced significantly more cracks, even though the increase in the first parameter did not produce the wear factor increase.

At low crack-growth rates (as in the case of dry sliding in our study), the crack is able to find the easiest path through the microstructure, perhaps around the PMMA beads themselves. Thus, the crack follows a torturous path, and the fracture surfaces are highly irregular and uneven. Here, the evidence of particulate wear debris was the most apparent. At higher fatigue crack-growth rates (as in the case of wet sliding here), the fracture surfaces are progressively less rough as the crack apparently becomes less sensitive to local microstructural features (Fig. 6b). In addition, the fracture surfaces exhibited significantly smaller amounts of the wear debris and began to show signs of PMMA bead cleavage (Fig. 3b). It was proved that physiological environment has a profound effect upon both the cyclic fatigue crack-growth and fracture toughness behaviour of PMMA bone cements [10, 16]. PMMA was found to be more resistant to both cyclic fatigue and fracture in Ringer's solution than in laboratory air with 45% relative humidity, which is due to both the lubricating effect of the aqueous environment and its effect on increasing ductility in the polymer [10]. During the toughness testing in Ringer's solution [10], in the case of fast fracture surfaces, the crack cleaved cleanly through all the PMMA beads in the bone cement, leaving behind a smooth, almost flat fracture surface. In contrast, during the testing in air, fracture surfaces were relatively rough, and some PMMA beads remain uncleaved [10]. This agrees with our results. Cleaved PMMA beads can be clearly observed in Figure 3b, while uncleaved PMMA beads can be observed in Figure 2a.

For both dry and wet sliding, comparison of appropriate wear tracks for the same load regimes indicated that the higher loads produced more uniform and less fragmented wear tracks, probably meaning that higher loads induced higher densification of the PMMA bone cement surface. But the wear factor did not significantly change with load changes, oscillating around a mean value, in both cases of dry and wet sliding. It seems that the load change is compensated by the induced plastic deformations in PMMA. Some authors proved that the maximal densification occurs at the temperature equal to the pressure induced glass transition temperature, Tg (around 105 ^{o}C for PMMA), and that PMMA densification starts well below Tg at zero pressure [23]. Temperature affects physical properties of polymers and hence storage modulus (elastic portion) of PMMA is almost two times lower at 80 ºC than at the room temperature [23].

Friction heating generated during the sliding contact, enhanced plastic deformation of the PMMA bone cement and its densification, which is achieved by the mass transport into the pores thus producing a decrease in the pore volume. However, different pressure holding times do not influence density profiles of PMMA and densification is not proportional to the pressure applied [2]. This is consistent with of the obtained results that the wear factor did not depend on the load change (Fig. 7a, c).

Due to multiple ions in Ringer solution (Na^+, K^+, Ca^{2+}, Cl^-), attraction and friction phenomena are difficult to identify. It can be expected that chlorides from the Ringer's solution produce metal dissolution. It was shown that chlorides induce disruption of passive films and promote dissolution of the metal due to the driving force by formation of metallic complexes on the 316L surface (*e.g.* α-Cr_2O_3, Fe_3O_4) [24]. However, the EDS analysis in our wet tests (Fig. 4) showed that steel was not transferred to the polymer. It was shown in literature that PMMA surface charges are negative while 316L surface charges are positive [24], so that the dissolution of metal ions reinforces attraction between the surfaces. On the other hand, high roughness of bone cement samples promotes disruption of the oxides film. Also, due to the high roughness, separation between the contact surfaces is too large to consider the contribution of electrostatic forces. According to literature [24], when the roughness is higher than 1 nm for bone cement samples, attraction does not occur between surfaces, indicating that the electrostatic forces can be neglected in the case of 316L - cement contact in our study.

However, Ringer's solution increased the wear factor if compared to dry sliding. It is probable that multiple ions in Ringer's solution influenced the 316L corrosion wear, producing corrosion debris thus adding to the third body wear (increasing PMMA worn particles) and promoting higher adhesion wear, and altogether increasing the wear level. Also, it was proved that the corrosion damage of steel increases when it is stressed, especially under compressive stresses [25]. The presence of the Ringer's solution in the contact zone prevented formation of large clusters of bone cement wear debris, otherwise promoted under dry conditions. Large PMMA clusters promote third-body abrasion and formed deep abrasive grooves (such as in Fig. 5), but they are also prone to easier ejection out of the contact zone. The PMMA wear debris in Ringer's solution consisted of small size particles, thus promoting polishing of the PMMA surface, which

can be clearly seen by comparison of Figures 1 and 3. On the other hand, flow of the erosive slurry formed by Ringer's solution and PMMA wear debris promotes early detachment of half broken pieces of surface layers in the wear track (Fig. 6d) thus increasing the wear level and producing large gouges and grooves (Fig. 6).

Several studies indicate that micromechanisms of fracture in PMMA promote formation of an energy dissipation zone surrounding the crack [16]. This zone arises primarily from crazing ahead of the crack tip but may lead to crack bridging on the subsequent crack extension by uncracked matrix ligaments and shielding of the crack tip by the dilated crazed zone in the wake of the crack [10]. These processes depend on the crack length and can have a profound effect on the toughness of the material. Whitening (crazing) of the bone cement around newly formed crack is evident in Figure 3. The stress whitening is a consequence of the craze cracks that appear prior to the crack propagation [16]. It was reported that a bone cement was considerably more resistant to fatigue-crack propagation in Ringer's solution than in air [10]. The increased PMMA toughness in Ringer's solution is thought to arise from the plasticizing effect of the environment [10,18]. A similar effect of has been also reported for other brittle materials, while such effect is not consistent with the fatigue crack-growth behaviour in metallic materials where toughness is relatively insensitive to crack growth rates [10]. On the other hand, the plasticizing effect enhances crazing in the crack tip region and leads to an increased fracture toughness. The presence of soluble environmental agents is well known to reduce the critical stress or strain required to initiate crazing [10]. Decreased stresses influenced by Ringer's solution result in a significantly larger craze or plastic zone size ahead of the crack tip as shown in Figures 3b and d.

Water has been known to have a plasticizing effect on polymers [16,18,26]. Water molecules act to break intermolecular bonds of the polymer, thus increasing the chain mobility and reducing the strength. Immersion in water is comparable to the effect of a rise in temperature according to literature [18]. This is consistent with results of our study where Ringer's solution increased the wear factor when compared to that under dry sliding, similarly as the increase of this parameter due to the increase in the sliding speed (due to the increase in the contact temperature). In a previous study it was shown that the influences of Ringer's solution and distilled water on curing or creep properties of PMMA bone cement were not significantly different [18], indicating that physiological salts present in Ringer's solution do not induce additional effects on curing or creep deformation. It is known that in glassy polymers (*e.g*. PMMA), water tends to move to free volume regions created by local defects [16]. This is also found in our study by the EDS analysis showing residual contents of Cl, Na and K from Ringer's solution only in voids and cavities observed on the sample surface (Fig. 4). On the other hand, these regions strongly contribute to deformation and fatigue crack initiation, as elaborated in literature [15]. The increase in the sliding speed had more drastic effects in the case of dry sliding, while under wet sliding conditions the increase in the wear factor was rather moderate. At sliding speeds and thus higher temperatures, the chain mobility of the PMMA has already increased to such an extent that additional water plasticization had little effects. This is the main difference of dry and wet sliding in relation to the wear factor dependences shown in Figures 7b and d: the wear factor has already been shifted to higher values at lower speeds and further increase is moderate under wet conditions, unlike for dry sliding where the wear factor increase is steeper.

PMMA wear debris has been studied in literature [27] showing that poorly mixed PMMA may release pre-polymerized spheres 25 - 35 μm in size. Small movements between the implant and the PMMA mantle or the PMMA implant and bone may constantly produce PMMA particles. For example, it was reported that micron and sub-micron particles or smaller particles of cement radiopaque agents such as ZrO_2 are contained in PMMA voids [27]. This is consistent with results obtained in our study (Figs. 1-4). Accumulation of ZrO_2 particles 10 - 15 μm in size, is clearly seen in Figure 3a while micron and sub-micron sized ZrO_2 particles or particle aggregates can be clearly observed in Figures 1c and d. In addition, pre-polymerized PMMA spheres in the size range 25 - 35 μm can be clearly seen in Figure 3b. According to literature [27] PMMA particles or associated voids can be described as: fine particles (<1 μm in size), multifaceted fragments with sharp edges (1 - 5 μm in size; more common than previous ones), spherical particles (5 - 25 μm in size), and even beads with pits and cracks (20 - 200 μm in size) or irregular chunks about 1 mm in length. One PMMA particle approximately 15 μm in size can be seen in Figure 6d, as a beginning of the wear debris formation by delamination. Hard debris such as PMMA particles and especially hard ZrO_2 particles induce scratching and produce plowing grooves, clearly visible in wear tracks (Figs. 5 and 6a). The effects of radiopaque agents (*e.g*. zirconium oxide

(ZrO_2)) on cement behaviour have been investigated in literature [8], especially regarding static mechanical properties, such as fatigue, while some studies considered also the physiological effects. Radiopaque agent particles (usually hard ceramic particles) could leach out of the material and find their way to the joints and become trapped in the joint component (if made of polymers), scratching the metallic component. They could also cause osteolysis if they penetrate the interface with the bone cavity. These particles in the cement produce worsening of the mechanical properties as a consequence of the stress concentration around the particles [8]. Some studies aimed to improve dispersion of the inorganic particles in order to improve the cement fatigue properties. The question of whether to perform the mixing in vacuum or manually in open atmosphere has been addressed by several researchers [1]. Ultimately, mixing in vacuum is widely recommended over the hand-mixing technique in order to obtain cements that will retain appropriate levels of hardness and elasticity for at least 2 or 3 decades whilst implanted *in vivo*, even though the optimal vacuum regime and optimal cement porosity are still under debate. Results obtained in our earlier study indicated that a combination of different periods of vacuum treatment of the bone cement produced good results regarding mechanical properties [6]. This in return, should induce less wear debris during sliding.

4. CONCLUSION

This research has aimed at the influence of the Ringer's solution on the wear of vacuum mixed PMMA bone cement during the reciprocating sliding with AISI 316L stainless steel, at low loads, in order to simulate the contacts that frequently appear in medical implants. Sliding in Ringer's solution was compared to dry sliding and crack initiation and development was analysed. Dry sliding produced discontinued, irregularly shaped wear tracks with a clear evidence of strong abrasive, adhesive wear, and plastic deformation grooves. The increase in the sliding speed produced smoother wear tracks with more pronounced adhesive wear. Plastic deformation along the sliding direction is more evident closer to the edges of the wear track. Also, under these conditions, aggregation and smearing of ZrO_2 particles occurred throughout the wear track. Larger clusters of ZrO_2 particles were mainly positioned in cavities and pores. Also, there was a slight transfer of stainless steel to the PMMA surface during sliding. Prominent fatigue wear and fatigue crack initiation were observed, as well as networks of fine random cracks on the cement surface. Fatigue cracks developed in the direction normal to sliding (perpendicular to abrasive scratches) growing into the large cracks and leading to chipping, spalling and detachment of large pieces of densified PMMA surface and producing three-body wear. The wear debris particles varied in size, from small fine particles, below 1 μm up to 15 μm and larger, according to associated voids formed on the polymer surface.

In the case of sliding in the presence of Ringer's solution, abrasive grooves could be seen but scratches were not as deep as in the case of dry sliding and adhesive wear was more prominent. Steel was not transferred to the polymer surface. Wear tracks were also discontinuous, consisting of many small mainly round-shaped areas. Aggregation of ZrO_2 particles was also exhibited but to a significantly smaller extent and the particles were mainly rounded without smearing along the sliding direction. Detached parts of the cement surface formed smooth edges further developing into rather regular ellipsoid-shaped cavities, showing the influence of the Ringer's solution flow within the contact zone. Erosion and abrasive wear were prominent, but fatigue failure was also present. Large erosion grooves, number of small pits and microcracks developing into fractures could be observed.

In both cases of dry and wet sliding, cavities and voids formed only on the surface of the wear track and did not extended into the bulk material beyond densified area of the wear track. Fragmentation of wear tracks observed in both cases was significantly higher in the case of wet sliding.

Changes in the load over the investigated range did not produce any significant effect on wear factor values for both test conditions. Higher loads produced more uniform and less fragmented wear tracks, probably meaning that higher loads induced higher densification of the PMMA bone cement surface. The increase in the sliding speed induced significant increases in the wear factor, more pronounced in the case of dry sliding. Wear factors were in average higher for sliding in Ringer's solution than under dry conditions.

These findings provide significant insights into the patterns of surface cracks in PMMA bone cements, during its contact with a steel implant in physiological environments. Results indicated that craze cracks have important role in

damage behaviour of PMMA cements, beside fatigue cracks that altogether determine the life of the implant subjected to a complex micromotions.

Acknowledgements: The research study was financed by the Ministry of Education, Science and Technological Development, Serbia, project No. 451-03-68/2020-14/200107, and project No. 451-03-68/2020-14/200105.

REFERENCES

[1] Boote AT, Bigsby RJ, Deehan DJ, Rankin KS, Swailes DC, Hyde PJ. Does vacuum mixing affect diameter shrinkage of a PMMA cement mantle during in vitro cemented acetabulum implantation? *Proc Inst Mech Eng, Part H.*2021; 235: 133–140.

[2] Lewis G. Viscoelastic properties of injectable bone cements for orthopaedic applications: State-of-the-art review. *J Biomed Mater Res, Part B*. 2011; 98B(1): 171-191.

[3] Stojkovic M, Milovanovic J, Vitkovic N, Trajanovic M, Grujovic N, Milivojevic V, Milisavljevic S, Mrvic S. Reverse modeling and solid free-form fabrication of sternum implant. *Australas Phys Eng Sci Med*. 2010; 33(3): 243-250.

[4] Garcés GA, Rojas VH, Bravo C, Sampaio CS. Shear bond strength evaluation of metallic brackets bonded to a CAD/CAM PMMA material compared to traditional prosthetic temporary materials: an in vitro study. *Dental Press J Orthod*. 2020; 25(3): 31-38.

[5] Reyes-Sevilla M, Kuijs RH, Werner A, Kleverlaan CJ, Lobbezoo F. Comparison of wear between occlusal splint materials and resin composite materials. *J Oral Rehabil*. 2018; 45(7): 539-544.

[6] Zivic F, Babic M, Grujovic N, Mitrovic S, Favaro G, Caunii M. Effect of vacuum-treatment on deformation properties of PMMA bone cement. *J Mech Behav Biomed Mater*. 2012; 5(1): 129-138.

[7] Kraaij G, Zadpoor AA, Tuijthof GJM, Dankelman J, Nelissen RGHH, Valstar ER. Mechanical properties of human bone–implant interface tissue in aseptically loose hip implants. *J Mech Behav Biomed Mater*. 2014; 38: 59-68.

[8] Wimhurst JA, Brooks RA, Rushton N. The effects of particulate bone cements at the bone-implant interface. *J Bone Jt Surg*. 2001; 83-B(4): 588-592.

[9] Sinnett-Jones PE, Browne M, Moffat AJ, Jeffers JRT, Saffari N, Buffière J-Y, Sinclair I. Crack initiation processes in acrylic bone cement. *J Biomed Mater Res A*. 2009; 89A(4): 1088-1097.

[10] Nguyen NC, Maloney WJ, Dauskardt RH. Reliability of PMMA bone cement fixation: fracture and fatigue crack-growth behaviour. *J Mater Sci Mater Med*. 1997; 8(8): 473-483.

[11] Shih C-C, Shih C-M, Su Y-Y, Lin S-J. Potential risk of sternal wires. *Eur J Cardiothorac Surg*. 2004; 25(5): 812-818.

[12] Geringer J, Pellier J, Cleymand F, Forest B. Atomic force microscopy investigations on pits and debris related to fretting-corrosion between 316L SS and PMMA. *Wear*. 2012; 292-293: 207-217.

[13] Koistinen AP, Korhonen H, Kröger H, Lappalainen R. Interfacial sliding properties of bone screw materials and their effect on screw fixation strength. *J Appl Biomater Func*. 2014; 12(2): 90-96.

[14] Takamizawa T, Barkmeier W, Tsujimoto A, Scheidel D, Erickson R, Latta M, Miyazaki M. Mechanical Properties and Simulated Wear of Provisional Resin Materials. *Oper*. 2015; 40(6): 603-613.

[15] Alexeev AA, Bolshev KN, Ivanov VA, Syromyatnikova AS, Bolshakov AM, Andreev AS. Experimental Study of Crack Branching Velocity in Polymers. *Inorg Mater*. 2019; 55(15): 1476-1480.

[16] Koch S, Meunier M, Hopmann C, Alperstein D. A combined experimental and computational study of environmental stress cracking of amorphous polymers. *Polym Adv Technol*. 2020; 31(2): 297-308.

[17] Zivic F, Babic M, Mitrovic S, Vencl A. Continuous control as alternative route for wear monitoring by measuring penetration depth during linear reciprocating sliding of Ti6Al4V alloy. *J Alloys Compd*. 2011; 509(19): 5748-5754.

[18] Arnold JC, Venditti NP. Effects of environment on the creep properties of a poly(ethylmethacrylate) based bone cement. *J Mater Sci: Mater Med*. 2001; 12(8): 707-717.

[19] Myshkin NK, Pesetskii SS, Grigoriev AY. Polymer Tribology: Current State and Applications. *Tribol Ind.* 2015; 37(3): 284-290.

[20] Tiainen V. Amorphous carbon as a bio-mechanical coating — mechanical properties and biological applications. *Diamond Relat Mater*. 2001; 10(2): 153-160.

[21] Gorham DA, Salman AD, Pitt MJ. Static and dynamic failure of PMMA spheres. *Powder Technol*. 2003; 138(2-3): 229-238.

[22] Pulos GC, Knauss WG. Nonsteady crack and craze behavior in PMMA under cyclical loading: I. Experimental preliminaries. *Int J Fract*. 1998; 93(1/4): 145-159.

[23] Etienne S, Becker C, Ruch D, Grignard B, Cartigny G, Detrembleur C, Calberg C, Jerome R. Effects of incorporation of modified silica nanoparticles on the mechanical and thermal properties of PMMA. *J Therm Anal Calorim*. 2007; 87(1): 101-104.

[24] Geringer J, Atmani F, Forest B. Friction–corrosion of AISI 316L/bone cement and AISI 316L/PMMA contacts: Ionic strength effect on tribological behaviour. *Wear*. 2009; 267(5-8): 763-769.

[25] Munir S, Walsh WR. The Quantification of Corrosion Damage for Pre-stressed Conditions: A Model Using Stainless Steel. *Journal of Bio- and Tribo-Corrosion*. 2016; 2(1): 4.

[26] Ayre WN, Denyer SP, Evans SL. Ageing and moisture uptake in polymethyl methacrylate (PMMA) bone cements. *J Mech Behav Biomed Mater*. 2014; 32: 76-88.

[27] Savio JA, Overcamp LM, Black J. Size and shape of biomaterial wear debris. *Clin Mater*. 1994; 15(2): 101-147.

[28] Capitanu L, Badita L-L, Florescu V. Stability Loss of the Cemented Stem of Hip Prosthesis due to Fretting Corrosion Fatigue. *Tribol Ind* 2017; 39(4): 536-546.
[29] De Baets T, Waelput W, Bellemans J. Analysis of third body particles generated during total knee arthroplasty: Is metal debris an issue? *The Knee*. 2008; 15(2): 95-97.

SAŽETAK

Uticaj Ringerovog rastvora na habanje vakuumski tretiranog koštanog cementa od poli(metil metakrilata) u kontaktu sa AISI 316L nerđajućim čelikom pri linearno naizmeničnom kretanju

Fatima Živić[1], Nenad Grujović[1], Slobodan Mitrović[1], Jovan Tanasković[2] i Petar Todorović[1]

[1]*Univerzitet u Kragujevcu, Fakultet inženjerskih nauka, Kragujevac, Srbija*
[2]*Univerzitet u Beogradu, Mašinski fakultet, Beograd, Srbija*

(Naučni rad)

U radu su prikazane mikrostrukturne karakteristike i ponašanje PMMA koštanog cementa mešanog u vakuumu, pri kontaktu sa AISI 316L nerđajućim čelikom, sa mikro opterećenjima i analiziran je uticaj prisustva Ringerovog rastvora na habanje u odnosu na suvi kontakt. Promena sile nije značajno uticala na faktor habanja dok je povećanje brzine klizanja uslovilo značajan porast faktora habanja, naročito u slučaju suvog kontakta. Faktori habanja su u proseku bili veći za klizanje u Ringerovom rastvoru od suvog kontakta. Uočena je značajna fragmentacija tragova habanja, nepravilnog oblika, sa izlomljenim ivicama, što je bilo više naglašeno pri suvom kontaktu. U tragovima habanja se uočavaju brojni otvori i šupljine, koji se ne šire u dubinu materijala. Veća opterećenja su uzrokovala uniformnije i manje fragmentirane tragove habanja. Uočeno je abrazivno i adhezivno habanje i tragovi plastične deformacije, kao i zamorno i erozivno habanje. Zamorne pukotine su se širile u pravcu normalnom na pravac klizanja. Fina mreža tankih površinskih lomnih pukotina je uočena na površini tragova habanja, posebno u slučaju suvog kontakta. Rezultati su značajni kao doprinos razumevanju inicijacije pukotina i mehanizmima njihovog razvoja na površini PMMA koštanog cementa, uključujući i sinergijske efekte fiziološke okoline s aspekta nestacionarnog ponašanja i modela razvoja pukotina kod PMMA.

Ključne reči: lomne pukotine; erozivni useci; lom; denzifikacija; frikciona toplota; zamorni lom.

Hidrodinamika i prenos mase u ekstrakcionim kolonama tipa Kini

Milan N. Sovilj[1] i Momčilo Đ. Spasojević[2]

[1]*Univerzitet u Novom Sadu, Tehnološki fakultet, Bulevar cara Lazara 1, Novi Sad, Srbija*
[2]*Univerzitet u Novom Sadu, Fakultet tehničkih nauka, Trg Dositeja Obradovića 6, Novi Sad, Srbija*

Izvod

U ovom radu dat je prikaz eksperimentalnih istraživanja vezanih za hidrodinamiku i prenos mase u ekstrakcionim kolonama tipa Kini (Kühni), koja su preuzeta iz literature. Prikazan je ispitivani uticaj radnih parametara na hidrodinamičke karakteristike u odabranim dvofaznim sistemima tečno-tečno. Utvrđeno je da broj obrtaja rotora i međufazni napon značajno utiču na Sauterov srednji prečnik kapi, dok je uticaj protoka kontinualne i dispergovane faze zanemarljiv. Istovremeno, konstatovano je da sadržaj dispergovane faze uglavnom zavisi od broja obrtaja rotora i protoka dispergovane faze. U radu je zaključeno da su empirijske korelacije, preuzete iz literature, adekvatne za proračun Sauterovog srednjeg prečnika kapi i sadržaja dispergovane faze, za odabrane dvofazne sisteme. U isto vreme, pokazano je da se brzina prenosa mase povećava sa povećanjem nivoa povratnog mešanja. Konstatovano je da koeficijent prenosa mase zavisi od broja obrtaja rotora i pravca prenosa mase između faza. Istovremeno, pokazano je da koeficijent prenosa mase relativno malo zavisi od protoka faza. U radu je prikazana i empirijska korelacija za određivanje koeficijenta prenosa mase koja se zasniva na bezdimenzionalnim brojevima.

Keywords: Sauterov srednji prečnik kapi, sadržaj dispergovane faze, brzina obrtanja rotora, povratno mešanje, koeficijent prenosa mase.

Available on-line at the Journal web address: http://www.ache.org.rs/HI/

STRUČNI RAD

UDK: 66.023.23:551.511.32: 544.431.11

Hem. Ind. **75 (2)** 93-101 (2021)

1. INTRODUCTION

Ekstrakcija tečno-tečno je jedna od najzastupljenijih separacionih operacija koja se primenjuje u postupcima prenosa mase i energije u hemijskoj i procesnoj industriji. Ona se široko primenjuje u industrijskoj proizvodnji goriva u naftnoj industriji, u nuklearnoj industriji, faramaceutskoj industriji, metalurgiji, pri proizvodnji katrana iz uglja, kao i pri razdvajanju ugljovodonika u petrohemijskoij industriji [1]. U ovim industrijskim granama koriste se različiti tipovi ekstrakcionih kolona, kao što su: kolona sa raspršivanjem, kolona sa punjenjem, pulzacione kolone sa punjenjem ili sa perforiramim podovima, Oldšue-Rašton (Oldshue-Ruschton) kolona, rotacioni disk kontaktor (RDK), Šajbelov (Scheibel) ekstraktor, Karova (Karr) kolona, Kinijeva (Kühni) kolona i dr. [2-4]. Jedna od najefikasnijih ekstrakcionih kolona u laboratorijskoj i industrijskoj praksi je kolona tipa Kini. Ona se sastoji od vertikalne cevi u kojoj se u centralnom delu nalazi osovina koja na sebi nosi specijalne turbinske mešalice (rotori), postavljene između perforiranih podova (statori) koji su pričvršćeni na unutrašnju površinu kolone (Slika 1.) [5]. Turbinske mešalice, zahvaljujući svojoj konstrukciji, izazivaju povećanje brzine kapi i međufazne površine unutar svake sekcije koju čine jedan rotor i dva statora. Perforirani podovi omogućavaju stvaranje aksijalnog toka fluida, čime se ostvaraje potpuna separacija faza, što je različito od postupka u rotacionom disk kontaktoru (RDK). Promenom geometrije statora, značajno se utiče na režim strujanja u dvofaznom sistemu unutar kolone. U procesima tečno-tečno najznačajniji hidrodinamički parametri su: sadržaj dispergovane faze, srednji prečnik kapi, brzina plavljenja i relativna brzina faza. Ovi parametri zavise od geometrije ekstrakcione kolone, površinskih brzina faza i fizičkih karakteristika sistema tečno-tečno. Istovremeno, oni se koriste i pri proračunima koeficijenta povratnog mešanja i brzine prenosa mase u dvofaznom sistemu [6]. Poluindustrijska ispitivanja u ekstrakcionim kolonama su relativno skupa i zahtevaju dosta vremena. Međutim, ova istraživanja se ipak koriste kao prvi korak u postupku projektovanja svih ekstrakcionih kolona. U ovakvim uređajima, kinetika ekstrakcije i brzina prenosa mase značajno zavise od međufazne površine. S druge strane,

Corresponding author: Milan N. Sovilj, Tehnološki fakultet, Bulevar cara Lazara 1, 21000 Novi Sad, Srbija
E-mail: miso@uns.ac.rs
Paper received: 4. decembar 2020.
Paper accepted: 31 March 2021.
https://doi.org/10.2298/HEMIND201204014S

međufazna površina je osetljiva na kontaminente i zavisi od geometrije kolone, hidrodinamike u koloni, radne visine kolone, protoka tečnih faza, temperatute, itd. Poznavanje srednjeg prečnika kapi dispergovane faze i raspodele veličina prečnika kapi duž visine kolone su od fundamentalnog značaja pri dobijanju realističnih parametara kolone (kapacitet i prečnik kolone), uzimajući u obzir da je ekstrakcioni sistem vrlo kompleksan i da se on ne može predvideti samo na osnovu teorije [7,8]. Ekstrakcione kolone tipa Kini projektuju se u širokom opsegu unutrašnjeg prečnika od laboratorijskih kolona (60 mm) do industrijske skale (2,0 m). Unos energije u dvofazni sistem pomoću turbinskih mešalica značajno utiče na prenos mase između faza. Vrlo važan korak u određivanju radne visine ekstrakcione kolone tipa Kini je poznavanje efikasnosti kolone, kao i vrednosti koeficijenta prenosa mase u dvofaznom sistemu. Za ovu svrhu razvijene su odgovarajuće empirijske korelacije, koje su funkcija hidrodinamičkih karakteristika, geometrije kolone i fizičkih svojstava sistema tečno-tečno.

Cilj ovog rada je da prikaže rezultate eksperimentalnih istraživanja hidrodinamičkih karakteristika i prenosa mase u ekstrakcionoj koloni tipa Kini, koja se mogu naći u dostupnoj literaturi. U eksperimentalnim merenjima korišćeni su dvofazni sistemi tečno-tečno u slučajevima sa i bez prenosa mase između faza. Kao radni parametri u toku ekstrakcije tečno-tečno poslužili su: broj obrtaja diskova, protoci dispergovane i kontinualne faze, gustine tečnih sistema i međufazni napon, kao i pravac prenosa mase između faza. Kao hidrodinamički parameteri, određivani u eksperimentalnom radu, bili su sadržaj dispergovane faze i srednji prečnik kapi u kolonskom ekstraktoru. U ovom radu je dat pregled empirijskih korelacija, koje su razvijene za slučaj proračunavanja Sauterovog srednjeg prečnika kapi dispergovane faze. S druge strane, prikazani su i postupci neophodni za određivanje koeficijenta prenosa mase u ekstrakcionim kolonama tipa Kini. Istovremeno, razmotrene su i empirijske korelacije koje daju zavisnost koeficijenta prenosa mase od radnih uslova, geometrije kolone i fizičkih karakteristika dvofaznih sistema.

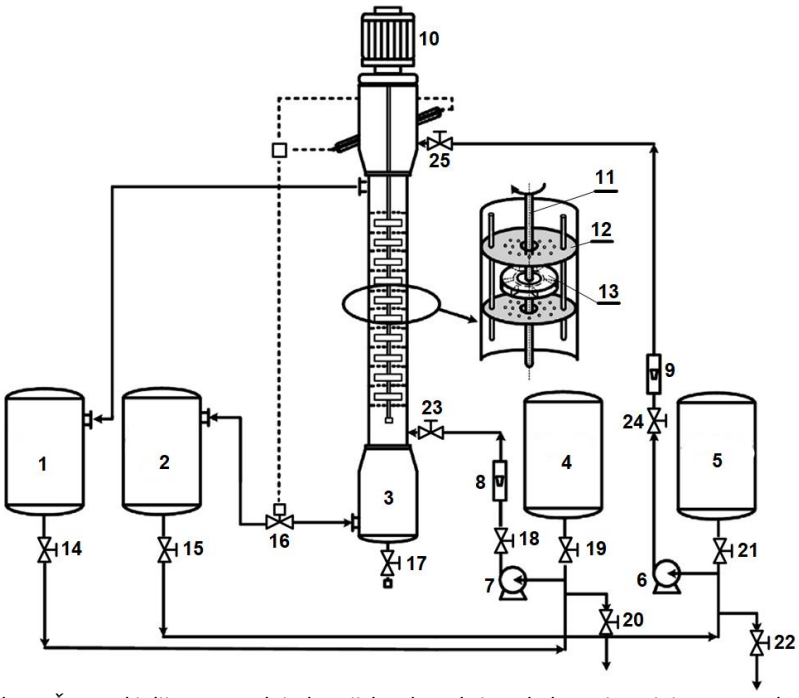

Slika 1. Šematski dijagram poluindustrijske ekstrakcione kolone tipa Kini; osnovna kolona, glavni elementi kolone i dizajn jednog stupnja kolone (Preuzeto i prevedeno iz Asadollahzadeh i sar. [5]). ***Legenda****: 1, 4 – rezervoari za organsku fazu; 3 – ekstrakciona kolona; 2, 5 – rezervoari za vodenu fazu; 6, 7 – pumpe; 8, 9 – rotameteri; 10 - elektromotor sa reduktorom; 11 – osovina; 12 – perforirani pod (stator); 13 – turbinska mešalica (rotor); 16 – elektromagnetni ventil za regulaciju nivoa; 14, 15, 17-25 – kuglasti ventili.*

Figure 1. Scheme of a Kühni extraction column at a pilot scale; extraction column with the main elements and design of an individual plate (Reproduced from Asadollahzadeh et al. [5]). ***Legend****: 1, 4 – reservoirs for the organic phase; 3 – extraction column; 2, 5 - reservoirs for the aqueous phase; 6, 7 – pumps; 8, 9 – rotameters; 10 – electric motor with a reducer; 11 – rod; 12 – perforated plate (stator); 13 – turbine mixer (rotor); 16 – solenoid valve for the level regulator; 14, 15, 17-25 - ball valves.*

2. HIDRODINAMIKA

2.1. Srednji prečnik kapi

Srednji prečnik kapi dispergovane faze u slučaju kapi eliptičnog oblika, čije su ose minimalna d_1 i maksimalna d_2, označava se kao ekvivalentni prečnik d_e i izračunava se primenom relacije [9]:

$$d_e = (d_1^2\, d_2)^{1/3} \quad (1)$$

S druge strane, zapreminsko-površinski prečnik kapi (Sauterov srednji prečnik kapi), d_{32}, se izračunava iz izraza [10]:

$$d_{32} = \sum_{i=1}^{NN} n_i d_i^3 \,/\, \sum_{i=1}^{NN} n_i d_i^2 \quad (2)$$

gde su: n_i – broj kapi prečnika d_i unutar određenog intervala i; NN – ukupan broj tačaka.

Srednji prečnik kapi dispergovane faze definiše se, u odsustvu turbulencija ili pri nivou male agitacije u koloni ($Re_R \leq 10\,000$), odnosom između sile uzgona i međufaznog napona, pa se Sauterov srednji prečnik kapi može izraziti sledećom jednačinom [11]:

$$d_{32} = C_1 \left(\frac{\sigma}{\Delta \rho g} \right)^{0,5} \quad (3)$$

gde je C_1 - empirijski parametar čija vrednost zavisi od geometrije kolone, pravca prenosa mase između faza i fizičkih osobina tečnih faza. U rotacionom disk kontaktoru određena je vrednost ovog parametra za kapi n-butil alkohola dispergovane u vodi, koja iznosi C_1 = 1,3 [12], dok je u drugoj studiji data vrednost od C_1 = 0,92 za pulzacionu kolonu sa perforiranim podovima [13].

U jednoj studiji, ispitivana je hidrodinamika kratke Kini kolone, pod uslovom da nije bilo prenosa mase, koristeći dvofazni sistem tečno-tečno Eksol D-80 (Exxsol D-80)-voda [7]. Eksol D-80 je korišćen kao dispergovana, a voda kao kontinualna faza. Ekstrakciona kolona je imala 5 stupnjeva, unutrašnji prečnik od 15,0 cm, a načinjena je od vertikalne staklene cevi. Svaki stupanj kolone sadržao je turbinsku mešalicu od šest lopatica (prečnik rotora = 8,5 cm, visina rotora = 1,0 cm, pri čemu je vršena tačna kontrola brzine obrtanja rotora). Statori u koloni su imali otvore od 7,0 cm i udeo otvora na perforiranom podu je bio 30 %. U ekstrakcionoj koloni je ostvarivan protivstrujni tok faza, pri čemu su određivani sledeći hidrodinamički parametri: Sauterov srednji prečnik kapi, raspodela veličina kapi i sadržaj dispergovane faze u radnom delu kolone. U radu je korišćena fotografska metoda za određivanje veličina prečnika kapi. Kao radni parametri korišćeni su: brzina obrtanja rotora, protoci obe faze i broj stupnjeva kolone. Utvrđeno je da je funkcija log-normalne verovatnoće gustine adekvatna za modelovanje eksperimentalnih vrednosti za raspodelu prečnika kapi duž kolonskog uređaja. U istom radu [7], pokazano je da se dobijaju kapi manjeg prečnika i znatno ravnomernija raspodela prečnika kapi kada se povećavaju vrednosti broja obrtaja rotora i koristi veći broj stupnjeva kolone. Predložena je, takođe, nova korelaciju za d_{32}, sledećeg oblika [7]:

$$d_{32} = (5{,}43 \pm 0{,}35) - (1{,}38 \pm 0{,}22)\, N + [(0{,}57 \pm 0{,}15) - (0{,}10 \pm 0,\, 2)\, E]\, V_c N \quad (4)$$

gde su: d_{32} / mm, V_c / L min^{-1} - protok kontinualne faze i N / o min^{-1} - broj obrtaja rotora. Ova relacija je primenljiva za sledeće vrednosti promenljivih:

$1{,}24 \leq V_c \leq 2{,}00$ / L min^{-1}, protok dispergovane faze u opsegu $1{,}24 \leq V_d \leq 2{,}00$ / L min^{-1} i $60 \leq N \leq 180$ / o min^{-1}.

Na Slici 2. prikazano je poređenje eksperimentalnih podataka za d_{32} u sistemu Eksol D-80-voda i računskih podataka dobijenih pomoću korelacije (4). Sa Slike 2. se može uočiti da se računski podaci za d_{32} nalaze u intervalu od ± 10 %.

Za slučaj prenosa mase iz dispergovane u kontinualnu fazu u jednoj studiji [9] primenjena je poznata univezalna jednačina Kumara i Hartlanda [13] za potrebe proračuna Sauterovog srednjeg prečnika kapi u ekstrakcionoj koloni Kini:

$$d_{32} = \frac{3{,}05\, e^{0,57}}{\left[\dfrac{1}{\left[2{,}49 \left(\dfrac{\sigma}{\Delta \rho g} \right)^{0,5} \right]^2} + \dfrac{1}{\left[0{,}52 \left(\varepsilon_d \right)^{-0,4} \left(\dfrac{\sigma}{\rho_c} \right)^{0,6} \right]^2} \right]^{0,5}} \quad (5)$$

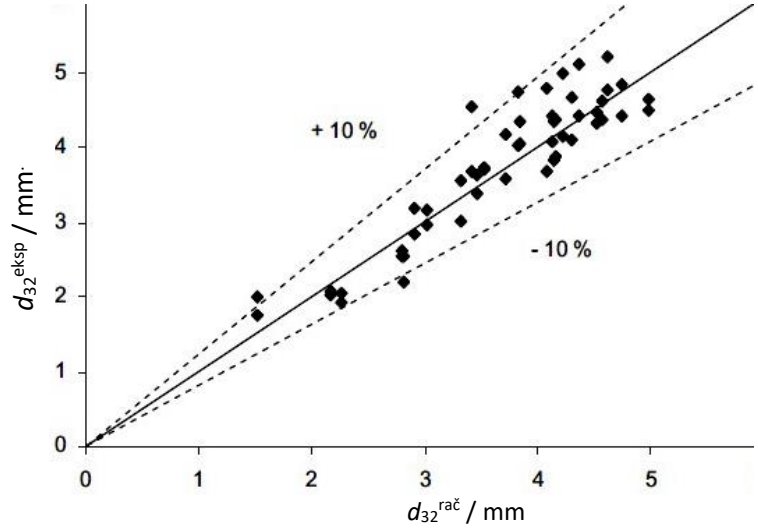

Slika 2. Poređenje eksperimentalnih (d_{32}^{eksp}) računskih ($d_{32}^{rač}$) podataka za Sauterov srednji prečnik kapi u sistemu Eksol D-80-voda (Preuzeto i prevedeno iz Oliveira i sar. [7]).
Figure 2. Compasion of experimental (d_{32}^{eksp}) and calculated ($d_{32}^{rač}$) data for the Sauter mean drop diameter in the Exxsol D-80-water system (Reproduced from Oliveira et al. [7])

Ispitivanja u ovom radu [9] su vršena u poluindustrijskoj ekstrakcionoj koloni tipa Kini, čije su geometrijske veličine bile: unutrašnji prečnik 11,7 cm, broj stupnjeva 10 i radna visina 75 cm. Dva separatora za odvajanje faza bila su prečnika 17,7 cm, a postavljena su na vrh i na dno kolone, redom. Istovremeno, korišćene su dve pumpe, jedna za kontinualnu a druga za dispergovanu fazu. Međufazna površina je automatski kontrolisana pomoću jednog optičkog senzora. U ovim istraživanjima, u ekstrakcionoj koloni su korišćeni dvofazni sistemi toluen-voda, n-butilacetat-voda i utvrđeno je da se kapi malih prečnika formiraju pri velikim vrednostima broja obrtaja rotora, što je rezultat povećanog razbijanja kapi dispergovane faze (Slika 3.). To znači da Sauterov srednji prečnik kapi značajno zavisi od broja brtaja rotora i međufaznog napona, dok je uticaj protoka dispergovane i kontinualne faze zanemarljiv. Koalescencija kapi pri velikim vrednostima broja obrtaja rotora se povećava zbog povećanja verovatnoće sudara kapi. To znači da se pri tim vrednostima broja obrtaja rotora stvaraju pogodni uslovi za razbijanje kapi, nakon čega se zatim veličina prečnika kapi postepeno stabilizuje.

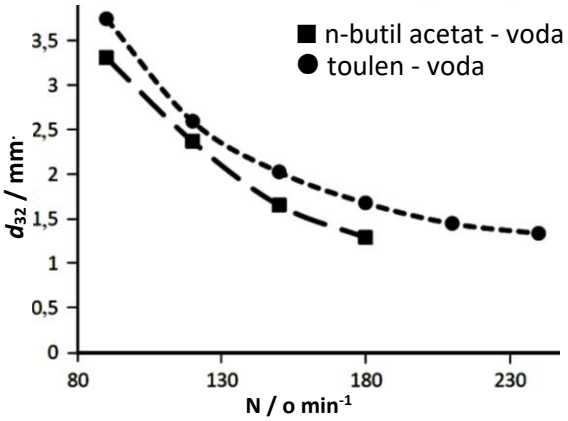

Slika 3. Uticaj broja obrtaja rotora (N) na Sauterov srednji prečnik kapi (d_{32}), $V_d = V_c = 24$ L h^{-1} (Preuzeto i prevedeno iz Shirvani i sar. [9])
Figure 3. Effect of the rotor speed (N) on the Sauter mean drop size (d_{32}), $V_d = V_c = 24$ L h^{-1} (Reproduced from Shirvani et al. [9])

S druge strane, na Slici 4. može se uočiti da povećanje brzine dispergovane faze relativno malo utiče na Sauterov srednji prečnik kapi, kao i da su srednji prečnici kapi značajno veći pri velikim vrednostima broja obrtaja rotora. Međutim, povećanje brzine dispergovane faze pozitivno utiče na formiranje većih kapi i veće učestalosti koalescencije.

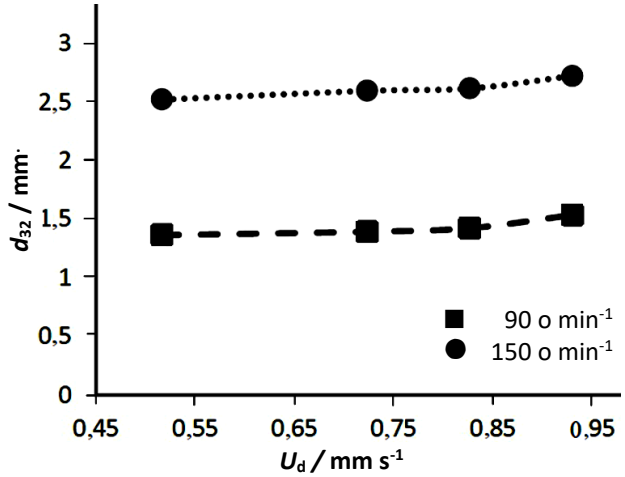

Slika 4. Uticaj brzine dispergovane faze (U_d) na Sauterov srednji prečnik kapi (d_{32}), V_c = 24 L h^{-1}, N –broj obrtaja rotora (Preuzeto i prevedeno iz Shirvani i sar. [9]) (sistem: n-butil acetat-voda).
Figure 4. Effect of the dispersed phase velocity (U_d) on the Sauter mean drop size (d_{32}), V_c = 24 L h^{-1}, N – the rotor speed (Reproduced from Shirvani et al. [9]) (system: n-butyl acetate-water)

U ovom istom istraživanju [9], razvijene su dve rigorozne empirijske korelacije koje su korišćene za predviđanje tačke plavljenja i Sauterovog srednjeg prečnika kapi, kod kojih su odstupanja računskih od eksperimentalnih rezultata bila 5,7 i 7,2 %, redom. Istovremeno, u radu je predložena i empirijska korelacija koja daje zavisnost srednjeg prečnika kapi od geometrije kolone, radnih parametara i fizičkih osobina dvofaznog sistema. Postignuto je dobro slaganje računskih i eksperimentalnih rezultata za sve radne uslove u koloni.

2. 2. Sadržaj dispergovane faze

U literaturi [14] su određene vrednosti sadržaja dispergovane faze u ekstrakcionoj koloni tipa Kini, pri čemu su korišćena tri dvofazna sistema: toluen-voda, n-butilacetat-voda i n-butanol-voda. Ispitivan je uticaj radnih parametara na hidrodinamičke karakteristike, i to, uticaj pravca prenosa mase rastvorka (aceton) između faza, broja obrtaja rotora i protoka dispergovane i kontinualne faze. U radu je još utvrđeno i da sadržaj dispergovane faze zavisi uglavnom od broja obrtaja rotora, pravca prenosa mase između faza i protoka dispergovane faze. U radu je razvijena univerzalna korelacija koja uključuje Frudov (Froude) broj, brzinu faza, kao i modifikovanu grupu koja sadrži geometrijske karakteristike ekstrakcione kolone za predviđanje sadržaja dispergovane faze. Primenom ove korelacije na dobijene eksperimentalne rezultate kao i rezultate preuzeteiz literature, zaključeno je da razvijena korelacija daje zadovoljavajuće predviđanje sadržaja dispergovane faze.

U drugoj studiji [6] eksperimentalno su određivani podaci za sadržaj dispergovane faze i relativnu brzina faza u poluindustrijskoj ekstrakcionoj koloni tipa Kini, pri čemu su korišćeni dvofazni sistemi toluen-aceton-voda i butil acetat-aceton-voda u slučaju kada nije postojao prenos mase između faza. Utvrđeno je da hidrodinamički parametri zavise od geometrije kolone, radnih parametara (broj obrtaja rotora i brzina kontinualne faze) i fizičkih karakteristika tečnih fluida u sistemu tečno-tečno, pri čemu se ovi parametri koriste u proračunima prenosa mase i protoka faza. Utvrđeno je da se sadržaj dispergovane faze povećava s porastom efekta mešanja u dvofaznom sistemu i odnosa protoka faza.

3. PRENOS MASE

3. 1. Koeficijent prenosa mase

Koncentracioni profili faza u Kini koloni su simulirani pomoću modela povratnog mešanja da bi se dobio stvarni koeficijenti prenosa mase koji su bili u funkciji Rejnoldsovog broja za pojedinančnu kap dispergovane faze [15]. Za date uslove međufaznog kontakta, koeficijent prenosa mase je zavisio samo od broja obrtaja rotora odnosno intenziteta mešanja u koloni, što je navelo autore na zaključak da je uvećanje razmera uređaja moguće izvesti samo ukoliko je poznata zavisnost promene povratnog mešanja od prečnika kolone. U sistemu metilizobutil keton (MIBK)-aceton-voda

u ekstrakcionoj koloni tipa Kini (prečnika 7,2 cm, 25 stupnjeva) su eksperimentalnio određeni koncentracioni profili obe faze, pri čemu su primenom modela povratnog mešanja numerički računati parametri prenosa mase i povratnog mešanja [16]. Konstatovano je da je povratno mešanje u kontinualnoj fazi relativno veliko, a u dispergovanoj fazi zanemarljivo. Iz ovog se može zaključiti da prisustvo povratnog mešanja u kontinualnoj fazi negativno utiče na brzinu prenosa mase između faza.

Koeficijenti prenosa mase su određivani u ekstrakcionoj koloni tipa Kini, prečnika 11,7 cm, visine 70 cm, broja stupnjeva 10, prečnika turbinskih mešalica 5 cm, a slobodna površina statora je bila 21,2 %, pri čemu su korišćena dva različita sistema tečno-tečno: toluen-aceton-voda i n-butilacetat-aceton-voda [17]. Na eksperimentalne rezultate koncentracije rastvorene komponente, primenjen je model aksijalne difuzije radi određivanja ukupnog zapreminskog koeficijenta prenosa mase u zavisnosti od radnih parametara (broj obrtaja rotora i protoci kontinualne i dispergovane faze). Iz tako određenih vrednosti ukupnog zapreminskog koeficijenta prenosa mase izračunate su vrednosti faktora poboljšanja prenosa mase koji predstavlja faktor povećanja koeficijenta difuzije dajući efektivni koeficijent difuzije. U radu je razvijena empirijska korelacija za proračun ovog faktora u zavisnost iod Rejnoldsovog broja i sadržaja dispergovane faze. Predviđanje vrednosti ukupnog koeficijenta prenosa mase na osnovu ove korelacije primenjene u prethodno predloženoj korelaciji u literaturi [18] je dalo dobro slaganje sa eksperimentalnim rezultatima. Ista ekstrakciona kolona i isti sistem tečno-tečno [17] su primenjeni za određivanje ukupnog zapreminskog koeficijenta prenosa mase u zavisnosti od radnih parametara (broj obrtaja rotora, pravac prenosa mase i protoci obe faze) [5]. I ovde je dobijeno da karakteristike prenosa mase strogo zavise od broja obrtaja rotora i pravca prenosa mase, s tim da postoji relativno mala zavisnost od protoka faza. U radu je razvijena empirijska korelacija za predviđanje ukupnog Šervudovog (Sherwood) broja u kontinualnoj fazi u zavisnosti od sadržaja dispergovane faze, Rejnoldsovog broja i pravca prenosa mase. Razvijena empirijska korelacija se zasniva na bezdimenzionalnim brojevima, odnosno data je kao kriterijalna jednačina za prenos mase i može se koristiti kao pogodan alat kod projektovanja ekstrakcionih kolona tipa Kini:

$$\mathrm{Sh}_{oc} = 4{,}89 + 2{,}19\ \mathrm{Re}\left(1-\varepsilon_d\right)^{0{,}65}\ \ (\mathrm{d}\rightarrow\mathrm{c}) \tag{6}$$

$$\mathrm{Sh}_{oc} = 5{,}19 + 5{,}39\ \mathrm{Re}\left(1-\varepsilon_d\right)^{0{,}46}\ \ (\mathrm{d}\rightarrow\mathrm{c}) \tag{7}$$

pri čemu oznaka (d → c) predstavlja pravac prenosa mase iz dispergovane u kontinualnu fazu, dok oznaka (c → d) predstavlja pravac prenosa mase iz kontinualne u dispergovanu fazu. Veličina ε_d predstavlja sadržaj dispergovane faze u disperziji.

Na slici 5. prikazana je zavisnost ukupnog zapreminskog koeficijenta prenosa mase od brzine dispergovane faze (U_d) za dvofazni sistem toluen-aceton-voda dobijena u ovom radu [5]. Sa slike se može videti da ovaj koeficijent ($K_{oc}a$) raste pri povećanju brzine kontinualne faze (U_d), kao i pri povećanju broja obrtaja rotora (N).

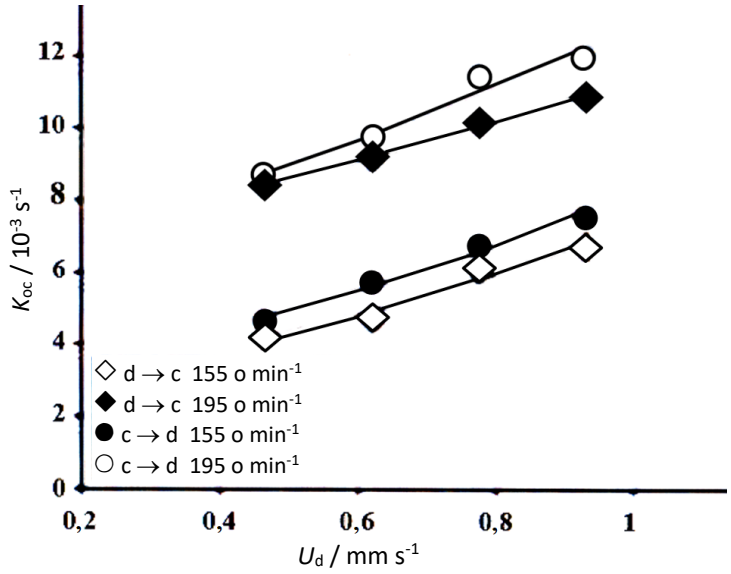

Slika 5. Zavisnost ukupnog zapreminskog koeficijenta prenosa mase (K_{oc} a) od brzine dispergovane faze (U_d) za različite vrednosti broja obrtaja rotora (N) i oba pravca prenosa mase za sistem toluen-aceton-voda (Preuzeto i prevedeno iz Asadollahzadeh i sar. [5]). Oznaka (c → d) predstavlja pravac prenosa mase iz kontinualne u dispergovanu fazu, dok oznaka (d → c) predstavlja pravac prenosa mase iz dispergovane u kontinualnu fazu.

Figure 5. Dependence of the overall volumetric mass transfer coefficient (K_{oc} a) on the dispersed phase velocity (U_d) for different rotor speeds (N) for the system toluene-acetone-water (Reproduced from Asadollahzadehet al. [5]). The notation (c → d) represents the mass transfer direction from the continuous to the dispersed phase, while the notation (d → c) represents the mass transfer direction from the dispersed to the continuous phase.

Slaganje eksperimentalnih i računskih podataka dobijenih pomoću korelacija (6) i (7) prikazano je na Slici 6., pri čemu je relativno odstupanje rezultata bilo 3,75 % [5].

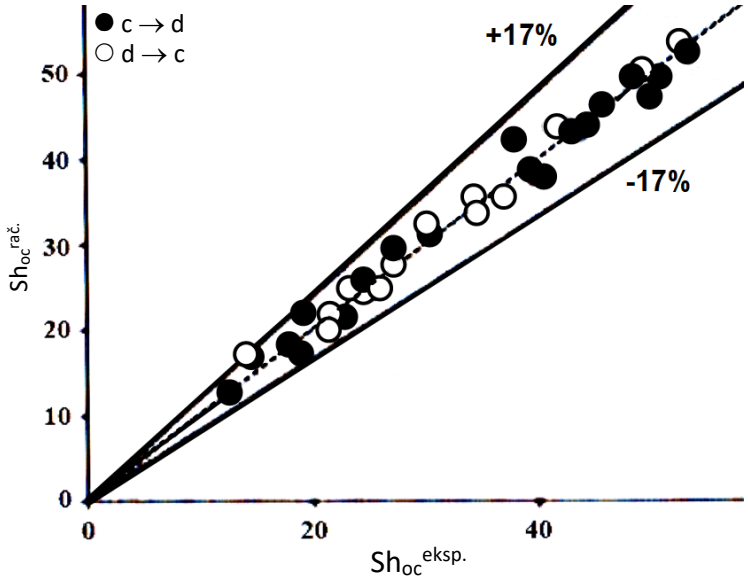

Slika 6. Poređenje eksperimentalnih($Sh_{oc}^{eksp.}$)i računskih ($Sh_{oc}^{rač.}$) podataka za Šervudov broj, redom, u sistemu toluen- aceton-voda (Preuzeto i prevedeno iz Asadollahzadeh i sar. [5]). Oznaka (c ⟶ d) predstavlja pravac prenosa mase iz kontinualne u dispergovanu fazu, dok oznaka (d ⟶ c) predstavlja pravac prenosa mase iz dispergovane u kontinualnu fazu.
Figure 6. Comparison of experimental ($Sh_{oc}^{eksp.}$) and calculated ($Sh_{oc}^{rač.}$) results for the Sherwood number, respectively, in the toluene-acetone-water system (Reproduced from Asadollahzadeh et al[5]).The notation (c → d) represents the mass transfer direction from the continuous to the dispersed phase, while the notation (d → c) represents the mass transfer direction from the dispersed to the continuous phase.

4. ZAKLJUČAK

U ovom radu su prikazani rezultati analize literaturnih podataka o hidrodinamici i prenosu mase u ekstrakcionim kolonama tipa Kini, pri čemu su korišćeni različiti dvofazni sistemi tečno-tečno. Prikazan je uticaj hidrodinamičkih parametara na Sauterov srednji prečnik kapi i sadržaj dispergovane faze u radnom delu kolone. Utvrđeno je da se Sauterov prečnik kapi smanjuje pri povećanju brzine obrtanja rotora, kao i pri povećanju međufaznog napona, dok je nezavisan od protoka faza. S druge strane, konstantovano je da sadržaj dispergovane faze uglavnom zavisi od broja obrtanja rotora i protoka dispergovane faze. Konstatovano je, takođe, da se sadržaaj dispergovane faze povećava s porastom efekta mešanja u dvofaznom sistemu i s povećanjem odnosa protoka faza. U literaturi je prikazano nekoliko empirijskih relacija koje se koriste za proračun srednjeg prečnika kapi, a zavise od radnih parametara, geometrije kolone i fizičkih katakteristika dvofazniog sistema. Predložene empirijske korelacije, preuzete iz literature, se mogu koristiti za predviđanje konačne vrednosti Sauterovog srednjeg prečnika i maksimalnog kapaciteta kolone. Pokazano je da koeficijent prenosa mase zavisi od broja obrtanja rotora i pravca prenosa mase, kao i od veličine povratnog mešanja, koje je funkciji prečnika kolone. S druge strane, koeficijent prenosa mase relativno malo zavisi od protoka faza. U literaturi je predložena empirijska kriterijalna jednačina za određivanje koeficijenta prenosa mase, koja se zasnivana bezdimenzionalnim brojevima i može se koristiti kao pogodan alat kod predskazivanja koeficijenta prenosa mase i pojektovanja ekstrakcionih kolonatipa Kini.

Poznavanje vrednosti hidrodinamičkih parametara i karakteristika prenosa mase u ekstrakcionim kolonama tipa Kini je od interesa za projektovanje ovih kolona. Proučavanje naučnih radova iz literature, koji su prikazani i kritički analizirani u ovom radu, a odnose se na određivanje nekih hidrodinamičkih parametara i koeficijenta prenosa mase, može biti od značaja istraživačima koji se bave projektovanjem i dizajnom kolonskih ekstraktora ovog tipa.

Lista oznaka

a / m^2 m^{-3} - međufazna površina
C_1 - empirijski parametar u jednačini (3)
c - kontinualna faza
D_c / m - prečnik kolone
D_s / m - prečnik otvora statora
d - dispergovana faza
d_e / m - ekvivalentni prečnik
d_i / m - srednji prečnik kapi u određenom intervalu i
d_1, d_2 / m - dužina minimalne i maksimalne ose eliptične kapi, redom
d_{32} / m - Sauterov srednji prečnik kapi
E - broj stupnjeva u koloni
E_c / m^2 s^{-1} - koeficijent molekulske difuzije
Fr - Frudov (Froude) broj, Fr = U_c^2 / $d_{32}g$
e - slobodna površina statora, e = (D_s / D_c)^2
K_{oc} / m s^{-1} - ukupan koeficijent prenosa mase
$K_{oc}a$ / s^{-1} - ukupan zapreminski koeficijent prenosa mase
N / o min^{-1} - broj obrtaja mešalice (rotora)
NN - ukupan broj tačaka
Re - Rejnoldsov (Reynolds) broj za kontinualnu fazu, Re =$U_s d_{32} r_c$ / μ_c
Re_R - Rejnoldsov broj baziran na brzini obrtanja rotora
U_c, U_d / m s^{-1} - brzina kontinualne i dispergovane faze, redom
U_s / m s^{-1} - relativna brzina faza, U_s = (U_d / ε_d) + (U_c / (1 - ε_d))
Sh_{oc} - ukupan Šervudov (Sherwood) broj za kontinualnu fazu, Sh_{oc}= K_{oc} d_{32} /E_c
V_c, V_d / m^3 s^{-1} - protoci kontinualne i dispergovane faze, redom

Oznake grčkim slovima

ε_d - sadržaj dispergovane faze u disperziji
ρ_d / kg m^{-3} - gustina dispergovane faze
μ_c / Pa s - dinamička viskoznost kontinualne faze
ρ_c / kg m^{-3} - gustina kontinualne faze
$\Delta\rho$ / kg m^{-3} - razlika gustina, $\Delta\rho$ = (ρ_c - ρ_d)
σ / N m^{-1} - međufazni napon.

REFERENCES

[1] Perry RH, Green DW. (eds.). *Perry`s Chemical Engineers Handbook,* 7th ed., McGraw-Hill, Inc., New York, NY: 1999, pp. 15-37 ÷ 15-47.
[2] Pratt HRC, Stevens GW. in *Science and Practice of Liquid-Liquid Extraction,* Thornton, JD. ed., Oxford University Press, London: 1992, pp. 492-589.
[3] Simons AJF. in *Handbook of Solvent Extraction*, Lo, TC, Baird, MHI, Hanson, C, eds., John Wiley & Sons, New York, NY: 1983, pp. 343-353.
[4] Sovilj MN. *Difuzione operacije*, Univerzitet u Novom Sadu, Tehnološki fakultet, Novi Sad: 2004, str. 172-193 (in Serbian).
[5] Asadollahzadeh M, Torkaman R, Torab-Mostaedi M, Experimental determination of continuous phase overall mass transfer coefficients case study: Kühni extraction column. *Iran J Chem Eng*. 2017; 36 (5): 149-161.
[6] Arab E, Ghaemi A. Experimental study of holdup and slip velocity in a Kühni extraction column. *Farayandno*, 2017; 12 (58): 70-85.
[7] Oliveira NS, Morales Silva D, Gondim MPC, Borges Mansur MA. A study of the drop size distributions and hold-up in short Kühni columns. *Brazil J Chem Eng*. 2008; 25 (4): 729 – 741.
[8] Pietsch W, Pilhofer T. Calculation of the drop size in pulsed sieve-plate extraction columns. *Chem Eng Sci.* 1984; 39 (6): 961-965.
[9] Shirvani AR, Ghaemi A, Torab-Mostaedi M. Experimental investigation of flooding and drop size in a Kühni extraction column. IJE Trans C.: Aspects. 2016; 29 (3): 288-296.
[10] Usman MR, Sattar H, Hussain SN, Muhammad H, Asghar A, Afzal W. Drop size in a liquid pulsed sieve-plate extraction column. *Brazil J Chem Eng.* 2009; 26(4): 677-683.
[11] Bailes PJ, Gledhill J, Godfrey J C, Slater M J. Hydrodynamic behavior of packed, rotating disc and Kühni liquid-liquid extraction columns. *Chem Eng Res Des.* 1986; 64: 43-55.
[12] Chang-Kakoti DK, Fei W-Y, Godfrey J C, Slater M J. Drop sizes and distributions in rotating disc contactors used for liquid-liquid extraction. *J Sep Process Technol.* 1985; *6:* 40- 48.

[13] Kumar A, Hartland S. Unified correlations for the prediction of drop size in liquid-liquid extraction columns. *Ind Eng Chem Res.* 1996; 35 (8): 2682-2695.
[14] Asadollahzadeh M, Torab-Mostaedi M, Shahhosseini S, Ghaemi A, Torkaman R. Unified new correlation for prediction of dispersed phase holdup in agitated extraction c*olumns. Separ Purif Technol*. 2016; 158: 275-285.
[15] Kumar A, Hartland S. Mass transfer in a Kühni extraction column. *Ind Eng Chem Res*. 1988; 27 (7): 1198-1203.
[16] Dongaonkar KR, Pratt HRC, Stevens GW. Mass transfer and axial dispersion in a Kühni extraction column. *AIChE J*, 1991; 37 (5): 694-704.
[17] Hemmati A, Torab-Mostaedi M, Asadollahzadeh M. Mass transfer coefficients in a Kühni extraction column. *Chem Eng Res Des*. 2015; 93: 747-754.
[18] Johnson AI, Hamielec AE. Mass transfer inside drops. *AIChE J.* 1960; 6: 145-149.

ABSTRACT

Hydrodynamics and mass transfer in Kühni extraction columns

Milan N. Sovilj[1] i Momčilo Đ. Spasojević[2]

[1]*University of Novi Sad, Faculty of Technology, Bulevar Cara Lazara 1, Novi Sad, Serbia*
[2]*University of Novi Sad, Faculty of Technical Sciences, Trg Dositeja Obradovića 6, Novi Sad, Serbia*

(Technical paper)

This work provides a review of hydrodynamic characteristics and mass transfer in the Kühni extraction columns. The experiments, as reported in the literature, were performed in the presence and absence of mass transfer. The results showed that the Sauter mean drop diameter was strongly affected by the rotor speed and interfacial tension, whereas the effects of the dispersed and continuous velocities were negligible. Empirical correlations for the Sauter mean drop diameter, taken from the literature, were discussed. It was experimentally determined that the dispersed-phase holdup depended to a great extent on the rotor speed, mass transfer direction between the phases, physical characteristics of fluids in the liquid-liquid system, and the dispersed-phase flowrate whereas it increased with the increase in mixing in the two-phase system and the ratio of phase flowrates. On the other hand, it has been shown that the mass transfer rate increases with increasing the level of back mixing. It was found that the mass transfer coefficient depends on the rotor speed and the direction of mass transfer between the phases. At the same time, it has been shown that the mass transfer coefficient depends relatively little on the phase flowrates. An empirical correlation was proposed for prediction of the overall mass transfer coefficient based on dimensionless numbers. Also, novel empirical correlations for prediction of the Sherwood number in the continuous phase were presented based on the dispersed-phase holdup, Reynolds number, and mass transfer direction between the phases. Empirical correlations based on dimensionless numbers can be considered as a useful tool for the design of the Kühni columns.

Keywords: Sauter mean drop diameter, dispersed-phase holdup, rotor speed, axial mixing, mass transfer.

Microbial bioremediation of heavy metals

Ana Volarić[1], Zorica Svirčev[1], Dragana Tamindžija[2] and Dragan Radnović[1]

[1]University of Novi Sad, Faculty of Sciences, Department of Biology and Ecology, Trg Dositeja Obradovića 2, Novi Sad, Serbia
[2] University of Novi Sad, Faculty of Sciences, Department of Chemistry, Biochemistry and Environmental Protection, Trg Dositeja Obradovića 3, Novi Sad, Serbia

Abstract

Heavy metal pollution is one of the most serious environmental problems, due to metal ions persistence, bioavailability, and toxicity. There are many conventional physical and chemical techniques traditionally used for environmental clean-up. Due to several drawbacks regarding these methods, the use of living organisms, or bioremediation, is becoming more prevalent. Biotechnological application of microorganisms is already successfully implemented and is in constant development, with many microbial strains successfully removing heavy metals. This paper provides an overview of the main heavy metal characteristics and describes the interactions with microorganisms. Key heavy metal resistance mechanisms in microorganisms are described, as well as the main principles and types of heavy metal bioremediation methods, with details on successful pilot scale bioreactor studies. Special attention should be given to indigenous bacteria isolated from the polluted environments since such species are already adapted to contamination and possess resistance mechanisms. Utilization of bacterial biofilms or consortia could be advantageous due to higher resistance and a combination of several metabolic pathways, and thus, the possibility to remove several heavy metals simultaneously. Novel technologies covered in this review, such as nanotechnology, genetic engineering, and metagenomics, are being introduced to the field of bioremediation in order to improve the process. To conclude, bioremediation is a potentially powerful solution for cleaning the environment.

Keywords: biotransformation; pollution; biotechnology; heavy metal resistance.

Available on-line at the Journal web address: http://www.ache.org.rs/HI/

REVIEW PAPER

UDC: 504.5+549.25:351.777.6

Hem. Ind. **75 (2)** 103-115 (2021)

1. INTRODUCTION

As a result of industrialization, the environment is being polluted with various types of hazardous wastes. Microorganisms have a crucial role in the pollutants fate in the environment, as they play a part in pollutant transport, distribution, properties, transformation, and mineralization. They have been successfully used for remediation of various types of environmental pollutants, including diverse organic compounds as well as heavy metals [1,2]. Organic compounds can be completely degraded by the microbial metabolism, resulting in the removal from the environment. Contrary, heavy metals persist in the environment due to their non-degradable nature [3]. As such, heavy metals cannot be completely degraded or eliminated, but only transformed by a microbial activity to a less toxic, bioavailable, or mobile form. Microorganisms can also adsorb and accumulate metals inside the cells, which can then be more easily removed from the contaminated environment. Thus, microorganisms are a valuable asset in combat against widespread pollution, with significant practical applicability.

In total, there are 53 heavy metals. Out of these, 22 are of some biological importance. Due to low solubility, tin (Sn), cerium (Ce), gallium (Ga), zirconium (Zr), and thorium (Th) do not exhibit biological influence. Trace elements with low toxicity and important roles in physiological, biochemical, and metabolic processes in living organisms (*e.g.* co-factors for some enzymes, micronutrients, regulators of osmotic pressure, etc.) are iron (Fe), molybdenum (Mo), and manganese (Mn). Heavy metals zinc (Zn), nickel (Ni), copper (Cu), vanadium (V), cobalt (Co), wolfram (W), and chromium

Corresponding author: Dragana Tamindžija; University of Novi Sad, Faculty of Sciences, Department of Chemistry, Biochemistry and Environmental Protection, Trg Dositeja Obradovića 3, Novi Sad, Serbia
E-mail: dragana.cucak@dh.uns.ac.com
Paper received: 15 September 2020
Paper accepted: 21 March 2021
https://doi.org/10.2298/HEMIND200915010V

(Cr) are considered toxic with high to moderate importance as trace elements. Arsenic (As), silver (Ag), antimony (Sb), cadmium (Cd), mercury (Hg), lead (Pb), and uranium (U) have limited beneficial functions and are considered toxic [4]. The most common metals found in the contaminated areas are lead (Pb), chromium (Cr), arsenic (As), zinc (Zn), cadmium (Cd), copper (Cu), and mercury (Hg) [5]. Most heavy metals are naturally present in the environment originating from pedogenetic processes of weathering of parent materials and are usually found in trace amounts in insoluble forms, not available for uptake by living organisms. Various anthropogenic activities are causing the disturbance and acceleration of slowly occurring natural geochemical cycles of metals, leading to accumulation of one or more heavy metals at concentrations higher than defined background values [6]. With the rapid expansion of many industries (*e.g*. mining, surface finishing, energy and fuel production, metallurgy, electroplating, *etc.*), wastes containing heavy metals are discharged into the environment [7]. Some heavy metals essential for plant growth (*e.g*. Cu, Mn, Co, Fe, Mo, Ni, and Zn) are introduced to soil in the form of fertilizers. Fertilizers can contain trace amounts of other heavy metals, such as Cd and Pb [6]. Several common pesticides used extensively in the past were based on the compounds containing Cu, Hg, Mn, Pb, or Zn. Certain animal wastes such as solids or slurries used in agriculture as fertilizers can contain elevated levels of Cu and Zn, which act as growth promoters in the pig and poultry industry. Long-term irrigation with wastewater containing low heavy metal concentrations can lead to accumulation of metals in soil.

2. INTERACTION OF HEAVY METALS WITH MICROORGANISMS

Microbial populations are often capable of surviving environmental stresses caused by accumulation of heavy metals, through the selection of the fittest and formation of heavy metal tolerant and/or resistant microbial populations [8]. Toxicity of metals, among other factors, depends on their chemical speciation, bioavailability, absorbed dose, route of exposure, and characteristics of the exposed individual [9,10]. Metal speciation and bioavailability are very important from the aspect of biological interactions. The speciation of any metal in nature depends on the combined effects of pH, redox potential, and ionic strength. Bioavailability of metals is a complex phenomenon, influenced by many physical, chemical, and biological factors such as pH, eH, ion exchange capacity, organic matter content, clay content, presence of ligands, metal concentration, and speciation [16,17].

Some heavy metals are essential for the normal function of a microbial cell, such as iron and copper contained in cytochrome c oxidase [13], and manganese, which is important for oxygen production during photosynthesis [14]. However, metals can be very toxic to cells, as a result of their affinity to bind to many cellular components, which can lead to cell membrane disruption, DNA damage, inhibition of transcription and translation, inhibition of enzymatic activities, protein denaturation, and inhibition of cell division. Environmental pollution caused by the heavy metal release can change microbial soil communities, with an inhibitory effect on microorganisms in most cases [15]. Some studies found that the culturable number of various microbial groups in the contaminated soil samples is decreased, compared to a number in uncontaminated samples [16]. Contrary, other studies did not find a statistically significant correlation between the metal concentration in soil (Cr) and cultivable bacteria count nor with the percentage of chromate tolerant cultivable bacteria [17,18]. The functional diversity and composition of the microbial community can be also assessed by using the Biolog-Microplate method [19], restriction fragment length polymorphism (RFLP) based on 16S rRNA sequence of microbes [20,21] as well as the PCR-DGGE analysis [22]. In a polluted environment, the response of microbial communities is determined by the metal type, nature of the substrate (pH, for example, which affects metal bioavailability), and microorganism species. In some cases strains both from polluted and clean environments have a similarly high level of heavy metal resistance indicating the presence of constitutive or intrinsic resistance mechanisms [23]. Microbial resistance mechanisms can be encoded by chromosomal or mostly, plasmid genes [24,25]. Microorganism species that possess plasmid-encoded resistance mechanisms are more important for eventual applications in bioremediation because those genes can easily become available for other microbial species through the horizontal gene transfer. There are five main heavy metal resistance mechanisms (Fig. 1): (I) extracellular (permeability) barrier, (ii) oxidation/reduction of heavy metal ions, (iii) intracellular sequestration, (iv) extracellular sequestration, and (v) efflux (active transport) of metal ions [26].

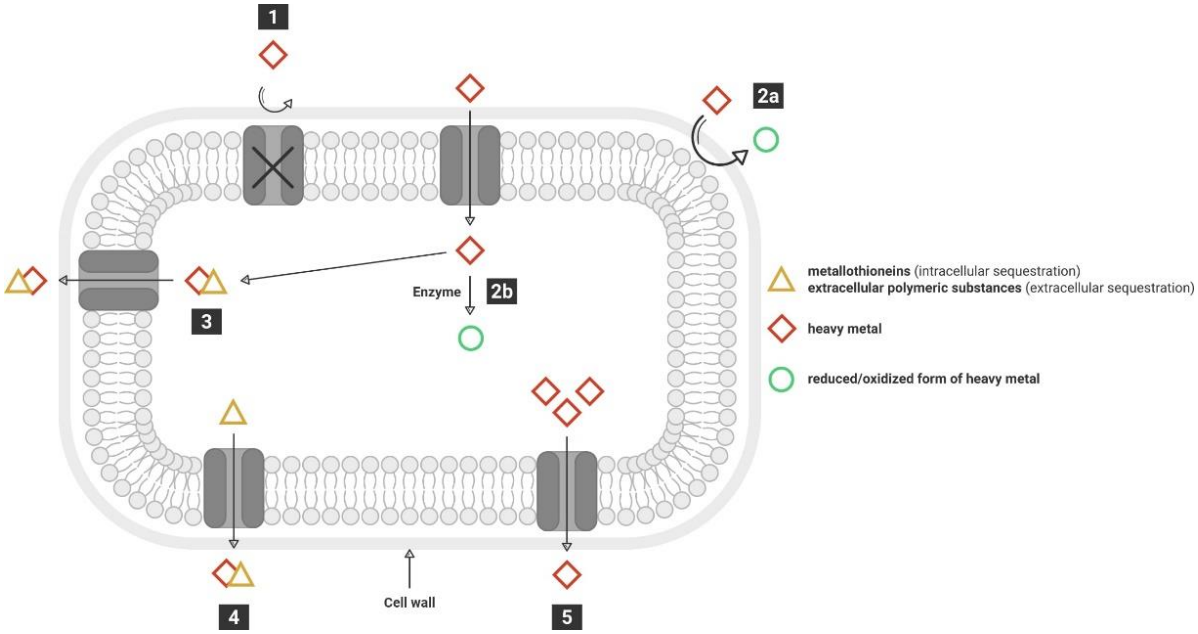

Figure 1. Five main heavy metal resistance mechanisms: (1) extracellular barrier – mutation of gene involved in transport; (2a) extracellular enzymatic oxidation/reduction; (2b) intracellular enzymatic oxidation/reduction; (3) intracellular sequestration; (4) extracellular sequestration; (5) efflux of metal ions.

Extracellular barrier, including cell membrane, cell wall, and extracellular polymers, is responsible for metal resistance by preventing the entrance of metal ions inside the cell [27]. Living or dead bacterial cells can adsorb metal ions by binding them to different moieties of the cell wall or capsule (carboxyl, amino, phosphate, and hydroxyl groups) [28]. Changes in the plasma membrane permeability, such as mutations of genes involved in transport, could prevent the entry of metal ions in the cell [29]. **Efflux or active transport of metal ions** outside of the cell is a widely present heavy metal resistance mechanism, which prevents accumulation of toxic ions inside the cell [29]. Following the metal uptake, some microorganisms sequestrate metal ions **intracellularly** using cysteine-rich peptides, called metallothioneins [26,30]. After the sequestration, the complexed metal can be transported out of the cell or stored in intracellular granules. **Extracellular sequestration** of metals can be carried out by binding to extracellular polymeric substances (EPS) or some other electronegative components of the cell membrane [31,32], metal precipitation [27], and with the help of biosurfactants and siderophores [31]. **Oxidation and reduction** lead to the formation of less toxic metal forms. In some metals higher oxidation state is more toxic (*e.g*. Hg, Cr, Se), while in others a higher state is less toxic (*e.g*. As). Many species, such as *Bacillus cereus*, *Bacillus subtilis*, *Pseudomonas aeruginosa*, *Pseudomonas fluorescens,* and *Escherichia coli*, are capable of reducing highly toxic hexavalent chromium to its biologically inert, less toxic trivalent form [8,17,33-38]. Besides chromium, it is reported that bacteria can reduce mercury [39], iron [40], arsenic [41], uranium [42], manganese [43], molybdenum [44], and other metals, and oxidize As [45,46].

3. REMOVAL OF HEAVY METALS FROM THE ENVIRONMENT

3. 1. Conventional remediation techniques

Physico-chemical remediation techniques such as excavation and disposal to a landfill, the containment of contaminated areas, incineration, chemical oxidation or reduction, extraction of pollutants with organic solvents, electroreclamation, and vitrification are already in use [47]. The excavation and disposal technique simply moves contaminated soil to another place and may create risks in excavation and transport of the contaminated soil [48]. Besides this, it is extremely hard to find new landfills for contamination disposal. The technique based on containing the contamination is a temporary solution, with the contamination remaining on site and requiring constant monitoring. A better approach would be to eliminate contaminants, or in the case of heavy metals, convert them to less toxic forms. However, those techniques can be very expensive, complicated, and they lack public acceptance. The most commonly

used techniques, in the case of heavy metal removal from the soil, are immobilization of metals by increasing the pH value, and the opposite process termed soil washing with acids, in order to increase metal solubility, followed by flocculation to remove metal ions [31]. In the case of sediment remediation, it is usually necessary to remove the sediment and treat it elsewhere, during which process the metal mobility and toxicity could be increased. Metal removal from aquatic systems can be achieved by using a wide range of techniques, including flocculation, precipitation, complexation, ion exchange, reverse osmosis, and electrochemical recovery. The downside of all techniques discussed is expensiveness, alongside with possible ineffectiveness, and negative ecological side effects.

3. 2. Bioremediation

Bioremediation is a process of biotransformation of the environment altered by contaminants, to its original state by using organisms to degrade pollutants [49]. The main focus is on the use of microorganisms and the variety of their metabolic processes to clean up the environment. The advantages of bioremediation are low cost and the use of natural processes for the pollution removal [50,51]. However, these processes can be time-consuming and affected by various environmental factors, such as climate and geological conditions [52]. Other drawbacks regarding applications of bioremediation processes are formation of possibly more toxic byproducts, limited effectiveness, and the specificity of biological processes [53]. As it was said earlier, heavy metals cannot be degraded, but only transformed from one oxidation form to another. When their oxidation state is altered, heavy metals can become (i) more water-soluble and removed by leaching, (ii) less toxic, (iii) less water-soluble, leading to their precipitation, or (iv) volatilized and removed from the contaminated area [49]. Distribution of heavy metals in the environment is regulated, to a large degree, by microbial activities [54]. Microorganisms used for bioremediation can be indigenous to the contaminated site, or isolated from elsewhere and introduced to the site [53]. The process of adding microorganisms to the site, in order to increase the removal of hazardous substances, is known as bioaugmentation [55]. For bioremediation to be successful, it is necessary to strictly control environmental conditions on the contaminated site (*i.e*. by adding the nutrients, controlling the temperature or the pH), due to the microbial sensitivity to even small fluctuations of some factors. There are two types of bioremediation (Fig. 2), based on the method of removal and transportation of toxic waste [53]:

1. ***In situ* bioremediation.** In this type of bioremediation, removal of the contaminated substrate is not needed. The process involves supplying oxygen and nutrients to the system to stimulate naturally occurring microbial population. *In situ* bioremediation can be intrinsic, based on the stimulation of indigenous microbial communities, and engineered, which involves the introduction of microorganisms to the site.

One of the biggest concerns associated with the treatment of heavy metals by *in situ* microbial reduction is the possibility of changes caused by environmental conditions that may influence metal speciation [56]. A reduced form of the metal in an ecosystem can be reoxidized by either physicochemical or biological processes, becoming toxic again. Therefore, it is important to monitor metal speciation to ensure that the chemical form does not change over time.

2. ***Ex situ* bioremediation.** This type of bioremediation requires excavation of the contaminated soil and sediment or pumping of the groundwater. Based on the state of the contaminant, *ex situ* bioremediation can be classified as:
   - *solid phase system* - includes organic (leaves, animal manures, and agricultural wastes) and problematic wastes (domestic and industrial wastes, sewage sludge, and municipal solid wastes). This kind of treatment includes landfarming, composting, and biopiles.
     Landfarming is a simple process that includes excavation of the contaminated soil, spreading it over a prepared bed, and tilling until the pollutants are degraded. It is based on the stimulation of indigenous microbial communities and their aerobic activities in the superficial layer of the soil.
     Composting involves mixing of the contaminated soil with organic wastes (such as manure and agricultural waste), which provide nutrients for microorganisms.
     Biopiles presents a hybrid method of landfarming and composting.
   - *slurry phase system* – the contaminated substrate is mixed with water in a large tank (bioreactor) at constant mixing in order to keep the microorganisms in contact with the pollutants. This kind of bioremediation can be performed by processes in bioreactors, or by bioventing, biosparging, and bioaugmentation.

Bioreactors. In bioreactors, bioremediation of soil, sediment, water, or sludge is conducted through an engineered containment system, which enables greater biodegradation, due to easily manageable conditions.
Bioventing. This technique is based on pumping of air and nutrients through wells to the contaminated soil into the unsaturated zone, in order to stimulate microbial communities.
Biosparging. Biosparging involves air injection below a water table to increase oxygen and nutrient levels in the saturated zone and groundwater, thus increasing the activity of microorganisms.
Bioaugmentation. This method is based on addition of microorganisms to the contaminated matrix, either indigenous or exogenous. Most soils after prolonged exposure to pollutants already possess a microbial community resistant to that pollution, in which case addition of exogenous microorganisms is not needed.

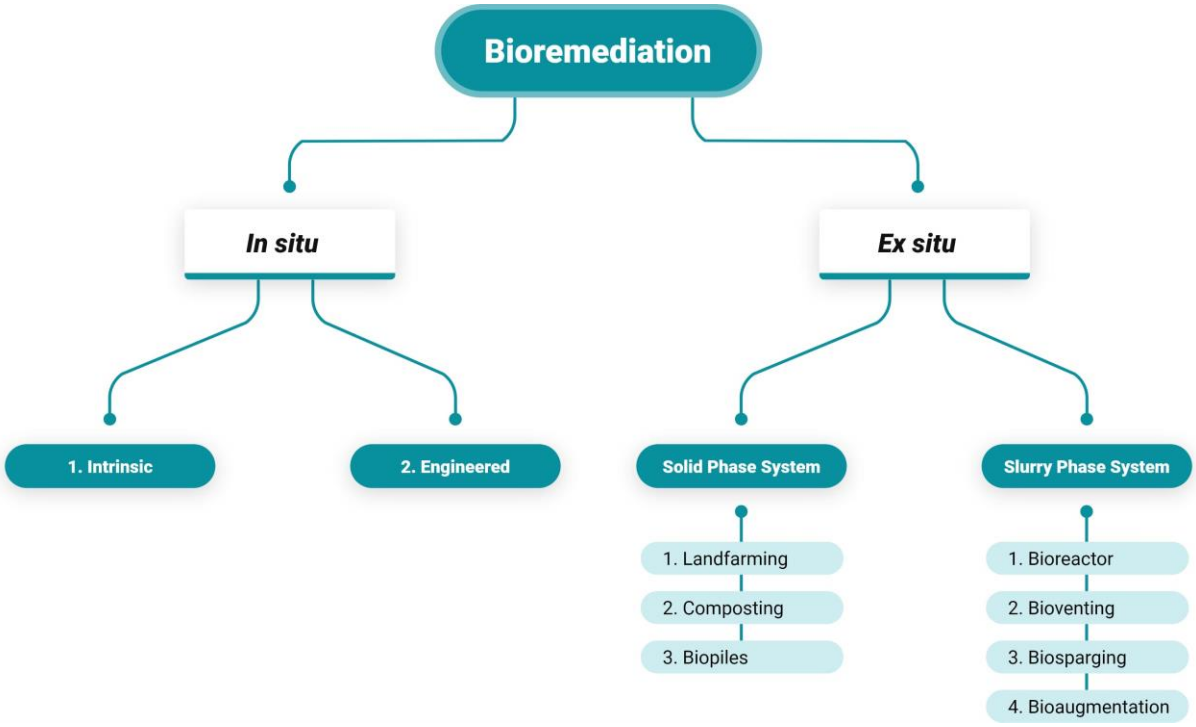

Figure 2. Overview of bioremediation methods.

3. 2. 1. Biotechnological applications of heavy metal resistant microorganisms

The ability to resist and detoxify heavy metals has been proven under laboratory conditions for many bacterial species, which can potentially be successfully used in bioremediation of heavy metal contamination. For successful design of a bioreactor system (Fig. 3) for heavy metal bioremediation, it is important to pay attention to the following factors: existence of a microbial population capable of detoxifying the contaminant, availability of the contaminant to the microbial cells, and the environmental factors, such as the type of soil, pH, temperature, and the presence of oxygen and nutrients [57]. Regarding the choice of the microbial population capable of heavy metal detoxification, use of the indigenous microorganisms would be the best solution, since they are already adapted to higher concentrations of heavy metals and other conditions in the contaminated substrate. In order to isolate such microorganisms, the soil, wastewater, or other samples that should be decontaminated from heavy metals, could be treated in a bioreactor. After the incubation, microorganisms could be isolated and used for creation of heavy metal resistant culture collections. To increase the number and variability of resistant microorganisms, some strains isolated from the other sources could be added into the culture collection. The best sources of heavy metal resistant microorganisms are mines, containing naturally high concentrations of various metals, and thus having highly resistant microbial communities. The use of a consortium consisting of resistant microorganisms could be more effective in heavy metal bioremediation than the use

of a single species or strain [58,59]. The main advantages of the consortium over single strains are a diversity of metabolic processes and resistance mechanisms, and the possibility to remove various heavy metals simultaneously.

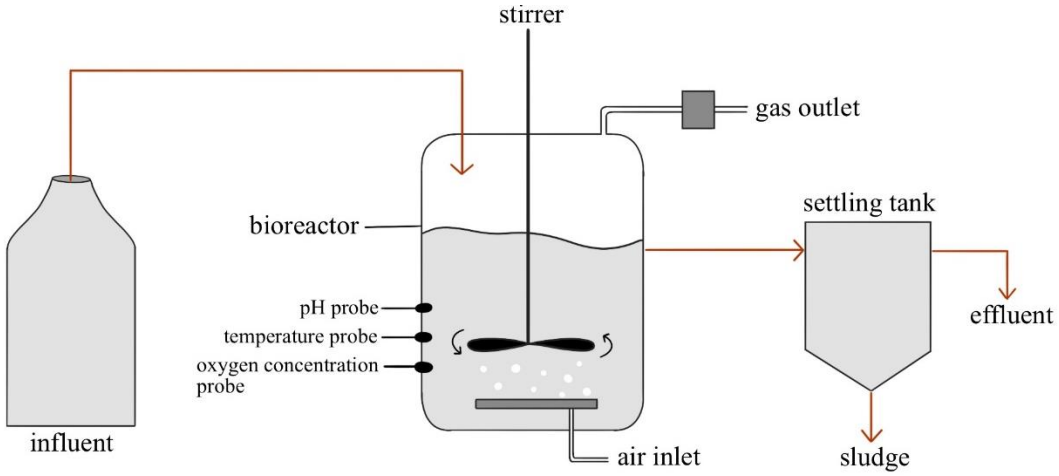

Figure 3. Scheme of a general bioreactor system for wastewater treatment

One of the successful studies was conducted on a continuous hexavalent chromium biological removal from wastewater by anaerobic-aerobic activated sludge process [60]. The bioreactor used in this study had two zones – aerobic, with the air pump, and anaerobic, with a stirrer, which are linked together by two holes on the bottom of the anaerobic tank. The influent containing hexavalent chromium is primarily added into the anaerobic tank, followed by passing through to the aerobic tank. In this experiment, a rapid increase in the chromium concentration in the effluent was observed during the first few days after the addition of higher Cr(VI) concentrations into the influent. After a short period of adaptation of the bacterial community to the new conditions, the concentration of chromium in the effluent significantly decreased, with the final values around 0 mg dm^{-3}. This system has been proven effective since the chromium removal efficiency was above 97% at influent Cr(VI) levels of 60 mg day^{-1}. From this experiment it can be concluded that for successful remediation by a continuous system, it is important to avoid sudden increases in the Cr(VI) concentrations in the influent, ensuring the effluent water quality.

Use of biofilms in bioremediation of heavy metals is also a very potent and promising method due to providing high biomass concentrations, while the bacteria can stay in the system for an unlimited time, thus providing a chance to adapt to various unfavorable conditions [61,62]. For the treatment of chromium solutions in one of the studies, *Arthrobacter viscosus* was chosen, due to its high production of exopolysaccharides and the ability of biofilm formation [61]. For the two tested concentrations of chromium of 10 and 100 mg dm^{-3} the removal efficiency was 100% during the first 26 days and 6 days, respectively. After that, the removal efficiency started to decrease. At the end of the experiment (226 days for 10 mg dm^{-3} and 104 days for 100 mg dm^{-3}), removal efficiencies were 36% and 38%, respectively. The authors of this study have concluded that with the increase in the chromium concentration, the removal ability decreases [61]. A possible explanation for this result is in the toxicity which hexavalent chromium has on living cells at high concentrations. Therefore, the influent concentration has to be optimized for each individual system. In order to improve the removal efficiency and activity period, biofilms are usually supported on some materials, such as granular activated carbon (GAC), zeolite, kaolin, etc. It was shown that even more successful could be combining these carriers, such as GAC and zeolite [63]. In this study, the chromium removal achieved by using an *Arthrobacter viscosus* biofilm supported on GAC was 19 %, similarly to the use of the biofilm supported on zeolite (18 %). However, better performances were reached when GAC and zeolite were used together (42 % of the Cr(VI) was removed). The main amount of the metallic ion in solution is adsorbed on GAC covered with biofilm. This allows more even distribution of the remaining ions on the surface of zeolite covered with biofilm. With zeolite not being as good adsorber as GAC, the combination of these two materials leads to the better heavy metal removal percentage [63].

In another study, it was shown that the bacterial strain *Acidithiobacillus ferooxidans* has the ability to completely remove hexavalent chromium at concentrations in the range 1 - 5 mg dm^{-3}, while the removal efficiency decreased to only 43% at 10 mg dm^{-3} Cr(VI) [64].

For the removal of arsenic in the form of arsenate (As^{5+}), a laboratory glass column was used as a fixed bed anaerobic reactor with commercially available sand as a biomass carriers [65]. The reactor was inoculated with sulfate-reducing bacteria, later proven to be the species of the genera *Desulfovibrio* and *Desulfomicrobium*. At first, under high sulfide concentrations arsenic was not removed, while after addition of 100 and 200 mg dm^{-3} Fe^{2+}, the arsenic removal increased to 63% and 80%, respectively. Further increase in the removal to ~96% was achieved by a decrease in the dissolved sulfide concentration and maintenance of the Fe^{2+} concentration at 200 mg dm^{-3} [65].

A completely automated pilot plant for the removal of mercury from industrial wastewater was designed and consisted of a pre-treatment and nutrient amendment units followed by a bioreactor and activated carbon filter, and supplied with measuring/control devices [66]. The plant was inoculated with 7 mercury-resistant *Pseudomonas* strains. Over the whole testing period of 8 months, 98% of the inflow mercury was removed [66].

Removal of mercury was also reported in a hybrid bioreactor for combined cadmium/mercury bioremediation [67]. This hybrid bioreactor comprised two systems: (i) anaerobic-anoxic-aerobic, and (ii) photoautotrophic, organized in 8 units: (1) depositional tank planted with macrophytes, (2) anaerobic tank, (3) overflow pool (used for reduction of suspended particles/materials), (4) settling tank (for further reduction of suspended materials), (5) anoxic bed, (6) aerobic bed, (7) clarification tank (also used for reduction of suspended materials), and (8) photoautotrophic system. The hybrid bioreactor supported both heterotrophic and autotrophic organisms and the presence of various bacterial species, *Cladophora* sp., diatoms, and cyanobacteria was observed. The average removal efficiencies achieved in this bioreactor were 79% for Cd and 62% for Hg. Advantages of this system are in mineralization of the sludge, its treatment by the photoautotrophic system, and conversion into organic fertilizer thus avoiding possible toxic sludge pollution.

A *Thiobacillus ferooxidans* strain was used for bio-dissolution of nickel-cadmium batteries in two percolator systems [68]. The first system was a sulfuric acid bioreactor with *T. ferooxidans* immobilized on elemental sulfur. The acidic medium produced in the first system was pumped to the second system containing Ni-Cd batteries. Extraction percentages at the end of the experiment were 100% for cadmium and 96.5% for nickel. This system has a great potential for use as a first step in recycling of nickel-cadmium batteries, thus preventing contamination arising from discarded batteries.

A laboratory scale anaerobic baffled bioreactor was successfully used for the treatment of acidic and zinc-containing wastewater [69]. The bioreactor was divided into four compartments and filled with sulfate-reducing bacteria. Throughout the process, the zinc removal efficiency was always higher than 99% achieved by Zn precipitation in the first compartment. Thus, a possibility for Zn recovery was provided without losing high amounts of sulfate-reducing bacteria, which may be reseeded from other compartments without a significant influence on the overall system [69].

A novel perspective approach in bioremediation is the next generation industrial biotechnology (NGIB) based on extremophilic bacteria [70]. The NGIB should overcome disadvantages of the current industrial biotechnology, such as heavy consumption of fresh water and energy, microbial contaminations, difficulty to develop fully automated processes, difficult and expensive product separation and purification, etc. The strains used in NGIB should be resistant to other microbial contaminations and grow rapidly under harsh conditions (*e.g*. very low or high temperatures, pH, osmotic pressure; growth on unusual substrates, or in the absence of water). Many bacterial groups, such as acidophiles, alkaliphiles, thermophiles, psychrophiles, xerophiles, methanotrophs, and halophiles possess one or more of the required characteristics and their biotechnological utilization is yet to be investigated.

Extremophilic microorganisms belonging to Archaea have been poorly studied in respect to bioremediation [71]. It is known that the strain *Sulfolobus acidocaldarius*, belonging to the domain Archaea, is capable of oxidizing arsenite to arsenate [72]. Another example of a heavy metal resistant Archaea is *Sulfolobus solfataricus*, having a mercury reductase [73]. It is necessary to further investigate this group of microorganisms, as it is possible that they would show greater efficacy in bioremediation under harsh conditions than the Eubacteria.

3. 2. 2. Novel technologies in bioremediation

Genetic engineering. Bioremediation with the use of genetically engineered bacteria is an emerging and promising technology based on addition of genes for metal homeostasis, survival in abiotic and biotic stresses, biodegradative enzymes, metal chelators and transport genes, metal uptake regulator genes, and risk-mitigating genes in the bacterial genome [74]. The advantage of such bacterial species is in the tolerance and resistance to heavy metal pollution. However, these species can be more vulnerable to impacts of various environmental stresses due to the addition of foreign genes. Besides, the competition for nutrients and other resources between genetically engineered and indigenous species can become a serious problem. Indigenous species can be superior because they are already adapted to the environmental conditions in the contaminated areas, and resistant strains are selected due to the exposure to heavy metal induced stress. On the other side, genetically engineered bacterial species can prevail because the addition of specific genes provides the advantage over the indigenous strains. The best solution is to use naturally occurring microorganisms for constructing the recombinant bacteria, because once genetically engineered, this species will have the same genetic base as the naturally occurring species, but will also be improved by the addition of the resistance genes. For example, cloning and expression of chromate efflux gene *chrA* from chromate resistant environmental isolate *B. pseudomycoides* in *B. subtilis* resulted in its improved survival [75]. A modified gene expression for metallothionein in *Ralstonia eutropha* CH34 led to improved bioremediation of cadmium under laboratory conditions [76]. Modifications in metalloregulatory protein ArsR in an *Escherichia coli* strain were shown to be responsible for successful bioremediation of arsenic in contaminated drinking water and groundwater [77]. A modified Hg^{2+} transporter in *E. coli* JM109 induced the increased resistance to mercury under laboratory conditions [78]. Modifications of genes encoding MerR, CadC, ZntR, P*mer*, P*cadA*, and P*zntA* proteins in *Pseudomonas fluorescens* OS8, *Escherichia coli* MC1061, *Bacillus subtilis* BR161, and *Staphylococcus aureus* RN4220 were shown to be responsible for cadmium, lead, zinc, and mercury biosensing in water-suspensions and extracts of soil [79].

Nanotechnology. Remediation of heavy metals can be achieved by the use of nanotechnology. A wide range of nanoparticles (iron, gold, silver, etc.) is known to enhance microbial activities with respect to bioremediation [80]. However, the use of toxic chemicals in the physical and chemical synthesis of nanomaterials is limiting applications of such materials in bioremediation. Nanoparticles produced by bacterial enzymatic activities are far more superior, exhibiting higher catalytic reactivity, better specific surface area, and improved contact between the enzyme and metal [81]. Nanoparticles are created by enzymatic processes when the bacteria uptake the metal ions from the environment and turn them into element metals. Biosynthesis of nanoparticles can be intracellular, following the uptake of metal ions, or extracellular, which involves trapping the metal ions on the cell surface, followed by enzymatic transformation. It was reported that *Rhodococcus* sp. can synthesize Au nanoparticles intracellularly [82], *Bacillus cereus* can synthesize Ag nanoparticles intracellularly [83], while magnetite is synthesized by *Shewanella oneidensis* extracellularly [84]. There are many other examples of nanoparticles synthesized by microbial activities [81]. Such nanoparticles can be used for the removal of heavy metals. For example, iron nanoparticles, among the mostly used nanoparticles in bioremediation, can reduce highly toxic hexavalent chromium into its innocuous trivalent form [85–87]. Bimetal oxide magnetic nanomaterials ($MnFe_2O_4$ and $CoFe_2O_4$) have shown higher adsorption capacity and removal of As^{3+} and As^{5+} than Fe_3O_4, possibly due to the increased content of surface hydroxyl groups in bimetal oxide nanoparticles [88]. Also, it was reported that the removal of Pb^{2+} from wastewater can be achieved rapidly *via* adsorption onto γ-Fe_2O_3 nanoparticles [89].

Metagenomics. It is of great importance to monitor the structure of microbial communities during the process of bioremediation. In the past, it presented a huge problem, due to the fact that only a small fraction of species (less than 1%) present in the soil is culturable under laboratory conditions [90]. The scientific developments have brought metagenomics, a method based on the analysis of the complete DNA extracted from the soil sample [91]. It is assumed that the isolated DNA, termed the soil metagenome, represents the collective DNA of all indigenous microorganisms from the sample [92,93]. The general procedure for metagenomic research includes several steps: (i) enrichment of samples, (ii) extraction of genomic DNA, (iii) construction of DNA library, (iv) screening of the target genes and (v) expression of the product of the target gene [94].

With the use of metagenomics, microbial diversity as well as the potential for heavy metal removal can be determined [95,96]. This approach allows scientists to investigate the overall metabolic capacity of a microbial community, including specific groups of genes encoding proteins responsible for heavy metal transformations. In addition, metagenomics provides the possibility to compare polluted with unpolluted sites in terms of functional diversity and community structures. For example, it was observed that functional diversity was higher in the community from an unpolluted soil sample, in comparison to the one in a soil polluted with Cd [97]. This finding implicates that pollution leads to changes in the functional diversity (usually decreasing it) and community structures over time.

4. CONCLUSION

Conventional remediation techniques have many drawbacks, including the secondary contamination of the environment with even more toxic pollutants, making them less suitable for further use. Therefore, turning to green remediation techniques is of great importance. Very potent tools in bioremediation of heavy metals are various microorganism species, capable of detoxifying a wide range of metal contaminants, due to versatile metabolic activities. There is already a vast number of laboratory scale studies of heavy metal removal, but currently the field studies are fewer. However, some of the developed bioreactor systems were proven to be very efficient in the removal of metal contamination. Beside bacterial species already used in such systems, it is important to investigate Archaea, as a very potent group of various extremophilic microorganisms. Several novel technologies, such as genetic engineering and nanotechnology are being developed and utilized in order to improve bioremediation processes. Overall, bioremediation represents a very powerful tool for the clean-up of the environment in the future.

REFERENCES

[1] Čučak DI, Spasojević JM, Babić OB, Maletić SP, Simeunović JB, Rončević SD, Dalmacija BD, Tamaš I, Radnović D V. A chemical and microbiological characterization and toxicity assessment of the Pančevo industrial complex wastewater canal sediments, Serbia. *Environ Sci Pollut Res*. 2017;24(9):8458-8468.

[2] Isakovski MK, Maletić S, Tamindžija D, Apostolović T, Petrović J, Tričković J, Agbaba J. Impact of hydrochar and biochar amendments on sorption and biodegradation of organophosphorus pesticides during transport through Danube alluvial sediment. *J Environ Manage*. 2020;274.

[3] Dhankhar R, Hooda A. Fungal biosorption-an alternative to meet the challenges of heavy metal pollution in aqueous solutions. *Environ Technol*. 2011;32(5):467-491.

[4] Fashola MO, Ngole-Jeme VM, Babalola OO. Heavy metal pollution from gold mines: Environmental effects and bacterial strategies for resistance. *Int J Environ Res Public Health*. 2016;13.

[5] USEPA. *Recent Developments for In Situ Treatment of Metal Contaminated Soils*.; 1997.

[6] Wuana RA, Okieimen FE. Heavy Metals in Contaminated Soils: A Review of Sources, Chemistry, Risks and Best Available Strategies for Remediation. *ISRN Ecol*. 2011;2011.

[7] Gupta A, Joia J. Microbes as Potential Tool for Remediation of Heavy Metals: A Review. *J Microb Biochem Technol*. 2016;8(4):364-372.

[8] Volarić A, Čučak D, Radnović D. Rezistentnost i sposobnost redukcije šestovalentnog hroma od strane bakterija izolovanih iz različitih sredina. In: Zivic M, Petkovic B, eds. *Drugi Kongresa Biologa Srbije Knjiga Sažetaka*. Beograd: Srpsko biološko društvo; 2018:241-242. (In Serbian)

[9] Tchounwou PB, Yedjou CG, Patlolla AK, Sutton DJ. Heavy metal toxicity and the Environment. In: Luch A, ed. *Molecular, Clinical and Environmental Toxicology*. Vol 101. Basel: Springer; 2012:133-164.

[10] Kastori R, Vukmirović Z, Polić P, Blagojević S, Bogdanović D, Ubavić M, Vapa L, Hadžić V, Govedarica M, Milošević N, Jarak M, Petrović N, Arsenijević-Maksimović I, Vapa M. *Teški Metali u Životnoj Sredini: Heavy Metals in the Environment*. Novi Sad: Naučni institut za ratarstvo i povrtarstvo; 1997.

[11] Spasojević JM, Maletić SP, Rončević SD, Radnović D V., Čučak DI, Tričković JS, Dalmacija BD. Using chemical desorption of PAHs from sediment to model biodegradation during bioavailability assessment. *J Hazard Mater*. 2015;283:60-69.

[12] John DA, Leventhal JS. Bioavailability of metals. In: du Bray EA, ed. *Preliminary Compilation of Descriptive Geoenvironmental Mineral Deposit Models*. ; 1995:10-18.

[13] Ludwig B. *Cytochrome c Oxidase in Prokaryotes*. Vol 16.; 1987.

[14] Nies DH. Microbial heavy-metal resistance. *Appl Microbiol Biotechnol*. 1999;51:730-750.

[15] Hassen A, Saidi N, Cherif M, Boudabous A. Resistance of environmental bacteria to heavy metals. *Bioresour Technol*. 1998;64:7-15.

[16] Oliveira A, Pampulha ME. Effects of long-term heavy metal contamination on soil microbial characteristics. *J Biosci Bioeng*. 2006;102(3):157-161.

[17] Tamindžija D, Chromikova Z, Spaić A, Barak I, Bernier-Latmani R, Radnović D. Chromate tolerance and removal of bacterial strains isolated from uncontaminated and chromium-polluted environments. *World J Microbiol Biotechnol*. 2019;35(4):56.

[18] Čučak DI, Pavlović A, Chromikova Z, Bernier-Latmani R, Barak I, Radnović D. Chromium impact on a cultivable soil bacterial community. In: *Abstract Book of the 19th International Conference on Bacilli & Gram-Positive Bacteria*. Berlin; 2017:267-268.

[19] Xie Y, Fan J, Zhu W, Amombo E, Lou Y, Chen L, Fu J. Effect of heavy metals pollution on soil microbial diversity and bermudagrass genetic variation. *Front Plant Sci*. 2016;7(755).

[20] Andronov EE, Petrova SN, Pinaev AG, Pershina E V., Rakhimgaliyeva S, Akhmedenov KM, Gorobets A V., Sergaliev NK. Analysis of the structure of microbial community in soils with different degrees of salinization using T-RFLP and real-time PCR techniques. *Eurasian Soil Sci*. 2012;45(2):147-156.

[21] Tipayno S, Kim CG, Sa T. T-RFLP analysis of structural changes in soil bacterial communities in response to metal and metalloid contamination and initial phytoremediation. *Appl Soil Ecol*. 2012;61:137-146.

[22] Yao X feng, Zhang J ming, Tian L, Guo J hua. The effect of heavy metal contamination on the bacterial community structure at Jiaozhou Bay, China. *Brazilian J Microbiol*. 2017;48:71-78.

[23] Čučak D, Pavlović A, Chromikova Z, Barak I, Bernier Latmani R, Radnović D. Comparison of chromate resistance of environmental and reference strains of Bacillus genus. In: Obradović D, Ranin L, eds. *Abstract Book of the XI Microbiology Congress- MIKROMED*. Belgrade: Serbian microbiology society; 2017.

[24] Cervantes C, Campos-García J. Reduction and Efflux of Chromate by Bacteria. In: Nies DH, Silve S, eds. *Microbiol Monogr*. Berlin: Springer; 2007.

[25] Nanda M, Kumar V, Sharma DK. Multimetal tolerance mechanisms in bacteria: The resistance strategies acquired by bacteria that can be exploited to 'clean-up' heavy metal contaminants from water. *Aquat Toxicol*. 2019;212:1-10.

[26] Choudhury R, Srivastava S. Zinc resistance mechanisms in bacteria. *Curr Sci*. 2001;81(7):768-775.

[27] Ianieva OD. Mechanisms of bacteria resistance to heavy metals. *Mikrobiol Zh*. 2009;71(6):54-65.

[28] El-Helow ER, Sabry SA, Amer RM. Cadmium biosorption by a cadmium resistant strain of Bacillus thuringiensis: Regulation and optimization of cell surface affinity for metal cations. *BioMetals*. 2000;13:273-280.

[29] Ramírez-Díaz MI, Díaz-Pérez C, Vargas E, Riveros-Rosas H, Campos-García J, Cervantes C. Mechanisms of bacterial resistance to chromium compounds. *BioMetals*. 2008;21:321-332.

[30] Pinto E, Sigaud-Kutner TCS, Leitão MAS, Okamoto OK, Morse D, Colepicolo P. Heavy metal-induced oxidative stress in algae. *J Phycol*. 2003;39:1008-1018.

[31] Roane TM, Pepper IL, Miller RM. Microbial remediation of metals. In: Lynch J, ed. *Bioremediation: Principles and Applications*. 2nd ed. New York: Cambridge University Press; 1996:312-340.

[32] Gupta P, Diwan B. Bacterial Exopolysaccharide mediated heavy metal removal: A Review on biosynthesis, mechanism and remediation strategies. *Biotechnol Reports*. 2017;13:58-71.

[33] Lovley DR. Dissimilatory Metal Reduction. *Annu Rev Microbiol*. 1993;47:263-290.

[34] Ishibashi Y, Cervantes C, Silver S. Chromium Reduction in Pseudomonas putida. *Appl Environ Microbiol*. 1990;56(7):2268-2270.

[35] Bopp LH, Ehrlich HL. Chromate resistance and reduction in Pseudomonas fluorescens strain LB300. *Arch Microbiol*. 1988;150:426-431.

[36] Dey S, Paul AK. Hexavalent Chromate Reduction During Growth and by Immobilized Cells of Arthrobacter sp . SUK 1205. *Sci Technol Dev*. 2015;34(3):158-168.

[37] Ackerley DF, Gonzalez CF, Keyhan M, Blake R, Matin A. Mechanism of chromate reduction by the Escherichia coli protein, NfsA, and the role of different chromate reductases in minimizing oxidative stress during chromate reduction. *Environ Microbiol*. 2004;6(8):851-860.

[38] Čučak DI, Chromikova Z, Pavlović A, Radnović D, Bernier-Latmani R, Barak I. Chromate tolerance and reduction of environmental Bacillus species isolates. In: *Abstract Book of the 19th International Conference on Bacilli & Gram-Positive Bacteria*. Berlin; 2017:266-267.

[39] Gupta A, Phung LT, Chakravarty L, Silver S. Mercury resistance in Bacillus cereus RC607: Transcriptional organization and two new open reading frames. *J Bacteriol*. 1999;181(22):7080-7086.

[40] Nevin KP, Lovley DR. Lack of production of electron-shuttling compounds or solubilization of Fe(III) during reduction of insoluble Fe(III) oxide by Geobacter metallireducens. *Appl Environ Microbiol*. 2000;66(5):2248-2251.

[41] Ji G, Silver S. Reduction of arsenate to arsenite by the ArsC protein of the arsenic resistance operon of Staphylococcus aureus plasmid pI258. *Proc Natl Acad Sci U S A*. 1992;89:9474-9478.

[42] Khijniak T V., Slobodkin AI, Coker V, Renshaw JC, Livens FR, Bonch-Osmolovskaya EA, Birkeland NK, Medvedeva-Lyalikova NN, Lloyd JR. Reduction of uranium(VI) phosphate during growth of the thermophilic bacterium Thermoterrabacterium ferrireducens. *Appl Environ Microbiol*. 2005;71(10):6423-6426.

[43] Myers CR, Nealson KH. Bacterial manganese reduction and growth with manganese oxide as the sole electron acceptor. *Science (80-)*. 1988;240(4857):1319-1321.

[44] Sugio T, Tsujita Y, Hirayama K, Inagaki K, Tano T. Reduction of Mo6+ with Elemental Sulfur by Thiobacillus ferrooxidans. *J Bacteriol*. 1988;170(12):5956-5959.

[45] Escudero L V., Casamayor EO, Chong G, Pedrós-Alió C, Demergasso C. Distribution of Microbial Arsenic Reduction, Oxidation and Extrusion Genes along a Wide Range of Environmental Arsenic Concentrations. Vos M, ed. *PLoS One*. 2013;8(10).

[46] Ghosh D, Bhadury P, Routh J. Diversity of arsenite oxidizing bacterial communities in arsenic-rich deltaic aquifers in West Bengal, India. *Front Microbiol*. 2014;5.

[47] Rulkens WH, Tichy R, Grotenhuis JTC. Remediation of Polluted Soil and Sediment: Perspectives and Failures. *Wat Sci Tech*. 1998;37(8):27-35.

[48] Vidali M. Bioremediation. An overview. *Pure Appl Chem*. 2001;73(7):1163-1172.

[49] Garbisu C, Alkorta I. Basic concepts on heavy metal soil bioremediation. *Eur J Miner Process Environ Prot*. 2003;3(1):58-66.

[50] Chibuike GU, Obiora SC. Heavy metal polluted soils: Effect on plants and bioremediation methods. *Appl Environ Soil Sci*. 2014;2014.

[51] Svirčev Z, Krstić S, Važić T. THE PHILOSOPHY AND APPLICABILITY OF ECOREMEDIATIONS FOR THE PROTECTION OF WATER ECOSYSTEMS. *Acta Geogr Slov*. 2014;54(1):179-188.

[52] Schmoger MEV, Oven M, Grill E. Detoxification of arsenic by phytochelatins in plants. *Plant Physiol*. 2000;122:793-801.

[53] Kumar A, Bisht B., Joshi V., Dhewa T. Review on Bioremediation of Polluted Environment : A Management Tool. *Int J Environ Sci*. 2011;1(6):1079-1093.

[54] Gupta R, Mittal A. Bioremediation: an inexpensive yet effective strategy for remediation of heavy metal contaminated sites. *Int J Adv Res*. 2016;4(4):519-530.

[55] Spasojević JM, Maletić SP, Rončević SD, Radnović D V., Čučak DI, Tričković JS, Dalmacija BD. Using chemical desorption of PAHs from sediment to model biodegradation during bioavailability assessment. *J Hazard Mater*. 2015;283:60-69.

[56] Bertrand J-C, Doumenq P, Guyoneaud R, Marrot B, Martin-Laurent F, Matheron R, Moulin P, Soulas G. Applied Microbial Ecology and Bioremediation. In: Bertrand JC, Caumette P, Lebaron P, Matheron R, Normand P, Sime-Ngando T, eds. *Environmental Microbiology: Fundamentals and Applications*. Springer; 2011.

[57] Joshi N. Bioremediation of heavy metals and organic pollutants through green technology. *Int J Adv Sci Res*. 2018;3(2):1-4.

[58] Panneerselvam P, Choppala G, Kunhikrishnan A, Bolan N. Potential of novel bacterial consortium for the remediation of chromium contamination. *Water Air Soil Pollut*. 2013;224(12).

[59] Volarić A, Tamindžija D, Radnović D. Hexavalent chromium reduction of individual bacterial strains and consortia. In: Šerbula S, ed. *27th International Conference Ecological Truth and Environmental Research - EcoTER'19*. Bor: University of Belgrade, Technical Faculty in Bor; 2019:240-246.

[60] Chen Y, Gu G. Preliminary studies on continuous chromium(VI) biological removal from wastewater by anaerobic-aerobic activated sludge process. *Bioresour Technol*. 2005;96:1713-1721.

[61] Quintelas C, Fonseca B, Silva B, Figueiredo H, Tavares T. Treatment of chromium(VI) solutions in a pilot-scale bioreactor through a biofilm of Arthrobacter viscosus supported on GAC. *Bioresour Technol*. 2009;100:220-226.

[62] Tamindžija D, Volarić A, Radnović D. Characterization of chromate resistant and reducing bacterial strains. In: Šerbula S, ed. *Proceedings 27th International Conference Ecological Truth and Environmental Research*. Bor: University of Belgrade, Technical Faculty in Bor; 2019:255 – 261.

[63] Lameiras S, Quintelas C, Tavares T. Biosorption of Cr (VI) using a bacterial biofilm supported on granular activated carbon and on zeolite. *Bioresour Technol*. 2008;99:801-806.

[64] Cabrera G, Viera M, Gómez JM, Cantero D, Donati E. Bacterial removal of chromium (VI) and (III) in a continuous system. *Biodegradation*. 2007;18:505-513.

[65] Altun M, Sahinkaya E, Durukan I, Bektas S, Komnitsas K. Arsenic removal in a sulfidogenic fixed-bed column bioreactor. *J Hazard Mater*. 2014;269:31-37.

[66] Wagner-Döbler I. Pilot plant for bioremediation of mercury-containing industrial wastewater. *Appl Microbiol Biotechnol*. 2003;62:124-133.

[67] Yan R, Yang F, Wu Y, Hu Z, Nath B, Yang L, Fang Y. Cadmium and mercury removal from non-point source wastewater by a hybrid bioreactor. *Bioresour Technol*. 2011;102:9927-9932.

[68] Cerruti C, Curutchet G, Donati E. Bio-dissolution of spent nickel-cadmium batteries using Thiobacillus ferrooxidans. *J Biotechnol*. 1998;62:209-219.

[69] Bayrakdar A, Sahinkaya E, Gungor M, Uyanik S, Atasoy AD. Performance of sulfidogenic anaerobic baffled reactor (ABR) treating acidic and zinc-containing wastewater. *Bioresour Technol*. 2009;100:4354-4360.

[70] Chen GQ, Jiang XR. Next generation industrial biotechnology based on extremophilic bacteria. *Curr Opin Biotechnol*. 2018;50:94-100.

[71] Krzmarzick MJ, Taylor DK, Fu X, McCutchan AL. Diversity and niche of archaea in bioremediation. *Archaea*. 2018;2018.

[72] Sehlin HM, Lindstrom EB. Oxidation and reduction of arsenic by Sulfolobus acidocaldarius strain BC. *FEMS Microbiol Lett*. 1992;93:87-92.

[73] Schelert J, Dixit V, Hoang V, Simbahan J, Drozda M, Blum P. Occurrence and Characterization of Mercury Resistance in the Hyperthermophilic Archaeon Sulfolobus solfataricus by Use of Gene Disruption. *J Bacteriol*. 2004;186(2):427-437.

[74] Singh JS, Abhilash PC, Singh HB, Singh RP, Singh DP. Genetically engineered bacteria: An emerging tool for environmental remediation and future research perspectives. *Gene*. 2011;480:1-9.

[75] Chromiková Z, Čučak D, Kučerová K, B. B, Radnović D, Bernier-Latmani R, Barak I. Microbial tolerance to heavy metal stress. In: Mandic-Mulec I, Danevcic T, Stefanic P, eds. *Abstract Book Bacell 2019*. Ljubljana: University of Ljubljana Biotechnical Faculty; 2019.

[76] Valls M, Atrian S, De Lorenzo V, Fernández LA. Engineering a mouse metallothionein on the cell surface of Ralstonia eutropha CH34 for immobilization of heavy metals in soil. *Nat Biotechnol*. 2000;18:661-665.

[77] Kostal J, Yang R, Wu CH, Mulchandani A, Chen W. Enhanced Arsenic Accumulation in Engineered Bacterial Cells Expressing ArsR. *Appl Environ Microbiol*. 2004;70(8):4582-4587.

[78] Zhao XW, Zhou MH, Li QB, Lu YH, He N, Sun DH, Deng X. Simultaneous mercury bioaccumulation and cell propagation by genetically engineered Escherichia coli. *Process Biochem*. 2005;40:1611-1616.

[79] Bondarenko O, Rõlova T, Kahru A, Ivask A. Bioavailability of Cd, Zn and Hg in soil to nine recombinant luminescent metal sensor bacteria. *Sensors*. 2008;8:6899-6923.

[80] Dixit R, Wasiullah, Malaviya D, Pandiyan K, Singh UB, Sahu A, Shukla R, Singh BP, Rai JP, Sharma PK, Lade H, Paul D. Bioremediation of heavy metals from soil and aquatic environment: An overview of principles and criteria of fundamental processes. *Sustainability*. 2015;7:2189-2212.

[81] Pandey S, Kumari M, Singh SP, Bhattacharya A, Mishra S, Chauhan PS, Mishra A. Bioremediation via nanoparticles: An innovative microbial approach. In: *Handbook of Research on Uncovering New Methods for Ecosystem Management Through Bioremediation*. IGI Global; 2015:491-515.

[82] Ahmad A, Senapati S, Khan MI, Kumar R, Ramani R, Srinivas V, Sastry M. Intracellular synthesis of gold nanoparticles by a novel alkalotolerant actinomycete, Rhodococcus species. *Nanotechnology*. 2003;14:824-828.

[83] Ganesh Babu MM, Gunasekaran P. Production and structural characterization of crystalline silver nanoparticles from Bacillus cereus isolate. *Colloids Surfaces B Biointerfaces*. 2009;74:191-195.

[84] Perez-Gonzalez T, Jimenez-Lopez C, Neal AL, Rull-Perez F, Rodriguez-Navarro A, Fernandez-Vivas A, Iañez-Pareja E. Magnetite biomineralization induced by Shewanella oneidensis. *Geochim Cosmochim Acta*. 2010;74:967-979.

[85] Němeček J, Lhotský O, Cajthaml T. Nanoscale zero-valent iron application for in situ reduction of hexavalent chromium and its effects on indigenous microorganism populations. *Sci Total Environ*. 2014;485-486(1):739-747.

[86] Ash A, Revati K, Pandey BD. Microbial synthesis of iron-based nanomaterials - A review. *Bull Mater Sci*. 2011;34(2):191-198.

[87] Abdeen M, Sabry S, Ghozlan H, El-Gendy AA, Carpenter EE. Microbial-Physical Synthesis of Fe and Fe3O4 Magnetic Nanoparticles Using Aspergillus Niger YESM1 and Supercritical Condition of Ethanol. *J Nanomater*. 2016;2016.

[88] Zhang S, Niu H, Cai Y, Zhao X, Shi Y. Arsenite and arsenate adsorption on coprecipitated bimetal oxide magnetic nanomaterials: MnFe2O4 and CoFe2O4. *Chem Eng J*. 2010;158:599-607.

[89] Cheng Z, Tan ALK, Tao Y, Shan D, Ting KE, Yin XJ. Synthesis and characterization of iron oxide nanoparticles and applications in the removal of heavy metals from industrial wastewater. *Int J Photoenergy*. 2012;2012.

[90] Kaeberlein T, Lewis K, Epstein SS. Isolating "Uncultivable" Microorganisms in Pure Culture in a Simulated Natural Environment. *Science (80-)*. 2002;296:1127-1130.

[91] Daniel R. The metagenomics of soil. *Nat Rev Microbiol*. 2005;3:470-478.

[92] Handelsman J, Rondon MR, Brady SF, Clardy J, Goodman RM. Molecular biological access to the chemistry of unknown soil microbes: A new frontier for natural products. *Chem Biol*. 1998;5(10):245-249.

[93] Rondon MR, Goodman RM, Handelsman J. The Earth's bounty: Assessing and accessing soil microbial diversity. *Trends Biotechnol*. 1999;17:403-409.

[94] Kumar Awasthi M, Ravindran B, Sarsaiya S, Chen H, Wainaina S, Singh E, Liu T, Kumar S, Pandey A, Singh L, Zhang Z. Metagenomics for taxonomy profiling: tools and approaches. *Bioengineered*. 2020;11(1):356-374.

[95] Drewniak L, Krawczyk PS, Mielnicki S, Adamska D, Sobczak A, Lipinski L, Burec-Drewniak W, Sklodowska A. Physiological and metagenomic analyses of microbial mats involved in self-purification of mine waters contaminated with heavy metals. *Front Microbiol*. 2016;7.

[96] Salam LB. Unravelling the antibiotic and heavy metal resistome of a chronically polluted soil. *3 Biotech*. 2020;10(238).

[97] Feng G, Xie T, Wang X, Bai J, Tang L, Zhao H, Wei W, Wang M, Zhao Y. Metagenomic analysis of microbial community and function involved in cd-contaminated soil. *BMC Microbiol*. 2018;18(11):1-13.

SAŽETAK

Bioremedijacija teških metala pomoću mikroorganizama

Ana Volarić[1], Zorica Svirčev[1], Dragana Tamindžija[2] i Dragan Radnović[1]

[1]Univerzitet u Novom Sadu, Prirodno-matematički fakultet, Departman za biologiju i ekologiju, Trg Dositeja Obradovića 2, Novi Sad, Srbija
[2]Univerzitet u Novom Sadu, Prirodno-matematički fakultet, Departman za hemiju, biohemiju I zaštitu životne sredine, Trg Dositeja Obradovića 3, Novi Sad, Srbija

(Pregledni rad)

Zagađenje teškim metalima je jedan od najozbiljnijih problema u životnoj sredini zbog perzistencije, biodostupnosti i toksičnosti. Brojne konvencionalne fizičke i hemijske metode se tradicionalno koriste za čišćenje životne sredine. S obzirom na to da ove metode imaju nekoliko značajnih mana, upotreba živih organizama, odnosno bioremedijacija, postaje sve zastupljenija. Biotehnološka primena mikroorganizama se već uspešno sprovodi i konstantno unapređuje, a mnogi bakterijski sojevi uspešno uklanjaju teške metale. Ovaj rad pruža pregled osnovnih karakteristika teških metala i opisuje njihovu interakciju sa mikroorganizmima. Opisani su ključni mehanizmi rezistencije mikroorganizama na teške metale, kao i osnovni principi i tipovi metoda bioremedijacije, sa posebnim osvrtom na pilot studije sa bioreaktorima. Posebnu pažnju bi trebalo obratiti na autohtone bakterije izolovane iz sredina prirodno zagađenih teškim metalima, jer su takve vrste već adaptirane na zagađenje i imaju razvijene mehanizme rezistencije. Upotreba biofilma ili konzorcijuma može biti efikasnija, zbog veće rezistencije i kombinacije nekoliko metaboličkih puteva, te samim tim mogućnosti za uklanjanje više teških metala istovremeno. Nove tehnologije opisane u ovom radu, poput nanotehnologije, genetičkog inženjerstva i metagenomike se sve više uvode u polje bioremedijacije u cilju poboljšanja procesa. Prema tome, bioremedijacija predstavlja moćno rešenje za čišćenje životne sredine.

Ključne reči: biotransformacija; zagađenje; biotehnologija; rezistencija na teške metale

Chemically modified *Jatropha curcas* oil for biolubricant applications

Nurazira Mohd Nor[1], Nadia Salih[2] and Jumat Salimon[2]

[1]*School of Chemistry and Environment, Faculty of Applied Sciences, Universiti Teknologi MARA, 72000 Kuala Pilah, Negeri Sembilan, Malaysia*
[2]*Department of Chemical Sciences, Faculty of Science and Technology, Universiti Kebangsaan Malaysia, 43600 Bangi, Selangor, Malaysia*

Abstract

Jatropha curcas oil is one of interesting renewable resources for preparation of biolubricants. However, direct application of this oil as a biolubricant is restricted due to its low oxidative stability. This drawback can be overcome by molecule structural redesign through a chemical modification process at its unsaturated functional groups. *Jatropha curcas* oil was modified *via* epoxidation, ring opening and esterification processes. Its conversion to the epoxidized oil was performed by using *in situ* performic acid as a catalyst, then reaction with oleic acid in the presence of *p*-toluenesulfonic acid as a catalyst in the ring opening process. The final esterification process with oleic acid was catalyzed by sulfuric acid. Molecular structures of the modified oil were determined by measurements of the oxirane oxygen content and by Fourier-transform infrared (FTIR), proton and carbon nuclear magnetic resonance (^{1}H NMR and ^{13}C NMR) spectroscopy analyses. The results showed that the oxidative stability, viscosity, flash point and pour point of the final product were significantly improved. In specific, the ring opening and esterification processes inducing branching and bending in the final oil molecular structure have resulted in the improved viscosity index of 135, the pour point of -29 °C and the increased flash point of 250 °C.

Keywords: epoxidation; ring opening; esterification; oleic acid; green biolubricant.

Available on-line at the Journal web address: http://www.ache.org.rs/HI/

ORIGINAL SCIENTIFIC PAPER

UDC: 665.345.5:621.892.8:677.027.622:66.094.39

Hem. Ind. **75 (2)** 117-128 (2021)

1. INTRODUCTION

In the last decade, a variety of new technologies have emerged aiming at development of products from renewable sources. to the reason is in increasing concerns over the use of petroleum-based products, which causes progressive reduction of fossil fuel reserves and has negative impacts on the environment [1,2]. In the field of the use of lubricant, there are wide ranges of lubricant base oils, which include mineral, synthetic, re-refined and plant oils. Among these, mineral oils are the most commonly used [3]. Mineral oils are more stable and readily available than natural oils and exhibit a wider range of viscosities [2]. However, they pose a constant threat to ecology and ground water reserves due to their inherent toxicity and non-biodegradable nature [3,4]. Reduction of petroleum oil resources and increasing greenhouse gas emissions give a clear picture of the importance of the move towards sustainable development [5] where the use of renewable sources in industry is vital. Such examples are studies on plant oils as a feedstock in the manufacture of products for daily use. Plant oils are found to be the best alternative source not only because they are renewable raw materials, but also because they are biodegradable and non-toxic [3,6], unlike conventional mineral based oils [2]. Plant oil-based biolubricants such as *Jatropha curcas* (*J. curcas*) oil and its derivatives have excellent lubricity and biodegradability properties for which they are being more closely examined as a base stock for lubricants and functional fluids [7,8]. Also, these oils exhibit high viscosity index [9]. However, plant oils, particularly *J. curcas* oil have several disadvantages including instability that limit their applications in biolubricant industries. Plant oil formulations provide many challenges such as low oxidative stability [2,10] and poor low temperature properties [5,11].

Corresponding author: Nadia Salih, Department of Chemical Sciences, Faculty of Science and Technology, Universiti Kebangsaan Malaysia, 43600 Bangi, Selangor, Malaysia
E-mail: nadiaalnami@hotmail.com
Paper received: 09 August 2020
Paper accepted: 09 March 2021
https://doi.org/10.2298/HEMIND200809009N

This is due to the presence of the weakest track of double bonds present in the unsaturated fatty acid structure [11,12] and instable β-hydrogen at glycerol backbone in the oil triacylglycerol molecule structure.

Many studies have reported production of *J. curcas* oil based biolubricants by improving the oxidative stability by the replacement of the glycerol backbone with polyhydric alcohols. Esterification or transesterification with polyhydric alcohols, especially with trimethylopropanol (TMP) in particular, are well documented. Some studies reported production of *J. curcas* biolubricants *via* esterification of the fatty acid methyl ester (FAME) and TMP [13-17] and direct transesterification of the oil with TMP [18]. Biolubricants based on the *J. curcas* oil showed varied properties depending on the production method. Utilization of 1 % $NaOCH_3$ as a catalyst resulted in 47% yield with a pour point (PP) of -3 °C and viscosity index (VI) of 178–183 [19]; use of 2 % $HClO_4$ has yielded 70 % with PP of -23 °C, flash point (FP) >130 °C and VI of 150 [20]; use of 0.9 % $NaOCH_3$, resulted in 98.2 % yield with PP of -3 °C, FP of 273 °C and VI of 140 [21]; finally the use of a calcium hydroxide catalyst produced a biolubricant with PP of −12 °C, FP of 178 °C and VI of 204 [22].

Scientific approaches have yet to be taken to improve the oxidative stability and low-temperature properties. With this aim, chemical modification of the *J. curcas* oil molecule structure can be carried out. The oil triacylglycerol structures have different functional sites and groups such as double bonds and allylic carbon, which are potential sites for chemical modification [23]. Double bonds present the weakest track being reactive and allowing addition of functional groups in fatty acids. Epoxidation is one of the most important functionalization reactions of double bonds to obtain stable functional groups in order to improve the plant oil oxidative stability [2,8,24].

Epoxidation of *J. curcas* oil using peracids is one of the most important steps and a useful modification process acting on double bonds since epoxides are reactive intermediates that can be converted into other functional groups by ring-opening reactions [25]. The oxirane ring opening by acidic or alkaline catalyzed reactions with a suitable reagent produces interesting poly-functional compounds [8,27] whereas reduction of the oil structural uniformity by attaching alkyl side chains would improve the low-temperature performance [8,26]. In general, plant oils with high contents of unsaturated fatty acid are used to produce high epoxy functionality materials [27]. Products obtained from epoxides can be used as high-temperature biolubricants, while the products obtained from ring opening can be used as low-temperature biolubricants [12]. Non-edible plant oils such as *J. curcas* oil have been studied as a better alternative source and more suitable in different industries such as biolubricant production [28].

However, until now modification of *J. curcas* oil was not attempted by reactions on double bonds or the unsaturated functional groups. Therefore, in this paper, we report the modification process by manipulation and making use of the oil unsaturated functional groups in the forms of oleyl and linolioyel which are present in J. *curcas* oil triacylglycerols. To enhance the lubrication properties, *J. curcas* oil was converted into the epoxidized oil followed by the oxirane ring opening and finally esterification reactions with oleic acid.

1. MATERIALS AND METHODS

1. 1. Materials

J. curcas seed was obtained from a Plant House Plot at the Universiti Kebangsaan Malaysia and extracted using the Soxhlet extraction method. Oleic acid (90 %) was purchased from Sigma Aldrich (USA). Ethyl acetate, toluene, sodium hydrogen carbonate and sodium chloride were purchased from Systerm (Malaysia). Formic acid (88 %) was obtained from Fisher Scientific (USA) and hydrogen peroxide 30% from Merck, Germany. All chemicals and solvents were either analytical grade or high performance liquid chromatography (HPLC) and used directly without further purification.

1. 2. Epoxidation reaction

The epoxidation process of *J. curcas* oil (JCO) was carried out according to Jumat *et al.* [29]. The molar ratio of double bonds in JCO to HCOOH to H_2O_2 was 1:1:2.5 and 100 g oil samples were used. JCO and formic acid were weighed and placed into a 250 cm^3 three neck round bottom flask, which was heated to 45 – 55 °C and continuously stirred by using a magnetic stirrer. When the temperature reached 40 °C, H_2O_2 was added slowly. The reaction was continued for 2.5 h with vigorous stirring of 900 rpm. At the end of reaction, the product was neutralized with sodium hydrogen carbonate solution, sodium

chloride solution and distilled water. The product, epoxidized *J. curcas* oil (EJCO), was kept overnight by adding anhydrous sodium sulfate to remove water. Then, the product was filtered using Whatmann No. 1 filter paper (Whatmann, Germany).

1. 3. Ring opening reaction

In the ring opening reaction [29,30], the mole ratio of EJCO and oleic acid was 1: 3. The EJCO and oleic acid were added to a 250 cm^3 three-neck round bottom flask and heated at 70 °C to 80 °C for 15 min. Then, 1 % of *p*-toluenesulfonic acid (PTSA) was added to yield the concentration of 1 wt.%. The reaction was carried out for 6 h at 100 – 140 °C at continuous stirring of 900 rpm using a magnetic stirrer. At the end of reaction, the product was neutralized with sodium hydrogen carbonate solution, sodium chloride solution and ethyl acetate. The product was kept overnight with the addition of anhydrous sodium sulfate. The product, *J. curcas* oil tetraester (JCOT), was filtered by using Whatmann No. 1 filter paper followed by solvent evaporation by using a rotary evaporator at 70 °C.

1. 4. Esterification reaction

In the esterification reaction [29], the mole ratio of the *J. curcas* oil tetraester (JCOT) and oleic acid was 1:3. The JCOT, oleic acid and sulfuric acid in 2 wt.% final concentration were added to a 500 cm^3 three-neck round bottom flask. 100 mL of toluene was added into the flask and the flask was connect to a Dean - Stark apparatus and a condenser and then heated in silicone oil. The esterification reaction was carried out at the temperature of 110-130 °C for 7-8 h. Once the reaction completed, the product was transferred into a separating flask and allowed to cool at room temperature. The product was neutralized with sodium hydrogen carbonate solution, sodium chloride solution and ethyl acetate to achieve pH of 6 - 7. The final product, *J. curcas* oil octaester (JCOO) was kept overnight with the addition of anhydrous sodium sulfate followed by filtration by using a Whatmann No. 1 filter paper and solvent evaporation by using a rotary evaporator at 70 °C. The esterification processes were repeated at least for three times.

1. 5. Structural characterizations

Formation of EJCO, JCOT and JCOO was confirmed first by using Fourier-transform infrared spectroscopy (FTIR). FTIR spectra were recorded on a Perkin Elmer Infrared Spectrophotometer (USA) in the range 400-4000 cm^{-1}. Nuclear magnetic resonance spectroscopy (NMR) was carried out to confirm the molecular structure of all products. ^1H and ^{13}C NMR were recorded on a JEOL-ECP 400 spectrometer (Japan) at 400 MHz ^1H/100.61 MHz ^{13}C using $CDCl_3$ as a solvent.

1. 6. Determination of the oxygen oxirane content

Evolution of the epoxidation reaction was monitored by measuring the oxygen oxirane content (OOC) in accordance with the official and recommended practice of AOCS Cd 9-57 [31]. Under the prescribed conditions of this method, oxygen was titrated directly using a hydrobromic acid solution in glacial acetic acid. From the OOC measurement, the relative conversion to oxirane (RCO) value was calculated by the following formula:

$$\mathrm{RCO}=\frac{\mathrm{OOC_{exp}}}{\mathrm{OOC_{the}}}100 \quad (1)$$

where OOC_{exp} is the experimentally determined oxirane oxygen and OOC_{the} is the theoretical maximum oxirane oxygen. These parameters were calculated according to eqs (2) and (3), respectively, as:

$$\mathrm{OOC_{exp}}=\frac{1.60VN}{Wt} \quad (2)$$

where *V* and *N* are the volume and normality of the HBr solution and *Wt* is the weight of the sample.

$$\mathrm{OOC_{the}}=\frac{IV_O/2A_\mathrm{i}}{100+\left(IV_O/2A_\mathrm{i}\right)A_\mathrm{O}}A_\mathrm{O}100 \quad (3)$$

where A_i (126.9) and A_o (16.0) are the atomic masses of iodine and oxygen, respectively and IV_o is the initial iodine value of the sample.

1. 7. Determination of the pour point

The lowest temperature at which a liquid can still be poured (still behaves like a fluid) is called the pour point (PP), which is used for investigation of the fluid flow behavior at low temperatures. The ASTM D97-17 method [32,33] was used to measure the PP of the biolubricants in this study, with some modifications. A U-tube and an attached thermometer were used in the experimental setup, with a temperature range of -80 to 0 °C. About 10 cm^3 of the sample was placed in the U-tube and the sample was placed in a freezer (at -80 °C). The sample (held inside the U-tube in a horizontal position) was left in the freezer for 24 h to ensure freezing [34]. Once frozen (after 24 h), the sample was taken out from the freezer and slowly thawed at room temperature monitoring for the start of the flow. The temperature measured at this point denotes the pour point. The pour point test was done in triplicate.

1. 8. Determination of the flash point

The lowest temperature at which a heated volatile liquid vaporizes and ignites is called the flash point (FP). The ASTM D 56-79 method was used to determine the flash point of the biolubricants in this study, using a Tag Closed Tester [33]. A 0 to 500 °C range thermometer was used for the test. First, a test cup was prepared, and approximately 10 cm^3 of the test specimen was filled into it. As a precaution due to using remarkably high temperatures, the flash point test was carried out in a fume chamber. At first, the heat was applied to the product rapidly increase the temperature to 100 °C. Then, the heating was slowed to a constant rate of 5 °C/min nearing the flash point. A spark plug with a test flame was passed across the cup at specified intervals. The lowest liquid temperature at which the vapor of the test specimen was ignited by the test is known as the flash point and the test was performed in triplicate.

1. 9. Determination of viscosity and the viscosity index

A good biolubricant should have a moderate viscosity index **(**VI). The VI value indicates the change in kinematic viscosity of a biolubricant with a change in temperature. Essentially, the VI indicates the quality of the biolubricant and the automotive industry uses this index to characterize lubricating oils. Kinematic viscosities of the biolubricants in this study were measured by using a rheometer model MCR 301, Anton Paar Instruments (Germany). The standard method ASTM D 2270-04 was used to calculate the viscosity and the viscosity index [33]. A hot plate heater was set to 40 and 100°C and the sample (1 cm^3) was added [37]. Then, the VI was determined by using the formula:

$$IV = \frac{L-U}{L-H}100 \quad (4)$$

where U is the kinematic viscosity at 40 °C of the oil sample (cSt), L is the kinematic viscosity at 40 °C of an oil with a zero-viscosity index having the same kinematic viscosity at 100 °C as the oil sample (cSt), H is the kinematic viscosity at 40 °C of an oil with a viscosity index 100, having the same kinematic viscosity at 100 °C as the oil sample (cSt).

1. 10. Determination of oxidative stability

The lubricant oil oxidizes faster when it is exposed to oxygen at elevated temperatures, which reduces the oil quality as it becomes more viscous. Pressure differential scanning calorimetry (PDSC) (model DSC822e Metter Toledo, Switzerland) was used to determine the oxidative stability temperature (OST) of the oil. Typically, a 2 µL sample resulting in a film thickness of less than 1 mm, was placed in an aluminium pan, which was hermetically sealed with a pinhole lid and oxidized in the presence of dry air (Gateway Airgas, St. Louis, MO), which was pressurized in the module at a constant pressure of 1378.95 kPa (200 psi). A 10 °C min^{-1} heating rate from 50 to 350 °C was used during each experiment. The oxidation stability temperature (OST) was calculated from the plot of the heat flow versus temperature for each experiment [35,38]. The OST test was performed in triplicate.

2. RESULTS AND DISCUSSION

2. 1. Epoxidation and ring opening reactions

In the epoxidation process, one oxygen atom will be attached to the active site of unsaturated double bonds to form an epoxide ring. Atomic oxygen from the oxygen donor was transferred to a position far from the carbonyl functional group. Performic acid was formed *in situ* after formic acid reacted with hydrogen peroxide (H_2O_2), which acts as an oxygen donor while formic acid as the active oxygen carrier [39]. Epoxidation of *J. curcas* oil (JCO) was successfully carried out to produce the epoxidized *J. curcas* oil (EJCO) with 87 % (w/w) yield. The OOC value was determined so to confirm the presence of oxirane oxygen ring in EJCO. The obtained OOC value was 4.92 while the theoretical value was 5.99. Based on both values, the relative conversion of oxirane oxygen in the epoxidation process is 82 %. The obtained EJCO was then submitted to the ring opening reaction with oleic acid to produce *J. curcas* oil tetraesters (JCOT). The average yield of the ring opening product was 68%. The ring opening process was monitored by the OOC value, which should be decreased as much as possible as the OOC reduction is proportional to the number of opened epoxide rings. The OOC value obtained after the ring opening process was significantly low approaching zero. A significant difference was observed between the OOC values of EJCO and JCOT and thus it is confirmed that all epoxide rings were successfully opened during the reaction with oleic acid. Further esterification of JCOT with oleic acid produced the final product *J. curcas* oil octaesters (JCOO) with the average yield of 64 %. Figure 1 shows the overall schematic reaction pathways in this research represented by dominant triacylglycerols (TAG) of 1-palmitoyl-2,3-dilinoleoyl-glycerol (PLL) found in JCO.

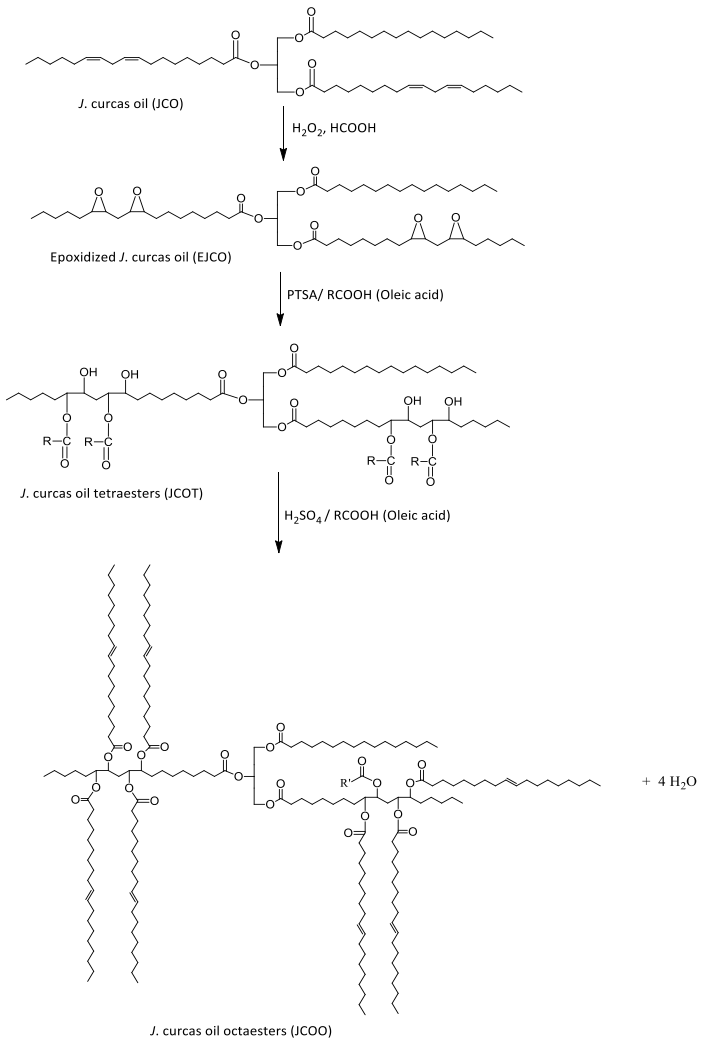

Fig 1. Schematic presentation of reactions used for modification of J. curcas oil

2. 2. FTIR spectra analysis

Presence of functional groups in all products was identified by using FTIR spectroscopy. Figure 2 shows the FTIR spectra of JCO, EJCO, JCOT and JCOO. The C=C olefin peak originates from the linolate acyl group, which was initially present in JCO appearing at 3007 cm^{-1} and was successfully converted into the epoxide ring. This is evidenced by the presence of the epoxide (oxirane) peak at 826 cm^{-1} in the EJCO spectrum. This value agrees with the literature reporting the wave number for the epoxide group in the range between 815-950 cm^{-1} [40]. Disappearance of the epoxide peak in the JCOT spectrum indicated that all epoxide rings have been successfully converted to hydroxyl ester functional groups in JCOT during the ring opening reaction with oleic acid. This is evidenced by the increase in the intensity of the peaks of the hydroxyl (OH) functional group at 3470 cm^{-1} and ester carbonyl C=O stretching at 1741 cm^{-1} in the JCOT spectrum. This agrees literature reports in which the wave number for the C=O ester group ranges from 1730-1750 cm^{-1} [40]. A significant change during the ring opening reaction is evidenced by the existence of a C=C olefin peak at 3005 cm^{-1} of oleate acyl group. Success of the final esterification reaction was evidenced by the reduction in peak intensity of the hydroxyl group at 3470 cm^{-1}, followed by an increase in the peak intensity of olefinic functional group at the wavenumber of 3005 cm^{-1} in the JCOO spectrum. The increase in the olefin (alkene) peak intensity showed that oleic acid has successfully reacted with the hydroxyl group and formed a big structure with branching esters.

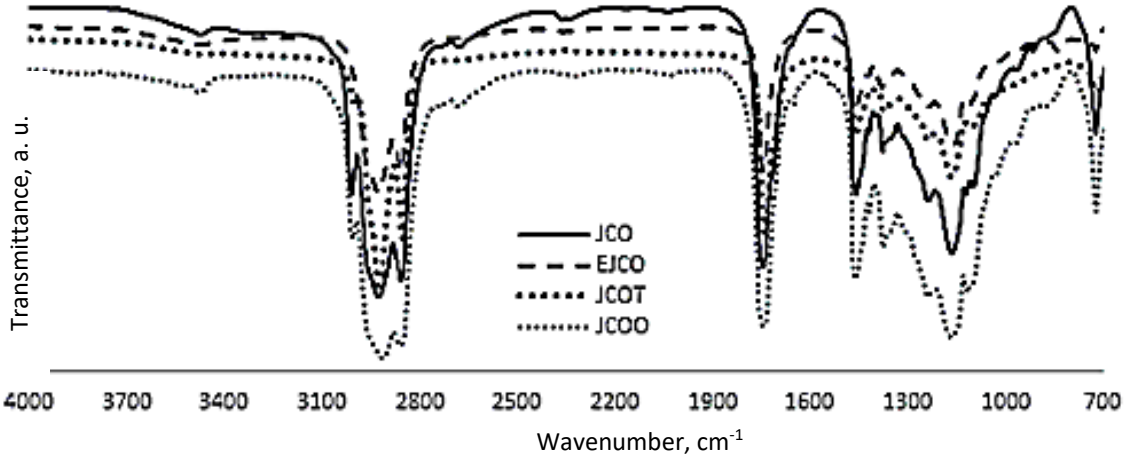

Figure 2. FTIR spectra of JCO, EJCO, JCOT and JCOO

2. 3. NMR spectra analysis

The epoxidation process (EJCO) can be proved by disappearances of the olefin proton at 5.340-5.311 ppm (C=C-H) and methylene proton at 2.029-1.975 ppm (-CH_2 methylene) which were initially present in the ^{1}H NMR JCO spectrum [41]. They are replaced by a peak at 3.013-2.863 ppm which corresponds to protons of oxirane ring (CHOCH) in the EJCO ^{1}H NMR spectrum. Result of the ring opening reaction can be confirmed by the disappearance of the peak of oxirane ring proton (CHOCH) in the ^{1}H NMR JCOT spectrum. Table 1 shows chemical shifts in ^{1}H NMR spectra for the JCO, EJCO, JCOT and JCOO.

Table 1. ^{1}H NMR chemical shifts of JCO, EJCO, JCOT and JCOO

Compound	Chemical shift, ppm	Remarks
JCO	5.340, 5.311	C=C-H
	2.319, 1.989, 1.615	-C-H_2 methylene
EJCO	3.013, 3.001, 2.863	CHOCH (oxirane ring)
JCOT	5.315	C=C-H
	2.311, 2.018	-C-H_2 methylene
	4.892	C-O-H
JCOO	5.334, 5.319, 5.304	C=C-H
	2.315, 2.017	-C-H_2 methylene
	4.892	C-O-H

Furthermore, the existence of hydroxyl group, which was formed during the ring opening reaction can be also confirmed by the existent peak for the hydroxyl proton at 4.89 ppm (C-O-H) in the JCOT spectrum. The existence and increase in the number of alkene groups due to further esterification by oleic acid can be evidenced by the existence of alkene C=C-H peak and methylene proton of $-CH_2$ in the JCOO spectrum. The spectrum also shows disappearance or a decrease in the hydroxyl group signal (C-O-H) in the JCOO spectrum [42].

The conversion of double bonds to oxirane ring can be proved by the disappearance of chemical shifts of olefin (C=C) at 130.217- 127.939 ppm, which initially existed in the ^{13}C NMR JCO spectrum and were replaced by chemical shifts at 57.159- 54.146 ppm, which represent the epoxy carbon atoms (C-O) in the ^{13}C NMR EJO spectrum. Results of the ring opening process can be evidenced by the disappearance of epoxy carbon and the existence of carbon olefin (C=C) at 130.240-129.759 ppm as well as the existence of peak at 73.590 ppm, which represents the carbon C-O next to the hydroxyl group in the ^{13}C NMR JCOT spectrum. The final product showed disappearance of the chemical shift of hydroxyl group and an increase in the intensity of carbon olefin (C=C) signal at 130.271-129.766 ppm in the ^{13}C NMR JCOO spectrum [43]. Table 2 shows chemical shifts in ^{13}C NMR spectra for JCO, EJCO, JCOT and JCOO. Figures 3 and 4 show ^{1}H and ^{13}C NMR spectra for JCO, EJCO, JCOT, and JCOO, respectively.

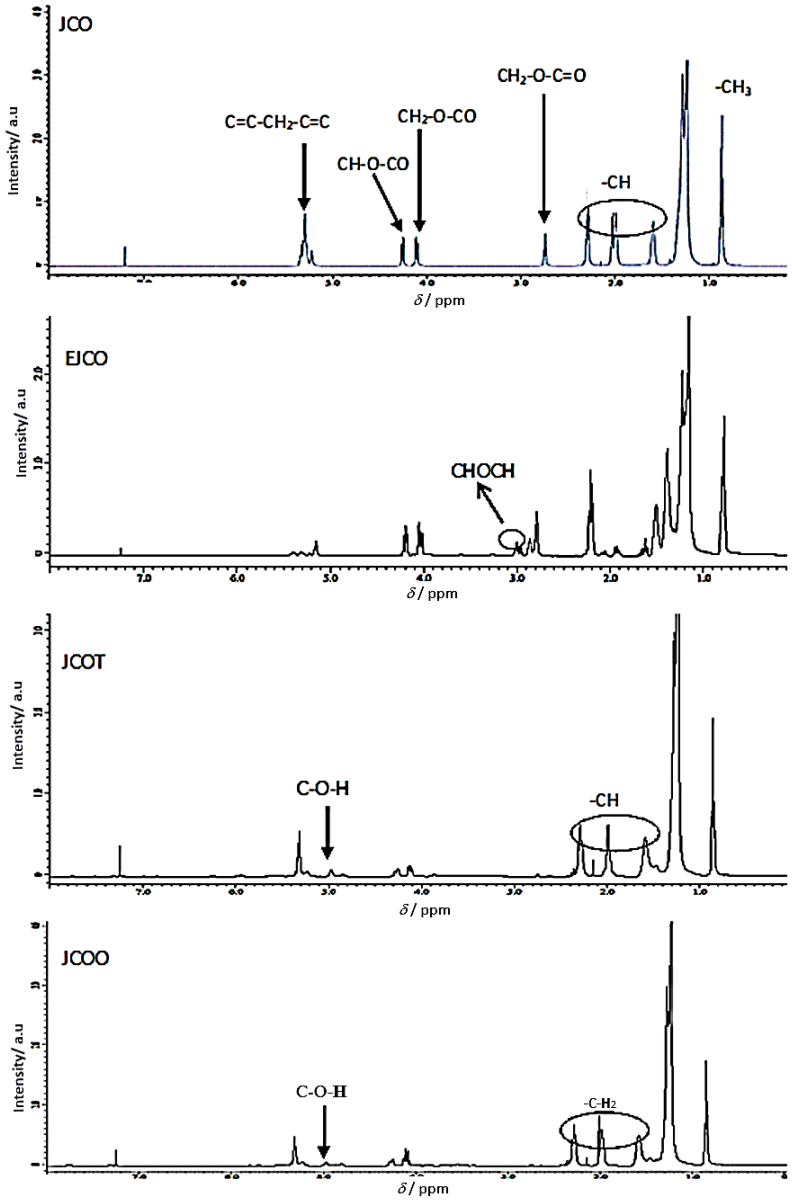

Figure 3. ^{1}H NMR spectra of JCO, EJCO, JCOT, and JCOO

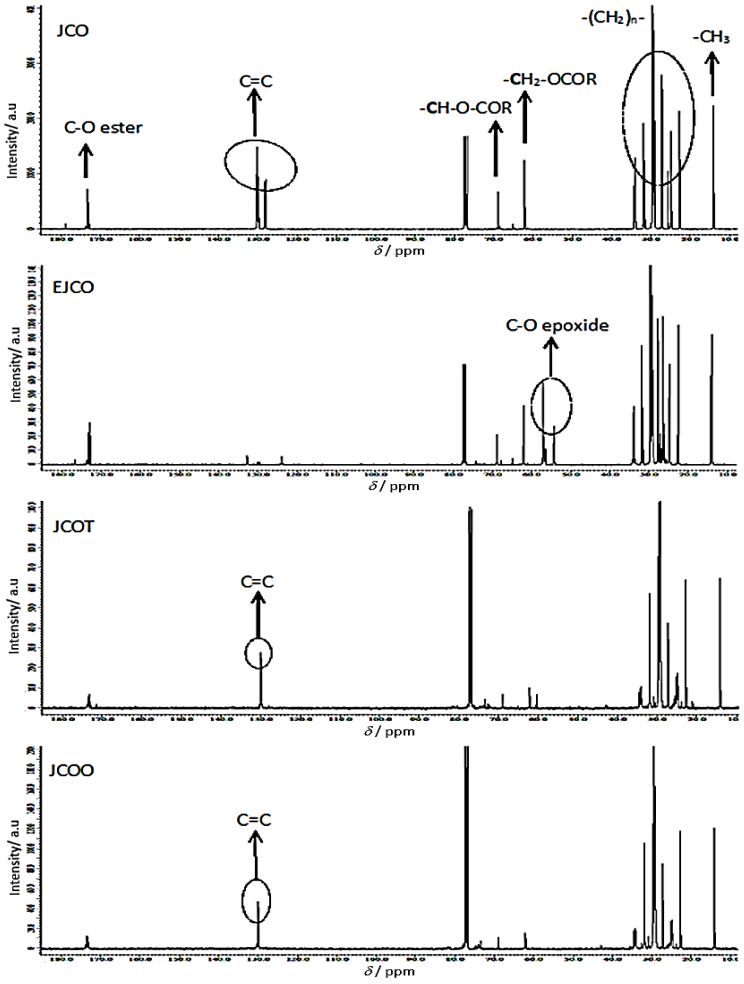

Figure 4. ^{13}C NMR spectra of JCO, EJCO, JCOT and JCOO

Table 2. ^{13}C NMR chemical shifts of JCO, EJCO, JCOT and JCOO

Compound	Chemical shift, ppm	Remarks
JCO	130.217, 130.026, 129.736, 128.115, 127.939	C=C
EJCO	57.159, 54.299, 54.146	C-O epoxide
JCOT	130.240, 130.057, 129.759	C=C
	73.590	C-O
JCOO	130.271, 130.065, 129.766	C=C

2. 4. Physicochemical properties

The obtained physicochemical properties are shown in Table 3. Increasing in the iodine values (IV) as the reaction product proceeds from JCO (113) to the final product of JCOO (660) proved that the esterification processes were successfully performed. Oxidative stability (OS) is determined by the onset temperature at which a sharp increase in the oxidation rate of the sample occurs. A high onset temperature indicates that the biolubricant has high OS [13]. Based on the DSC analysis, there is an improvement in OS for EJCO compared to JCO. This is due to the reduction in the content of double bonds that contributed to the reduction in the number of active sites for the oxidation process. However, JCOT and JCOO showed insignificant differences in OS due to the increasing carbon chain number and double bond content in the oil structure.

The ability of a substance to remain liquid at low temperatures is an important attribute for a number of industrial materials, such as biolubricants, surfactants and fuels [11]. The cold flow property of plant oils is extremely poor and this limits their use at low operating temperatures especially as automotive and industrial fluids. Plant oils tend to form

macro-crystalline structures at low temperatures through uniform self-stacking of the linear triacylglycerol molecules. Such macro-crystals restrict flow of the system due to the loss of kinetic energy of individual molecules during self-stacking [2, 3, 13]. JCOO has a lowest PP compared to the other products due to branching in the carbon chain and a bent structure. Self-stacking is thus restricted, and more hollow structure provide easier flowing which contributed to the lowest PP. In general, the presence of a branching group at the end of the molecule will disrupt the stacking process, create a steric barrier around the individual molecules and inhibits crystallization [11]. This will result in the formation of microcrystalline structures rather than macro-structures. At lower temperatures, such microcrystalline structures can easily tumble and glide over one another resulting in better fluidity of the total matrix [2], resulting in a lower PP [11]. Moreover, disappearance of hydroxyl groups in JCOO esters means that hydrogen bonds do not exist in the molecule, which causes lower bonding of the molecules to each other and easier moving around [2].

Viscosity is one of the most important quality parameters for biolubricant oils. Efficiency of the biolubricant in reducing friction and wear is greatly influenced by its viscosity. Viscosity of oils decreases as temperature increases. It is desired to use a biolubricant with the lowest viscosity but still separating two moving surfaces. If the biolubricant is too viscous, it will require a large amount of energy to move, while if it is too thin, the surfaces will rub and friction will increase [2]. The VI value highlights how viscosity of a biolubricant changes with variations in temperature [2]. JCOT has a higher viscosity due to the presence of inter and intramolecular hydrogen bonding originating from hydroxyl groups as results of the ring opening reaction. Hydroxyl groups cause higher polarity that influences viscosity of the oil so that the more polar molecules, the higher the viscosity [13]. In general, hydroxyl groups will form bonds between molecules, which will cause that the lubricating oil becomes more viscous. After the final esterification process, viscosity of JCOO decreased due the disappearance of hydroxyl groups.

Table 3. Physicochemical properties of JCO, EJCO, JCOT and JCOO

Compound	JCO	EJCO	JCOT	JCOO	PAO6*
Iodine value, mg I_2 /100 g oil	113	5	330	660	-
Oxidative stability temperature, °C	174	179	169	170	201
Pour point, °C	-17	-9	-21	-29	-57
Flash point, °C	230	235	245	250	226
Kinematic viscosity at 40 °C, cSt	23.76	165.29	365.88	220.00	30.6
Kinematic viscosity at 100 °C, cSt	4.60	20.00	40.65	22.29	5.8
Viscosity index	111	124	127	135	132

*PAO6 = Polyalphaolefin lubricant

The FP value is often used as a descriptive characteristic of fuel oils as well as other oils such as biolubricants [2]. FP refers to both flammable and combustible oils [2]. Oils with a FP lower than 43 °C are flammable, while those with a FP above this temperature are combustible [2]. High FP is important to ensure that the biolubricant is not burned in the engine during its operation. A biolubricant with a low FP value is usually considered to be contaminated by volatile substances and usually requires precautions in handling [2]. JCOO shows the highest FP compared to the other products based on JCO due to the increase in the carbon number and consequently, increased molecular weight inducing a higher FP. In addition, JCOO also has a big branched carbon chain molecular structure, which requires more energy to burn and it will increase the FP.

For assessment purposes, the JCOO biolubricant produced in this work shows better lubrication properties as compared to those reported in literature for other biolubricants, especially regarding the oxidative stability (OS). In specific, JCOO shows high OS at 167 °C as well as values of PP (-29 °C), VI (135) and FP (250 °C). In comparison, a biolubricant in the same class, produced from a trimethylopropanol (TMP) ester of *J. curcas* oil showed significantly poorer low temperature properties with a high PP at -3°C and VI of 178 [26]. Other reports show moderate properties for similar biolubricants PP at –23 °C, FP (>130 °C) and VI (150) for 9(10)-hydroxy-10(9)-ester derivatives of methyl oleate [27]; PP at -3 °C, FP of 273 °C and VI at 140 for trimethylolpropane ester of *Jatropha curcas* oil [20]; and PP at −12°Cm FP of 178°C and VI at 204, for 9(12)-hydroxy-10(13)-oleoxy-12(9)-octadecanoic acid [29]. JCOO has also comparatively good lubrication properties as compared to a commercial PAO6 based lubricant (Table 3).

3. CONCLUSION

Chemical modification processes have been successfully performed significantly improving physicochemical and lubrication properties of the final product as compared to JCO itself. The epoxidation process has improved the OS and VI of the oil. The ring opening reaction has improved PP and FP values. Further esterification process with oleic acid has additionally improved the PP, FP and VI values of JCOO. The final product, JCOO has greater branching of ester functional groups with more bends and holes in its molecule structure. This makes the molecular arrangement less compact which improves the lubrication properties. Based on the obtained results, it is plausible that JCOO could be used as an industrial biolubricant with adequate lubrication properties.

Acknowledgements: Authors would like to acknowledge Universiti Kebangsaan Malaysia for the financial support through a research grant (DPP-2014-058, FRGS/2/2014/ ST01/UKM/01/2) as well as for the research facilities provided and to the Ministry of Education of Malaysia.

REFERENCES

[1] Campanella A, Rustoy E, Baldessari A, Baltanas M.A. Lubricants from chemically modified vegetable oils. *Bioresour Technol*. 2010; 101: 245–254.

[2] Jumat S, Nadia S, Yousif E. Chemically modified biolubricant basestocks from epoxidized oleic acid: Improved low temperature properties and oxidative stability. *J Saudi Chem Soc.* 2011; 15: 195–201.

[3] Jumat S, Nadia J. Oleic acid diesters: Synthesis, characterization and low temperature properties. *Eur J Sci Res.* 2009; 32; 216–222.

[4] Farhoosh R, Einafshar S, Sharayei P. The effect of commercial refining steps on the rancidity measures of soybean and canola oils. *Food Chem.* 2009; 115: 933–938.

[5] Erhan SZ, Asadauskas S. Lubricant basestocks from vegetable oils. *Ind Crops Prod.* 2000; 11: 277–282.

[6] Cerretani L, Bendini A, Rodriguez-Estrada MT, Vittadini E, Chiavaro E. Microwave heating of different commercial categories of olive oil: Part I. Effect on chemical oxidative stability indices and phenolic compounds. *Food Chem.* 2009; 115: 1381–1388.

[7] Moser BR, Sharma BK, Doll KM, Erhan SZ. Diesters from oleic acid:synthesis, low temperature properties, and oxidative stability. *J Am Oil Chem Soc.* 2007; 84: 675–680.

[8] Jumat S, Nadia S. Substituted esters of octadecanoic acid as potential biolubricants. *Eur J Sci Res.* 2009; 31: 273–279.

[9] Nirmal VP, Dineshbabu D. Performance and emission of *Pongamia Pinnata* oil as a lubricant in diesel engine. *Int J Innov Res Sci Eng Technol.* 2015; 4: 435–441.

[10] Wu X, Zhang X, Yang S, Chen H, Wang D. The Study of epoxidized rapeseed oil used as a potential biodegradable lubricant. *J Am Oil Chem Soc.* 2000; 77: 561–563.

[11] Jumat S, Nadia S. Modification of epoxidized ricinoleic acid for biolubricant base oil with improved flash and pour points. *Asian J Chem.* 2010; 22: 5468–5476.

[12] Lathi P, Mattiasson B. Green approach for the preparation of biodegradable lubricant base stock from epoxidized vegetable oil. *Appl Catal B.* 2007; 69: 207-212.

[13] Ebtisam KH, Elmelawy MS, Salah AK, Elbasuny NM. Manufacturing of environment friendly biolubricants from vegetable oils. *Egypt. J. Pet*. 2017; 26: 53–59.

[14] Endalew AK, Kiros Y, Zanzi R. Inorganic heterogeneous catalysts for biodiesel production from vegetable oils. *Biomass Bioenergy*. 2011; 35: 3787–3809.

[15] Tahira F, Hussain ST, Ali SD, Iqbal Z, Ahmad W. Homogeneous catalysis of high free fatty acid of waste cooking oil to fatty acid methyl esters (biodiesel). *Int J Energy Power*. 2012; 1: 31–36.

[16] Hassani M, Amini G, Najafpour GD, Rabiee M. A two-step catalytic production of biodiesel from waste cooking oil. *Int J Eng*. 2013; 26: 563–570.

[17] Panadare DC, Rathod VK. Applications of waste cooking oil other than biodiesel: A review. *Iran J Chem Eng*. 2015; 12: 55–76.

[18] Arbain N, Jumat S. Synthesis and characterization of ester trimethylolpropane *Jatropha curcas* oil as biolubricant base stock. *J Sci Technol*. 2010; 2: 47–58.

[19] Muhammad FM, Gunam R, Tinia IMG, Azni I. Temperature dependence on the synthesis of Jatropha biolubricant. *IOP Conf Series: Mater Sci Eng*. 2011; 17: 1–11.

[20] Jumat S, Noor HA. The effects of various acid catalyst on the esterification of *Jatropha curcas* oil based trimethylolpropane ester as biolubricant base stock. *J Chem*. 2011; 8: 33–40.

[21] Sharma A, Adhvaryu A, Liu Z, Erhan SZ. Chemical modification of vegetable oils for lubricant applications. *J Am Oil Chem Soc.* 2006; 83: 129–136.

[22] Menkiti MC, Ocheje O, Agu CM. Production of environmentally adapted lubricant basestock from *Jatropha curcas* specie seed oil. Int J Ind Chem. 2017; 8: 133–144.

[23] Sharma A, Adhvaryu A, Liu Z, Erhan SZ. Chemical modification of vegetable oils for lubricant applications. *J Am Oil Chem Soc.* 2006; 83: 129–136.

[24] Moser BR, Erhan SZ. Preparation and evaluation of a series of α-hydroxy ethers from 9, 10-epoxystreates. *Eur J Lipid Sci Technol.* 2007; 109: 206–213.

[25] Wang R, Schuman TP. Vegetable oil-derived epoxy monomers and polymer blends: A comparative study with review. *eXPRESS Polym Lett.* 2013; 7:272–292.

[26] Yunus R, Razi AF, Iyuke TL, Idris A. Preparation and characterization of trimethylolpropane esters from palm kernel oil methyl esters. *J Oil Palm Res.* 2003; 15: 42–49.

[27] Sharma BK, Doll KM, Erhan SZ. Ester hydroxy derivatives of methyl oleate: Tribological, oxidation and low temperature properties. *Bioresour Technol.* 2008; 99:7333–7340.

[28] Akbar E, Yaakob Z, Kamarudin SK, Ismail M, Jumat S. Characteristic and composition of *Jatropha curcas* oil seed from Malaysia and its potential as biodiesel feedstock. *Eur J Sci Res*. 2009; 29: 396-403.

[29] Jumat S, Abdullah BM, Nadia S. Improvement of physicochemical characteristics of monoepoxide linoleic acid ring opening for biolubricant base oil. *J Biomed Biotechnol*. 2011; 2011: 1–8.

[30] Jumat S, Abdullah BM, Rahimi MY, Nadia S. Synthesis, reactivity and application studies for different biolubricants. *Chem Cen J*. 2014; 8: 1–11.

[31] AOCS, Official methods and recommended practices of the American Oil Chemists' Society, 4th ed., Champaign Illinois, USA, 1989.

[32] Nadia S, Jumat S, Jantan F. Synthesis and characterization of palm kernel oil based trimethylolpropane ester. *Asian J Chem*. 2013; 25: 9751–9754.

[33] Kishore, N.A. 2007. Guide to ASTM test methods for the analysis of petroleum products and lubricants, 2nd ed., ASTM International, West Conshohocken, PA, USA.

[34] Yunus R, Fakhru'l-Razi A, Ooi TL, Omar R, Idris A. Synthesis of palm oil based trimethylolpropane esters with improved pour points. *Ind Eng Chem Res*. 2005; 44: 8178–8183.

[35] Nadia S, Jumat J, Emad Y. The physicochemical and tribological properties of oleic acid based triester biolubricants. *Ind Crops Prod*. 2011; 34: 1089–1096.

[36] Abdo Ahmed W, Jumat S, Ambar YM. Lubricity characterizations of sebacic acid based ester. *Int J Adv Sci Eng Inf Technol.* 2014; 4: 1–6.

[37] Stachowiak GW, Batchelor AW. *Engineering Tribology*, 3th ed., USA, New York, Elsevier: Butterworth-Heinemann; 2005.

[38] Nor NM, Derawi D, Jumat S. Esterification and evaluation of palm oil as biolubricant base stock. *Malaysian J Chem*. 2019; 21: 28–35.

[39] Owuna FJ, Dabai MU, Sokoto MA, Dangoggo SM, Bagudo BU, Birnin-Yauri UA, Hassan LG, Sada I, Abubakar AL, Jibrin MS. Chemical modification of vegetable oils for the production of biolubricants using trimethylolpropane: A review. *Egypt J Pet*. 2020; 29: 75–82.

[40] Timothy YW, Sunday AL, Asipita SA, Moses AO. Nigeria Jatropha oil as suitable basestock for biolubricant production. *J Tribol*. 2019; 23: 97–112.

[41] Jagadeesh KM, Satish VK, Venkatesh K, Kathyayini N. Evironmentally friendly functional fluids from renewable and sustainable sources – A review. *Renew Sustain Energy Rev*. 2018; 18: 1787–1801.

[42] Jumat S, Abdullah BM, Yusop RM, Nadia S. Synthesis and optimization ring opening of monoepoxide linoleic acid using *p*-toluenesulfonic acid. *SpringerPlus*. 2013; 2: 1–14.

[43] Bilal S, Mohammed-Dabo I, Nuhu M, Kasim S, Almustapha I, Yamusa Y. Production of biolubricant from *Jatropha curcas* seed oil. *J Chem Eng Mater Sci*. 2013; 4: 72-79.

SAŽETAK

Hemijski modifikovano ulje biljke Jatrofa curcas za primenu kao biomazivo

Nurazira Mohd Nor[1], Nadia Salih[2] and Jumat Salimon[2]

[1]School of Chemistry and Environment, Faculty of Applied Sciences, Universiti Teknologi MARA, 72000 Kuala Pilah, Negeri Sembilan, Malaysia
[2]Department of Chemical Sciences, Faculty of Science and Technology, Universiti Kebangsaan Malaysia, 43600 Bangi, Selangor, Malaysia

(Naučni rad)

Ulje biljke *Jatropha curcas* jedan je od zanimljivih obnovljivih izvora za proizvodnju biomaziva. Međutim, direktna primena ovog ulja kao biomaziva je ograničena zbog njegove male oksidativne stabilnosti. Ovaj nedostatak može se prevazići modifikacijom strukture reakcijama epoksidacije, otvaranja prstena i esterifikacije. Epoksidacija ulja izvršena je *in situ* generisanom permravljom kiselinom, a otvaranje prstena reakcijom sa oleinskom kiselinom u prisustvu *p*-toluensulfonske kiseline . Potpuna esterifikacija oleinskom kiselinom izvršena je u prisustvu sumporne kiseline. Struktura modifikovanog ulja određena je merenjem sadržaja epoksi kiseonika, infracrvenom spektroskopijom sa Furijeovom transformacijom (engl. Fourier-transform infrared spectroscopy, FTIR) i nuklearno-magnetno-rezonantnom spektroskopijom (^{1}H NMR i ^{13}C NMR). Rezultati su pokazali da su oksidativna stabilnost, viskoznost, tačka paljenja i tačka tečenja krajnjeg proizvoda značajno poboljšani. Konkretno, postupci otvaranja i esterifikacije prstena koji dovode do grananja i savijanja u konačnoj molekulskoj strukturi ulja, doveli su do poboljšanja indeksa viskoznosti na vrednost od 135, tačke tečenja na -29 ° C i povećanja tačke paljenja na 250 ° C..

Ključne reči: epoksidacija; otvaranje prstena; esterifikacija; oleinska kiselina; ekološko biomazivo

Хемијско-технолошка пракса у Научно-технолошком центру НИС-Нафтагас

Научно-технолошки центар НИС-Нафтагас послује као регионални центар југоисточне Европе за научно праћење пројеката истраживања, производње и прераде угљоводоника. Основне делатности НТЦ-а су извођење научно - истраживачких и развојних радова, геолошко - истражни радови, пројектовање и надзор геофизичких радова, обрада и интерпретација геолошко - физичких података, геолошко моделирање, прорачун резерви, праћење и испитивање нових технологија, аналитички послови при мониторингу производње, пројектовање и надзор бушотина, примена хемикалија у процесима производње, лабораторијске и консултантске услуге.

ВЕСТИ
Hem. Ind. **74 (2)** 129-000 (2020)

Available on-line at the Journal web address: http://www.ache.org.rs/HI/

Научно-технолошки центар НИС-Нафтагас послује као регионални центар југоисточне Европе за научно праћење пројеката истраживања, производње и прераде угљоводоника. Основне делатности НТЦ-а су извођење научно - истраживачких и развојних радова, геолошко - истражни радови, пројектовање и надзор геофизичких радова, обрада и интерпретација геолошко - физичких података, геолошко моделирање, прорачун резерви, праћење и испитивање нових технологија, аналитички послови при мониторингу производње, пројектовање и надзор бушотина, примена хемикалија у процесима производње, лабораторијске и консултантске услуге.

Департман за технику и технологију производње нафте и гаса Научно-технолошког центра се бави пројектовањем израде и опремања бушотина различитих конструкција, одабиром и испитивањем нових техника и технологија, аналитичким пословима на откривању проблематике при производњи нафте и гаса, одабиром,

испитивањем и препорукама хемикалија за решавање проблематике прибушотинске зоне, производње, транспорта и припреме флуида, разрадом нових производа и спровођењем професионалних техничких обука. У овом департману ради велики број висококвалификованих и искусних стручњака, а послови се обављају применом најсавременијих софтверских пакета.

У оквиру Департмана за технику и технологију производње нафте и гаса, функционише Сектор за хемизацију који је подршка свим процесима у току производње и припреме нафте и гаса где се користе хемикалије. Овај сектор обавља активности као што су одабир, испитивање и препорука хемикалија за решавање проблематике прибушотинске зоне, производње, транспорта и припреме флуида.

Области којима се бави Сектор за хемизацију су:

- хемизација слоја и интензификација дотока: решавање проблема везаних за проблематику гушења бушотина, изучавање проблема негативног ефекта киселинске обраде и проналажење решења за минимизацију негативних ефеката, проналажење иновативних решења и истраживање нових технологија за контролу песка, изучавање примењивости раствора за изолацију водоносних слојева, испитивање интеракције са слојним флуидима;
- хемизација бушотина и технолошких процеса: анализа и израда предлога за решавање проблема са асфалтно-смоластим и парафинским наслагама (АСПН), као и проблема великих вискозности флуида у бушотинама, цевоводима и објектима за припрему и отпрему нафте, затим анализа и израда предлога за решавање проблема таложења каменца у бушотинама и објектима за припрему и отпрему нафте, анализа и израда предлога за решавање проблема корозије опреме у бушотинама, цевоводима и објектима за припрему и отпрему нафте, анализа и израда препорука за решавање проблема демулгације у процесима припреме нафте;
- нове технологије и погонска тестирања: развој хемијских реагенса и технологија за процесе бушења нафтних бушотина, заштите опреме и цевовода од парафина, асфалтена, каменца, корозије и других проблема, припрема и транспорт нафте, интензификација протока нафте, гушење бушотина и прерада нафте. У оквиру ове области рада се врше погонска тестирања развијених хемијских реагенаса, као и анализа резултата погонског тестирања са препорукама за даљу имплементацију, и коначно подршка имплементацији развијених хемијских реагенаса.

Један од значајнијих пројеката је пилот пројекат развоја нових хемикалија. Хемикалија, развијена и која се тестира у Научно-технолошком центру, има улогу спречавања стварања наслага парафина, асфалтена и смоле

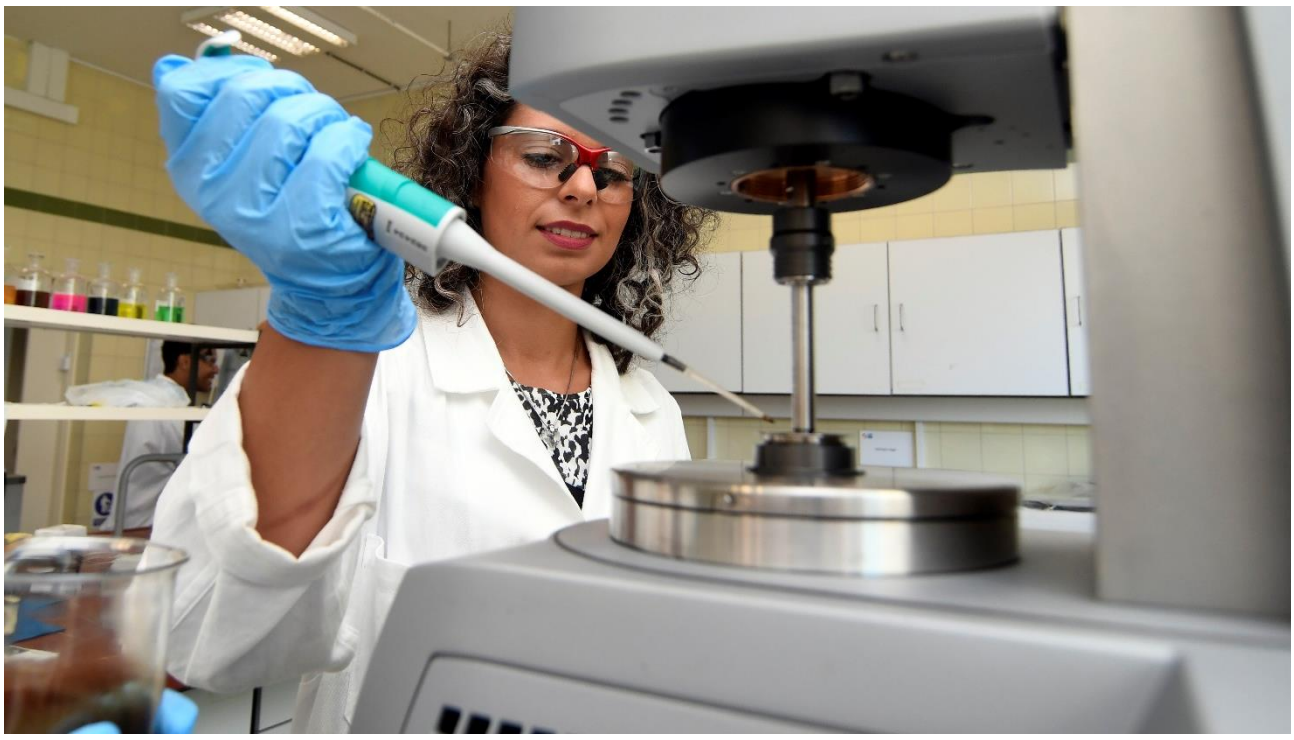

током производње и транспорта нафте. У Сектору за хемизацију реализован је пилот пројекат ''Развој сопствених хемикалија'', који је, у сарадњи са фирмом *ISS Chemicals d.o.o*, као експертском подршком при развоју хемикалија, започет у 2019. години. Кроз овај пилот пројекат проширили су се компетенције у виду сазнања о селекцији активних компоненти, избора растварача и адитива, до намешавања и тестирања хемикалије на нафтном пољу. Циљ овог пројекта је био да се изради хемикалија која ће решити проблематику таложења парафина, смола и асфалтена на нафтном пољу. Тим приступом се сама формулација хемикалије прилагођавала карактеристикама одређеног поља и проблематици која се на њему јавља. Тренутно развијена хемикалија, као и већина других које се примењују у нафтној индустрији, захтева безбедно руковање. Будући да је реч о материјама различитих нивоа опасности, кроз безбедносне листове који прате хемикалију прецизирани су начини складиштења, руковања и обавезне личне заштитне опреме чије поштовање омогућава заштиту запослених и безбедно руковање хемикалијама.

Производњом сопствених хемикалија компанија би могла да смањи зависност од иностраних произвођача и оперативне трошкове, о чему је још увек рано говорити, с обзиром да је у току погонско тестирање. Овај пилот пројекат би требало да укаже на могућности и проблеме развоја и производње хемикалија. Успостављање новог правца производње, као и дистрибуција и продаја нових производа је сложен процес, али свакако би помогао ширењу компетенција Научно-технолошког центра НИС-Нафтагас.

Директор НТЦ НИС-Нафтагас д.о.о
Леонид Стулов

Извршилац
Јелена Зелинчевић
e-mail: jelena.zelincevic@nis.eu

Chemical engineering practice in the Science and Technology Centre of NIS-Naftagas

The NIS - Naftagas Science and Technology Centre (Naučno-tehnološki centar) operates as the regional centre of Southeast Europe for scientific monitoring of hydrocarbon exploration, production and processing projects. The main direction of the business is performing scientific research and development, geological research, design and supervision of geophysical works, processing and interpretation of geological - physical data, geological modelling, reserve calculation, monitoring and testing of new technologies, analytical work in production monitoring, well design and monitoring, application of chemicals in production processes, and laboratory and consulting services.

NEWS

Available on-line at the Journal web address: http://www.ache.org.rs/HI/

The Department of Oil and Gas Production Engineering and Technology at the Science and Technology Centre deals with: the design of construction and completion of wells with different structures, selection and testing of new techniques and technologies, analytical work on detecting problems in oil and gas production, selection, testing and recommendation of chemicals for solving problems in the near-well zone, production, transport and preparation of fluids, development of new products and implementation of professional technical training. This department employs a large number of highly qualified and experienced specialised professionals, and the work is performed by using state-of-the-art software.

The Chemicalisation Sector within the Department for Oil and Gas Production Engineering and Technology provides support to all oil and gas production and preparation processes involving the use of chemicals. This sector performs

activities such as the selection, testing and recommendation of chemicals to resolve problems in the near-well zone, as well as for production, transport and preparation of fluids.

Areas covered by the Chemicalisation Sector are:

- layer chemicalisation and inflow enhancement: solving problems related to well killing, studying the negative effects of acid treatment and finding solutions to minimize negative effects, finding innovative solutions and investigating new technologies for sand control, studying the applicability of solutions for insulating aquifers, and testing interactions with fluids;
- chemicalisation of wells and processes: analysis and development of proposals for solving problems with asphalt-resin and paraffin deposits (ASPD) as well as high viscosity of fluids in wells, pipelines and facilities for oil preparation and shipment, analysis and development of proposals for solving problems of scale deposition in wells and facilities for oil preparation and shipment, analysis and development of proposals for solving the problem of corrosion of equipment in wells, pipelines and facilities for oil preparation and shipment, analysing and making recommendations for solving the problems of demulsification in oil preparation processes;
- new technologies and operational testing: development of chemical reagents and technologies for drilling oil wells, technologies for equipment and pipeline protection from paraffin, asphaltene, limestone, corrosion and other issues, oil preparation and transport, oil flow enhancement, well killing and oil refining. Within this area of work, operational tests of developed chemical reagents are performed, and analysis of the results of operational testing and recommendations for further implementation, and finally, support for implementing developed chemical reagents.

One of the most important projects is a pilot project for the development of new chemicals. The chemical developed and tested at the Science and Technology Centre, acts so to prevent formation of paraffin, asphaltene and resin deposits during oil production and transportation. The Chemicalisation Sector implemented the pilot project called "Development of Own Chemicals" which was initiated in 2019, in cooperation with the company ISS Chemicals doo, our specialised support for the chemicals development process. This pilot project resulted in broadening the competencies

of personnel in terms of knowledge about the selection of active components, the choice of solvents and additives, and mixing and testing of chemicals in the oil field. The goal of this project was to develop a chemical that would solve the problem of paraffin, resin and asphaltene deposits in the oil field. Under this approach, the very formulation of the chemical was adapted to the characteristics of a certain field and the corresponding problems. The chemical that has been developed, like most others used in the oil industry, requires safe handling. Since these are substances characterised by different hazards, the material safety data sheets that accompany the chemical specify the storage and handling methods and the mandatory personal protective equipment. Compliance with MSDS ensures employee protection and the safe handling of chemicals.

By producing its own chemicals, the company could reduce its dependence on foreign manufacturers and operating expenses, which is currently too early to claim, given that operational testing is underway. This pilot project should indicate the possibilities and problems in the development and production of chemicals. A new direction in production, as well as distribution and sale of new products, is a complex process, but would certainly help broaden the competencies of the Science and Technology Centre NIS-Naftagas.

Director of Science and Technology Centre NIS-Naftagas Ltd.
Leonid Stulov

Implementer
Jelena Zelinčević
e-mail: jelena.zelincevic@nis.eu